1 Introduction

This thesis is concerned with *diffusion* of *confined colloidal particles*. Diffusion can be illustrated with the spreading of an ink drop in a glass of water. After the ink has been dropped into the water, it will diffuse. As a result the colour of the water will, if given sufficient time, become homogeneous. As an example we will follow the trajectory of an imaginary individual ink particle, shown in figure 1.1. The random motion consisting

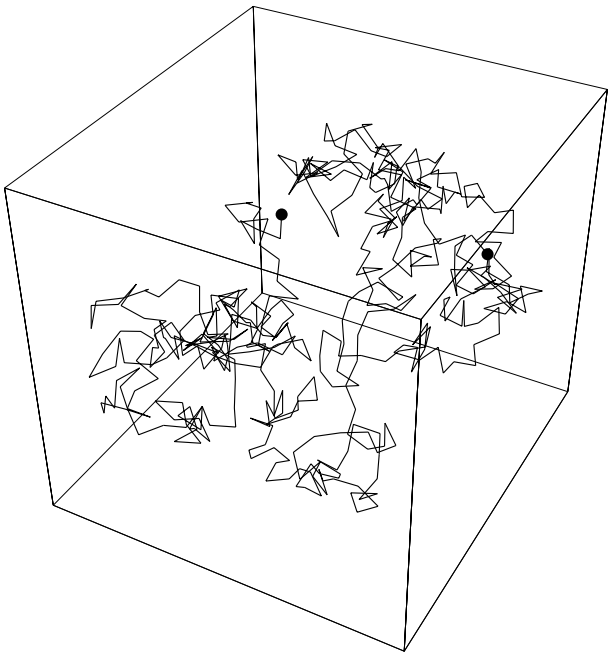

Figure 1.1
Random walk for an ink particle in water. The points denote the begin and end points.

of a sequence of apparently discrete steps is often referred to as a random walk. The random motion can be described by the diffusion equation

$$\frac{\partial n(\mathbf{r},t)}{\partial t} = D\nabla^2 n(\mathbf{r},t), \tag{1.1}$$

where the coefficient D is the diffusion constant, and $n(\mathbf{r},t)$ is the number density of the ink molecules. The diffusion equation describes quantitatively how a spatially non-uniform density will relax to spatial uniformity.

If we consider some every day fluids, like paint, blood milk and also ink, there is a remarkable similarity. In all these examples there are small particles, typically with a size of 10 nm to 10 μm present in the fluid. These particles, colloidal particles, which are suspended in a solvent, are in size much larger than the solvent molecules. Because they are large, compared to atoms for instance, it is possible to see colloidal particles with an optical microscope. The motion of the colloidal particle is determined by all constituents of the suspension. However, due to the size difference between the colloidal particles and the molecules, the effect of the molecules on the motion of the colloidal particle can be approximated by the motion of a particle in a continuum fluid. The fluid is thus taken into account in an effective way, by various parameters which specify the nature of the solvent. Parameters might include, for instance, the viscosity or the temperature of the solvent. These are not however the only parameters which influence the diffusion of colloidal particles. Diffusion might be modified by the presence of walls.

If we consider the motion of colloidal particles in a glass of milk, we encounter two limits for diffusion. First there is diffusion of the colloidal particle on short times, which might already be affected by hydrodynamic (mediated by the solvent) interactions with the wall. Secondly, at even longer times, when the particle displaces significantly compared to its size it will physically "feel" that it is confined by boundaries set by the medium, here the glass. In fact, here, the (long-time) diffusion coefficient of the colloidal particle vanishes, because the colloidal particles are confined to be in the container. Compared to the size of the colloidal particle, the glass is rather large. In this thesis we will study the effect of the confining medium on the diffusion of the colloidal particle when the size of the confining medium is comparable to the size of the colloidal particle.

Although the examples of colloidal suspensions we have mentioned are "real-world" examples, the behaviour of these systems can be mimicked by computer simulation. In computer simulation one considers a simplified version of the "real-world" system, the model. The model consists of the set of assumptions made, and the resulting method to calculate the quantities in which one is interested. In our case we do *not* consider the motion of every molecule in the system, we only take into account the effect which the continuum solvent has on the motion of the colloidal particles. The colloidal particle is assumed to be spherical. After the validity of these models is established one can "dress up" these models and apply them to more complex situations, like systems with walls.

In chapter 2 we discuss in more detail the background for this thesis. In chapter 3 we study the effect of walls on diffusion of a single colloidal particle. In chapter 4 we discuss the rotational diffusion coefficient for a suspension of colloidal particles. In chapter 5 we continue with a study of the diffusion of tracer particles in a porous medium. Chapter 6 discusses deviations from "classical diffusion" for a) a colloidal suspension b) a colloidal particle confined between plates. In chapter 7 we discuss the effect of the finite size of

a colloidal particle, which diffuses in a porous medium. The final chapter of this thesis, chapter 8, is concerned with diffusion of a colloidal particle near a single wall.

2 Background

2.1 Brownian motion in the early days

The central theme of this thesis is the Brownian motion of particles suspended in fluids. Brownian motion was first observed by botanist Robert Brown, who in 1828 saw the erratic motion of pollen floating on the surface of water. It was Einstein, who was, incidentally, at the time unaware of the work by Brown, who gave an explanation for the observed motion at the beginning of this century. The erratic motion is caused by random collisions of fluid molecules with the particle. Einstein's theory of Brownian motion allowed him to write down an expression that could be used to determine Boltzmann's constant k_{B}

$$< (\Delta \mathbf{r})^2 >=< (\mathbf{r}(t) - \mathbf{r}(0))^2 >= 6D_0 t = \frac{k_{\mathrm{B}} T}{\pi \eta R}, \tag{2.1}$$

where $< (\Delta \mathbf{r})^2 >$ is the average mean-squared displacement of the particle during a time t, D_0 is the (Stokes-Einstein) diffusion coefficient of the particle, T is the absolute temperature, η is the fluid viscosity and R is the particle radius. To give a specific example, equation 2.1 predicts that in water a particle with a radius of 0.1 μm will diffuse over a distance of about 1 μm in 1 second. Such displacements are observable under an optical microscope. Let us now consider what forces act on the Brownian particle. First of all, there are direct interparticle forces, such as Van der Waals and electrostatic forces. In addition there are indirect, hydrodynamic forces, where the effect of the motion of a particle on its own motion, or on that of another particle, is mediated by the flow induced in the solvent.

When studying the effect of hydrodynamic interactions on the motion of the particles, it is often convenient to minimize the range of the direct interactions. In practice this is often achieved by studying hard-sphere suspensions. In such systems, the direct forces act only when particles are in close contact. As pointed out by Einstein, the hydrodynamic force acting on a colloidal particle can be separated into two parts. First of all there is the random force, and secondly a systematic force, which is due to hydrodynamic friction. The systematic force exerted by the fluid on a spherical particle

moving with small, constant velocity $\mathbf{v}$ is given by Stokes Law, $\mathbf{F} = -\gamma\mathbf{v}$, where the friction coefficient γ is given by

$$\gamma = 6\pi\eta R, \tag{2.2}$$

provided that the solvent at the surface of the particle obeys "stick" boundary conditions, i.e., the fluid velocity at the surface of the sphere is taken to be the velocity of the sphere. Combining the random and systematic forces on the particle, Langevin introduced the following equation of motion for the suspended particle

$$M\dot{\mathbf{v}} + \gamma\mathbf{v} = \mathbf{f}(t), \tag{2.3}$$

where M is the mass of the particle, and $\mathbf{f}(t)$ is the random force. We still have to supply the properties of $\mathbf{f}$ to give a full description. Langevin made the following assumptions

$$\begin{aligned} &< \mathbf{f}(t) > = \mathbf{0} \\ &< \mathbf{f}(t) \cdot \mathbf{f}(t') > = < \mathbf{f}^2 > \delta(t - t') \\ &< \mathbf{f}(t) \cdot \mathbf{v}(\mathbf{t}) > = 0, \end{aligned} \tag{2.4}$$

where the brackets $< >$ denote a statistical average. Combination of equation 2.4 with the Langevin equation (eq. 2.3) leads to information on the velocity correlation function

$$C_v(t) = \frac{1}{d} < \mathbf{v}(0) \cdot \mathbf{v}(t) >, \tag{2.5}$$

which expresses the covariance of the initial velocity $\mathbf{v}(0)$ of a particle with $\mathbf{v}(t)$, its velocity some later time, t, d is the dimensionality. This type of correlation function will play a key role in this thesis. According to the Langevin equation (2.3) the velocity correlation function is

$$C_v(t) = < \mathbf{v}^2(0) > e^{-\gamma t/M}, \tag{2.6}$$

with relaxation time

$$\tau_1 = \frac{M}{\gamma} = \frac{2}{9}\frac{R^2\rho_{\mathrm{obj}}}{\eta}, \tag{2.7}$$

where ρ_{obj} is the density of the suspended particle. The velocity correlation function gives information on the motion of the particle, and can be related to the diffusion coefficient via the following 'Green-Kubo' relation

$$D = \int_0^\infty C_v(\tau)d\tau, \tag{2.8}$$

In equation 2.8 it is implicitly assumed that the integral converges. Even when the Langevin equation is not valid, the Green-Kubo relation is. Hence, knowledge of the velocity correlation function *always* allows us to compute the diffusion coefficient.

2.2 The "revolution" starting from 1970

It came as a surprise when, in 1970, Alder and Wainwright [1] reported simulations that showed that the velocity correlation function in a system of hard spheres decayed with an algebraic long-time tail

$$C_v(t) \sim \frac{1}{t^{d/2}}. \tag{2.9}$$

This finding contradicted both the "macroscopic" picture of Langevin and the microscopic picture of Boltzmann (1872) who, in deriving his kinetic theory of gases, assumed that successive collisions experienced by a fluid particle are uncorrelated. The latter assumption also leads to the prediction that the velocity correlation function decays exponentially. The simple qualitative explanation of the long-time tail given by Alder and Wainwright is the following: assume that initially a small fluid element of fluid δV is given an initial momentum, $p(0)$ in an otherwise quiescent fluid. Then, according to hydrodynamics, part of this momentum will diffuse away with a rate determined by the kinematic shear viscosity $\nu = \eta/\rho$, where ρ is the density of the fluid. The remainder is propagated by sound waves. The latter is a fast process, and can be neglected (at least for the time being). The part of the initial momentum that is transported away diffusively will, after some time t, be contained in a volume with radius $(2d\nu t)^{1/2}$, where we assumed that the diffusion coefficient is much smaller than the viscosity. If we now assume that the momentum is evenly distributed over this volume, then the part of the momentum in the fluid element is given by $\delta V/(2d\nu t)^{d/2}$, and hence the velocity correlation function decays as $C_v(t) \sim 1/t^{d/2}$. It is important to note that, in this simple derivation, *no* assumption was made about the way the initial momentum was introduced into the fluid, only the amount is important. From this we conclude that the velocity correlation function of a particle suspended in fluid will have the same form. The difference between the Langevin result (eq.2.6) and the long-time tail in equation 2.9 is caused by the memory of the fluid, i.e., momentum diffuses away at a finite rate. After the discovery of the long-time tail Ernst et al. [2] and Dorfman and Cohen [3] gave a detailed theoretical treatment of the velocity correlation function, and were able to calculate the prefactor of the velocity correlation function. For a comprehensive review of time dependent correlation functions see ref. [4]. After the discovery of the "hydrodynamic" long-time tail, many others were to follow. In 1971 Ernst and Weyland [5] predicted that in a Lorentz gas, i.e., a model where a point particle moves among a collection of fixed obstacles,the following *negative* velocity correlation function should be found

$$C_v(t) \sim -\frac{1}{t^{(d+2)/2}}, \tag{2.10}$$

which was also confirmed by computer simulation [6].

2.3 Computational fluid dynamics

We argued above that the hydrodynamic long time tail should not depend on molecular details. Alder and Wainwright performed an explicit calculation of the motion of the trajectories of the hard-sphere "atoms". But the long-time tail can be found in even simpler models. In 1986 Frisch, Hasslacher and Pomeau [7] introduced a discretized model for a hydrodynamic medium. The so-called FHP model belongs to the class of lattice-gas cellular automata-models where space and time are discrete. In these models, discrete particles travel along links between sites, where particles collide. During the collision momentum and number of particles are conserved. The special feature of the FHP-model was that it was the first lattice model that exhibited isotropic hydrodynamic behaviour. This is demonstrated in ref. [8]. A disadvantage of the lattice-gas cellular automata is that they are intrinsicly noisy, and that they lack Gallilean invariance. Nevertheless, for some problems it proved possible to get accurate results. An example is the calculation of the velocity correlation function for a lattice-gas particle, using the moment-propagation method [9]. These simulations made it possible to verify the predicted long-time behaviour of the velocity correlation function, given by equation 2.9, in lattice gases. Ladd, Colvin and Frenkel [10] showed that it was possible to implement moving boundary conditions in lattice gases. This made it possible to study the dynamics of suspended colloidal particles. Using this approach, Van der Hoef [11] showed that the velocity correlation function of a disk suspended in a two-dimensional fluid decayed faster than $1/t$. As we stated, before a drawback of the lattice-gas method are the inherent fluctuations, and the lack of Gallilean invariance. The large statistical fluctuations in the flow field, are effectively suppressed in a closely related model: the lattice- Boltzmann model [12–14]. In this model the Boltzmann equation of a lattice gas is solved, rather than the lattice gas itself. This model also proved to be a full-time dependent Navier-Stokes solver, with the added advantage that hydrodynamic fluctuations [15] could be added correctly [16]. The method of simulating colloidal particle dynamics using lattice gases was extended by Ladd to lattice-Boltzmann fluids [15, 17, 18]. This opened the way to direct numerical simulations of hydrodynamic interactions between colloidal particles in suspension. It should be mentioned that the lattice-Boltzmann model is not the only particle-based model that can be used to calculate (time-dependent) hydrodynamic interactions. There exist other simulation techniques that can be used to study hydrodynamic effects. Each technique has its specific advantages, and disadvantages. First of all, there is conventional Molecular Dynamics and secondly there is Dissipative Particle Dynamics. In Molecular Dynamics, see for instance refs. [19, 20], the natural time evolution of a system of particles is followed. In the case of colloidal suspensions the number of particles needed to represent the solvent surrounding realistically sized colloidal particles is prohibitively large. This makes brute force MD very expensive. As

a consequence that technique can only be used to study the very short-time dynamics of colloidal suspensions. Dissipative particle dynamics [21, 22] combines concepts from Molecular Dynamics with certain features of the lattice-gas method. The method is less well studied than the other techniques, and its theoretical foundation is still under discussion [23–27]. In addition there exist techniques to calculate hydrodynamic interactions, assuming that the interactions are fully developed before the velocity of the particle changes significantly. An example is Stokesian Dynamics [28].

What makes lattice Boltzmann unique is the fact that it is suitable for studying the short-time dynamics of colloidal suspensions, in the time regime where the the hydrodynamic interactions propagate. The same phenomena could also be studied with Molecular Dynamics. That is, in principle, but not in practice, at least not in the foreseeable future. For a comparable problem the lattice-Boltzmann simulation method is currently orders of magnitude faster than Molecular Dynamics. The schematic situation for simulation of colloidal suspension is depicted in figure 2.1. Finally, we mention one other method that is frequently used to simulate colloidal dynamics, viz. Brownian dynamics [29]. In this method the solvent molecules are omitted from the simulation, but their effect is incorporated by a combination of random forces, and frictional terms. This method is useful for studies of colloidal motion on time-scales in which particles diffuse over considerable distances. At this point it is important to identify the two time scales considered in this thesis. The first is the (short) time, in which the hydrodynamic interactions propagate. The particle does *not* move over a significant distance compared to its radius on this time scale. As an example, for a particle of radius 0.1 μm suspended in water the relaxation time τ_1 is about 10^{-9} s (from equation 2.7), during which it diffuses a distance of about 10^{-3} of its radius. It is only on this short-time scale that we can observe hydrodynamic effects (such as the long-time tail) in the colloidal particle dynamics. After this short-time regime the diffusion coefficient has reached a plateau value and all dynamics is dominated by particle diffusion. An estimate of the time scale for particle diffusion is given by

$$\tau_2 \sim \frac{R^2}{D_0}. \tag{2.11}$$

On this time scale the particles move over significant distances, the diffusion coefficient changes. Experimentally it is observed that it eventually reaches another plateau value. For a particle of radius 0.1 μm suspended in water the time scale for particle diffusion is about 10^{-3} s. The time scales for short-time and long-time diffusion are separated by $\tau_2/\tau_1 \approx 10^6$. All the simulations performed in this thesis rely on the time scale separation between short- and long-time motion.

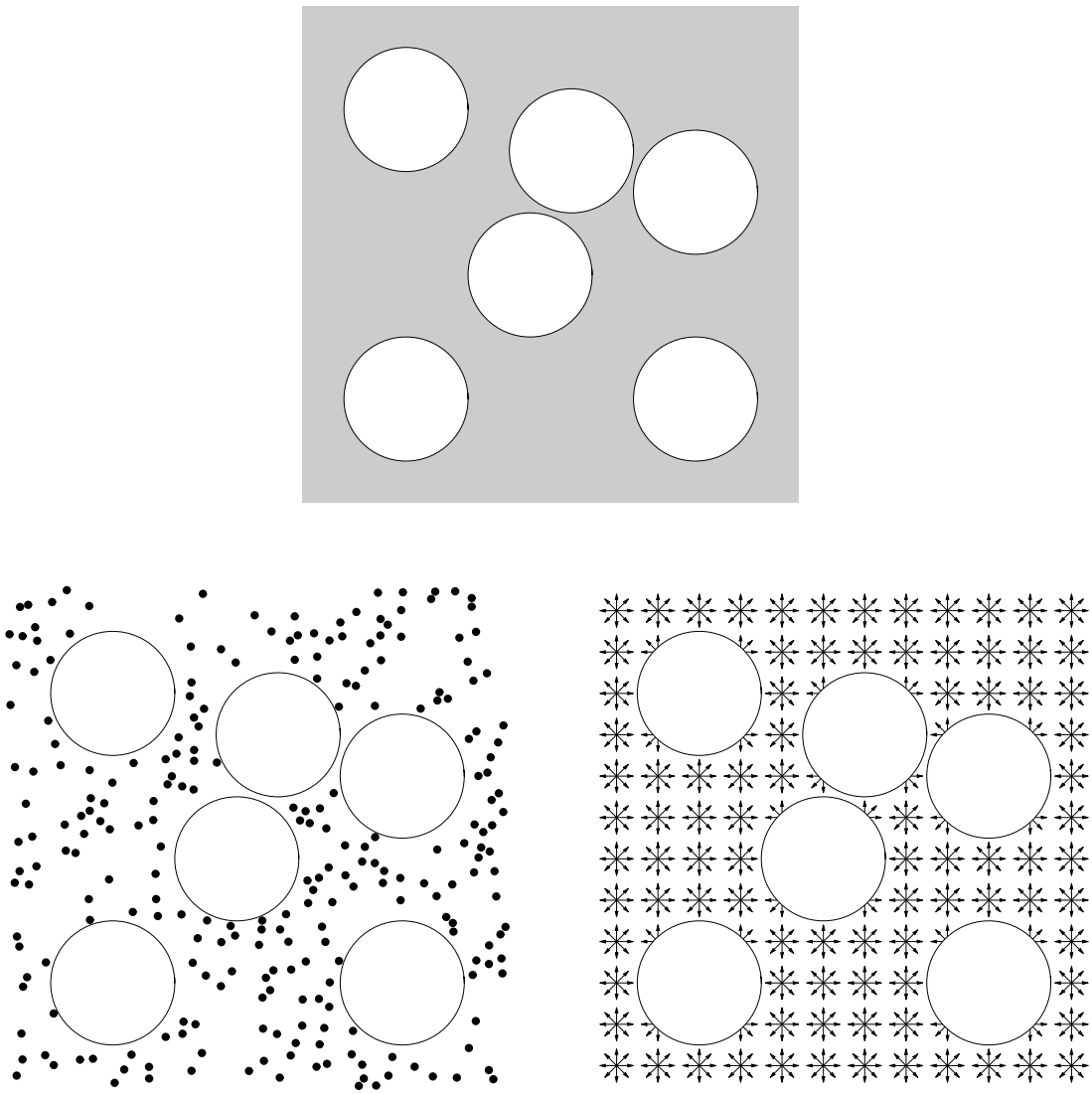

Figure 2.1 Models of colloidal suspension. Top: particles suspended in a continuum fluid. Lower left: particles suspended in a fluid represented by a molecular solvent. Lower right: particles suspended in a lattice-Boltzmann fluid.

2.4 Experimental techniques

Wherever possible, we compare our numerical data with experimental results. Here we briefly list the most important techniques to probe colloidal particle diffusion, and we indicate the nature of the information that they provide. We have listed the techniques in order of increasing time scale. The first technique we mention is Diffusing Wave Spectroscopy (DWS). This technique is particularly suited to probe short-time dynamics [30]. For instance, using DWS the $C_v(t) \sim t^{-3/2}$ long-time tail for the velocity correlation function for a particle diffusing in a suspension could be observed directly [31]. Secondly there is Dynamic Light Scattering (DLS), see for instance ref. [32]. One quantity that

is often obtained from dynamic light scattering is the self-dynamic structure factor

$$F(k,t) =< \exp\{i\mathbf{k}\cdot(\mathbf{r}_i(t)-\mathbf{r}_i(0))\} >, \tag{2.12}$$

where $\mathbf{k}$ is the wavevector, and $\mathbf{r}_i(t)-\mathbf{r}_i(0)$ is the displacement of particle i in time t. If the diffusion process under consideration is described by the diffusion equation, then $F(k,t)$ is given by

$$F(k,t) = \exp(-k^2Dt), \tag{2.13}$$

from which the diffusion coefficient can easily be obtained. DLS is suited to measure the intermediate to long-time dynamics of colloidal particles. The last technique in our (incomplete) list is Fluorescence Recovery After Photobleaching (FRAP). In this technique one bleaches a pattern on fluorescent colloidal particles. The pattern washes out due the Brownian motion of the particles [33]. FRAP also provides information about $F(k,t)$, and can hence be used to estimate D. FRAP is ideally suited for the measurement of the long-time self diffusion coefficient of colloidal particles.

2.5 Theoretical background

The present section summarizes some of the theoretical results concerning the dynamics of colloidal particles that are directly relevant to the work presented in this thesis. It is not our intention to give a complete description of the theoretical approach, but rather to indicate the approach used to calculate transport coefficients. For other aspects we refer the reader to the book on low Reynolds number hydrodynamics by Happel and Brenner [34]. Most theoretical treatments of the transport coefficients of suspensions begin with the Navier-Stokes (NS) equations for steady-state flow, at low Reynolds number. In this regime the non-linear term in the NS equations can be ignored, and we obtain the equations for Stokes flow

$$\begin{aligned} \nabla\cdot\mathbf{u}(\mathbf{r}) &= 0, \\ \nabla p(\mathbf{r}) &= \eta\nabla^2\mathbf{u}(\mathbf{r}) + \mathbf{F}_{\text{ext}}, \end{aligned} \tag{2.14}$$

where $\mathbf{u}(\mathbf{r})$ is the fluid velocity at position $\mathbf{r}$ and $p(\mathbf{r})$ is the pressure, ρ is the density and $\mathbf{F}_{\text{ext}}$ is any external force. These equations need to be supplied with the appropriate boundary conditions at the surface of the colloidal particle

$$\mathbf{u}(\mathbf{r}-\mathbf{R}) = \mathbf{v} + \omega\times(\mathbf{r}-\mathbf{R}), \tag{2.15}$$

where $\mathbf{v}$ is the velocity of the object, and ω is the angular velocity, and $\mathbf{r}-\mathbf{R}$ is a vector on the surface of the sphere, with $\mathbf{R}$ denoting the position of the center of the sphere. This is the so-called stick boundary condition: it implies that the fluid velocity matches that of the object at the boundary. For an isolated sphere, it is straightforward

to calculate both the translational and rotational drag

$$\begin{aligned} \mathbf{F}_{\text{drag}} &= 6\pi\eta R\mathbf{v}, \\ \mathbf{T}_{\text{drag}} &= 8\pi\eta R^3\omega. \end{aligned} \tag{2.16}$$

Einstein [35] and Debye [36] showed that knowledge of these drag coefficients allows one to compute the translational and rotational diffusion coefficients of the sphere. If one were to solve the equations for the case of two spheres then one could obtain information on the volume-fraction dependence of the diffusion coefficient. This was, in fact, done by Batchelor [37]. He found that for a dilute suspension of hard spheres the dependence of the short-time diffusion coefficient on the volume fraction ϕ is given by

$$D_s = D_0(1 - 1.83\phi), \tag{2.17}$$

where D_0 is the diffusion coefficient at infinite dilution (equation 2.1). Even though this is the lowest order correction to the dynamics to the diffusion coefficient, the actual derivation of equation 2.17 is non-trivial. If one could include more-particle interactions, one would obtain information about the following terms in the series expansion of equation 2.17. The first successful approach to this problem was developed by Beenakker and Mazur [38, 39]. It should be stressed that the success of the approach of refs. [38, 39] is due to the choices of the approximations made in the calculation of the higher-order hydrodynamic interactions. For more details see refs. [40, 41].

2.6 Lattice-Boltzmann method

In this section we outline the lattice Boltzmann method for simulation of colloidal suspensions. The lattice-Boltzmann model is a pre-averaged version of a lattice-gas cellular automaton (LGCA) model of a fluid. In lattice-gas cellular automaton the state of the fluid at any (discrete) time is specified by the number of particles at every lattice site and their velocity. Particles can only move in a limited number of directions (towards neighboring lattice points) and there can be at most one particle moving on a given 'link'. The time evolution of the LGCA consists of two steps - 1. Propagation: every particle moves in one time step, along its link to the next lattice site. 2. Collision: at every lattice site particles can change their velocities by collision, subject to the condition that these collisions conserve number of particles and momentum (and retain the full symmetry of the lattice). In the lattice-Boltzmann method (see e.g., ref. [14]) the state of the fluid system is no longer characterized by the number of particles that move in direction $\mathbf{c}_i$ on lattice site $\mathbf{r}$, but by the *probability* to find such a particle. The single-particle distribution function $n_i(\mathbf{r}, t)$, describes the average number of particles at a particular node of the lattice $\mathbf{r}$, at a time t, with the discrete velocity $\mathbf{c}_i$. The hydrodynamic fields, mass density ρ, momentum density $\mathbf{j}$, and the momentum flux density Π are simply

moments of this distribution

$$\begin{aligned} \rho &= \sum_i n_i, \\ \mathbf{j} &= \sum_i n_i \mathbf{c}_i, \\ \Pi &= \sum_i n_i \mathbf{c}_i \mathbf{c}_i. \end{aligned} \tag{2.18}$$

The lattice model used in this thesis is a three dimensional projection of the four dimensional Face-Centered Hyper Cubic (FCHC) lattice. The vectors spanning this lattice are given in table 2.1. A two dimensional model can be obtained by further projection.

i	1	2	3	4	5	6	7	8	9	10	11	12	13	14	15	16	17	18
c_{ix}	1	-1	0	0	0	0	1	-1	1	-1	1	-1	1	-1	0	0	0	0
c_{iy}	0	0	1	-1	0	0	1	-1	-1	1	0	0	0	0	1	-1	1	-1
c_{iz}	0	0	0	0	1	-1	0	0	0	0	1	-1	-1	1	1	-1	-1	1
c_i^2	1	1	1	1	1	1	2	2	2	2	2	2	2	2	2	2	2	2

Table 2.1 Velocity vectors used in the Lattice-Boltzmann model. For $i = 1, \ldots, 6$ the vectors are used twice in the simulation, due to the projection from the four dimensional Face-Centered Hyper Cubic (FCHC) lattice.

This FCHC model is used because three-dimensional cubic lattices do not have a high enough symmetry to ensure that the hydrodynamic transport coefficients are isotropic.

The time evolution of the distribution functions n_i is described by the discretized analogue of the Boltzmann equation [8]

$$n_i(\mathbf{r} + \mathbf{c}_i, t+1) = n_i(\mathbf{r}, t) + \Delta_i(\mathbf{r}, t), \tag{2.19}$$

where Δ_i is the change in n_i due to instantaneous molecular collisions at the lattice nodes. We now separate the distribution function into a local equilibrium part and a non-equilibrium part

$$n_i = n_i^{\mathrm{eq}} + n_i^{\mathrm{neq}} \tag{2.20}$$

If we demand that from the equilibrium part of the distribution function we recover the correct description of the fluid at the Euler level, i.e. non-dissipative hydrodynamics, then the required form of the moments of the velocity distribution are

$$\begin{aligned} \rho &= \sum_i n_i^{\mathrm{eq}}, \\ \mathbf{j} &= \sum_i n_i^{\mathrm{eq}} \mathbf{c}_i, \\ \Pi^{\mathrm{eq}} &= \sum_i n_i^{\mathrm{eq}} \mathbf{c}_i \mathbf{c}_i = p\mathbf{I}, \end{aligned} \tag{2.21}$$

with p the local pressure and Π^{eq} is the non-dissipative part of the momentum flux, $\mathbf{I}$ the unit tensor. The local equilibrium distribution can be expressed as a series in the flow velocity $\mathbf{u}$

$$n_i^{\mathrm{eq}} = \rho[a_0^{c_i} + a_1^{c_i}\mathbf{u}\cdot\mathbf{c}_i + a_2^{c_i}\overline{\mathbf{uu}} : \overline{\mathbf{c}_i\mathbf{c}_i} + a_3^{c_i}u^2], \tag{2.22}$$

where $\overline{\mathbf{uu}} = \mathbf{uu} - \frac{1}{3}u^2\mathbf{I}$ is the traceless part of $\mathbf{uu}$. If we combine equation 2.22 and equation 2.21, and supply a condition to guarantee isotropy [17], then we can solve for the coefficients in equation 2.22. The result of this is given in table 2.2. We have chosen

i	0	1	2	3
a_i^1	$\frac{1}{12}$	$\frac{1}{6}$	$\frac{1}{4}$	$\frac{1}{6}$
$a_i^{\sqrt{2}}$	$\frac{1}{24}$	$\frac{1}{12}$	$\frac{1}{8}$	$\frac{1}{12}$

Table 2.2 Coefficients used in equation 2.22.

the velocity of sound to be $c_{\mathrm{s}}^2 = \frac{1}{2}$ as this is the velocity of sound which maximizes the stability with respect to variations in fluid velocity [17].

Now that the local equilibrium part of the momentum flux tensor is known, we come to the relaxation of the non-equilibrium, or viscous part. The momentum flux density is updated according to

$$\Pi'_{\alpha\beta} = \Pi^{\mathrm{eq}}_{\alpha\beta} + (1+\lambda)(\overline{\Pi}_{\alpha\beta} - \overline{\Pi}^{\mathrm{eq}}_{\alpha\beta}) + \frac{1}{3}(1+\lambda_{\mathrm{B}})(\Pi_{\gamma\gamma} - \Pi^{\mathrm{eq}}_{\gamma\gamma})\delta_{\alpha\beta}, \tag{2.23}$$

where λ and λ_{B} relate to the shear and bulk viscosities

$$\eta = -\frac{1}{6}\rho(2/\lambda + 1). \tag{2.24}$$

In appendix A we show the calculation of the stress autocorrelation function, and how it can be related to the viscosity. The post-collision distribution, $n_i + \Delta_i(n)$, is determined by the requirement that the new probability densities are consistent with equation 2.18, thus

$$n_i + \Delta_i(n) = a_0^{c_i} + a_1^{c_i} j_\alpha c_{i\alpha} + a_2^{c_i}\Pi'_{\alpha\beta}\overline{c_{i\alpha}c_{i\beta}} + a_3^{c_i}(\Pi'_{\alpha\alpha} - \frac{3}{2}\rho). \tag{2.25}$$

The procedure to update the lattice Boltzmann equation consists of the following steps. First one calculates the moments ρ, $\mathbf{j}$, Π, and the equilibrium momentum flux Π^{eq}. This enables us to calculate the post-collision distribution, which is then propagated according to equation 2.19. Now that the update procedure for the lattice-Boltzmann equation is known, one needs to examine the macroscopic behaviour one obtains from it. This was discussed in ref. [17] where it was shown that the Navier-Stokes equations for an isothermal, compressible fluid are recovered.

If we want to study the motion of particles suspended in a lattice-Boltzmann fluid, we need to define a boundary surface, and the boundary condition, which is imposed on the surface of the particle. The motion of the colloidal particle is determined by

the force and torque exerted on it by the fluid. These are, in turn, the result of the boundary condition supplied at the fluid-solid interface. For a non-moving boundary a simple "bounce back" on the link leads to the stick boundary condition, with $\mathbf{v} = \mathbf{0}$ at the boundary. Implementation of the bounce-back rule is shown in figure 2.2. For a

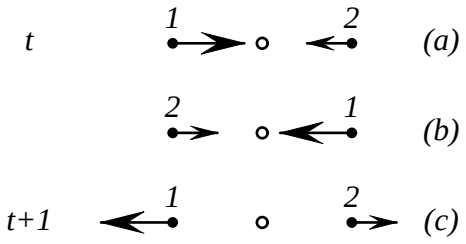

Figure 2.2 Implementation of the bounce back rule. The location of the boundary node is shown by an open circle, and the lattice points by closed circles. (*a*) Shows the densities n_1 and n_2 propagating in the direction of the boundary node. (*b*) Shows the intermediate step, where the densities are reversed. (*c*) Shows the propagated version of (*b*). In effect the densities have "bounced" of the boundary link.

moving boundary the boundary update needs to be modified. This leads to the modified bounce-back rule [17]. For a colloidal particle with linear and angular velocities of $\mathbf{u}$ and ω respectively, the local boundary velocity is just

$$\mathbf{u}_b(t) = \mathbf{u}(t) + \omega(t) \times \mathbf{r}_b, \tag{2.26}$$

where $\mathbf{r}_b$ is the vector connecting the center of the particle to the midpoint of the boundary link. The location of the boundary links is shown in figure 2.3. The force and the torque exerted by the fluid on each individual boundary link $\mathbf{F}_{ib}$ is given by

$$\mathbf{F}_{ib}(\mathbf{r}_b) = 2[n_{ib}(\mathbf{r}_b) - n_{-ib}(\mathbf{r}_b) - 4n_0(\rho)\mathbf{u}_b \cdot \mathbf{c}_{ib}]\mathbf{c}_{ib}, \tag{2.27}$$

where ib denotes the link connecting the inside to outside and $-ib$ its partner $n_0(\rho)$ is the zero velocity distribution. The total force and torque acting on the object are obtained by summing the forces over the links

$$\begin{aligned} \mathbf{F} &= \sum_{ib} F_{ib}(\mathbf{r}_b), \\ \mathbf{T} &= \sum_{ib} F_{ib}(\mathbf{r}_b) \times \mathbf{r}_b. \end{aligned} \tag{2.28}$$

If we now take the simplest discretized form of the equation of motion and define the time-step as unity, we calculate the new velocities

$$\begin{aligned} \mathbf{u}' &= \mathbf{u}(t+1) = \mathbf{u}(t) + \mathbf{F}/M, \\ \omega' &= \omega(t+1) = \omega(t) + \mathbf{T}/I, \end{aligned} \tag{2.29}$$

where M and I are the mass and the moment of inertia, respectively. Combination of the equations 2.26 - 2.29 define a possible method for updating the particle velocity [17].

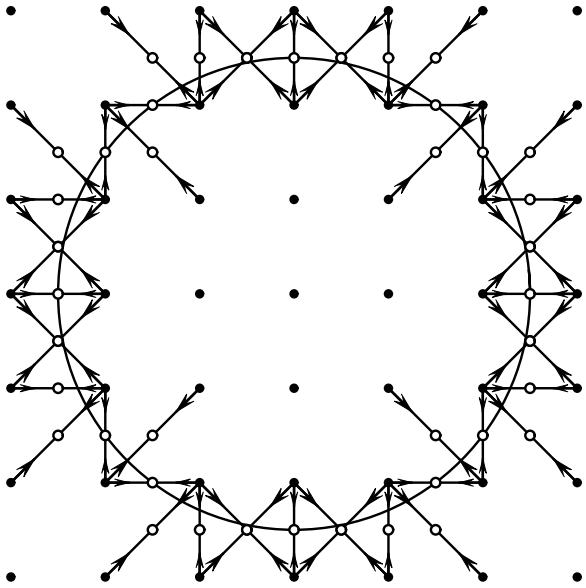

Figure 2.3 Location of the boundary nodes for a disk of radius 2.5 lattice spacings. The velocities along links cutting the surface are indicated by arrows. The locations of the boundary nodes are shown by open circles and the lattice nodes by solid circles.

However, using this scheme one matches the velocity of the fluid at the boundary with the "old" velocity of the particle, rather than the new velocity. This makes the equations of motion inherently unstable. In order to suppress this instability, the density of the particle must be chosen several times larger than the density of the fluid [17]. In contrast, if we match "new" velocity of the particle with the velocity at the boundary, the update rule is made self-consistent. This was first proposed by Lowe et al. [42]. With this approach it became possible to simulate particles with an arbitrary density ratio compared to the solvent (see ref. [42]).

The ability to simulate particles with an arbitrary density (ρ_{obj}) compared to the fluid density (ρ_{fluid}) facilitates the accurate determination of the velocity correlation function of the suspended particle. When $\rho_{\mathrm{obj}}/\rho_{\mathrm{fluid}} \approx 1$, the long-time tail in the velocity correlation function has to be taken into account [43]. A density ratio of order one is also appropriate when modelling "real" colloidal particles in suspension. In contrast, in the limit $\rho_{\mathrm{obj}}/\rho_{\mathrm{fluid}} \to \infty$ the exponentially decaying velocity correlation function is obtained.

In this thesis we use the dissipative method for the calculation of the diffusion coefficient. In this method we study the decay of an imposed initial velocity on the particle in an otherwise quiescent fluid. Correlating the initial velocity to with the subsequent velocity is according to Onsager's regression hypothesis, equivalent to calculation of the velocity correlation function in a "real" fluctuating system. In appendix B we show how the velocity correlation function can be related to the short-time diffusion coefficient.

3 Motion of a particle in a tube

3.1 Introduction

In order to investigate the dynamics of particles in confined media, we first focus on a simple geometry: a particle diffusing in a tube. A sketch of this system is given in figure 3.1. We focus on the short-time dynamics of the particle. A theoretical expression for the diffusion coefficient of a particle in the center of the tube has been derived by Bungay and Brenner [44]. In this theory the particle is assumed to diffuse along the direction of the tube. In the present chapter we focus on the following question: What is the dynamics of the particle diffusing in a tube? That is, we are interested in the short-time regime before the diffusion coefficient has reached its steady-state value. As in ref. [44], we shall study diffusion along the tube axis.

3.2 The velocity correlation function

In order to determine the velocity correlation function of a particle diffusing along the tube axis, we use the lattice-Boltzmann method as outlined in chapter 2 for neutrally buoyant particles. We impose a stick boundary condition at the wall of the tube (using the bounce-back rule described in the previous chapter). This ensures that the flow velocity vanishes on the tube boundary. We calculated the velocity correlation function of the particle by studying the decay of an initial velocity $v_x(0)$ of the particle in an otherwise quiescent fluid. In figure 3.2 we show the velocity correlation function of a colloidal particle with radius $r = 2.5$ lattice units in a tube with radius $R = 4.5$ lattice units. The time is expressed in dimensionless units $\tau = t\nu/r^2$. One might expect that the "hydrodynamic" long-time tail is suppressed, as the presence of the wall should lead to an exponential damping of vortices. This was indeed the conclusion reached by Bocquet and Barrat, in their analysis of the problem [45]. Surprisingly, we still observe a powerlaw decay of $C_x(t) \equiv < v_x(0)v_x(t) >$. In fact, we find that this quantity decays as $C_x(t) = -1/t^{3/2}$. This is qualitatively different from the behaviour expected for hydrodynamic tails (these algebraic tails are positive) and from single exponential decay. In order to check whether this behaviour is unique for the tube geometry, the

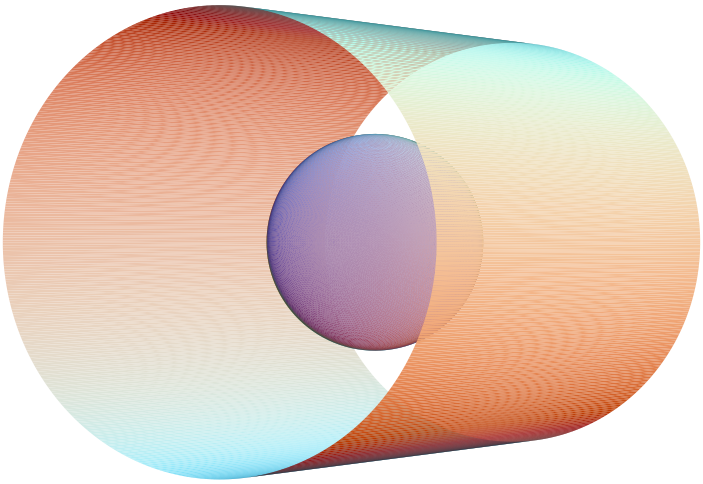

Figure 3.1 Particle in a (liquid-filled) tube.

calculation was repeated for a disk a two dimensional "tube". It was found that the decay of the velocity correlation function was the same $C_x(t) = -1/t^{3/2}$. Note that again this contrasts with the "normal" hydrodynamic tails which always depend on dimensionality. In order to clarify the origin of the long time tail we considered the long-time decay of a velocity perturbation in an initially quiescent fluid.

3.3 Theory

For simplicity, we discuss the two-dimensional case with an initial perturbation $\mathbf{v}(\mathbf{r}, 0) = (v_0\delta(\mathbf{r}), 0)$. The evolution of this disturbance is determined by the usual hydrodynamic equations

$$\frac{\partial \rho}{\partial t} + \rho_0 \nabla \cdot \mathbf{v} = 0, \tag{3.1}$$

and

$$\frac{\partial \mathbf{v}}{\partial t} + \alpha \nabla \rho - \nu \nabla^2 \mathbf{v} - \xi \nabla \nabla \cdot \mathbf{v} = 0, \tag{3.2}$$

where $\mathbf{v}(\mathbf{r}, t)$ and $\rho(\mathbf{r}, t)$ are the disturbance velocity and density field respectively, ρ_0 is the equilibrium density, ν the shear viscosity, ξ the bulk viscosity, and $\alpha = c^2/\rho_0$, with c the velocity of sound (for a three dimensional fluid, ξ in equation 3.2 is replaced by $\xi + \nu/3$). The stick boundary conditions should be supplemented to equations 3.1

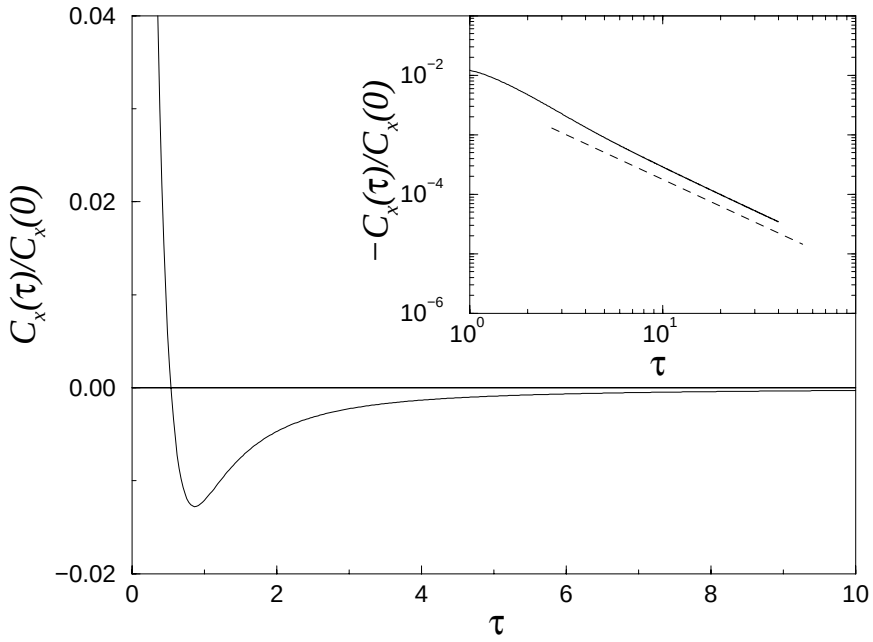

Figure 3.2 Normalized velocity correlation function $C_x(\tau)/C_x(0)$ of a colloidal particle with radius $r = 2.5$ in a cylindrical tube with radius $R = 4.5$ (drawn line). The dashed line denotes a line with $C_x(\tau) \sim -1/\tau^{3/2}$. The reduced time τ is defined by $\tau = t\nu/r^2$.

and 3.2. For the sake of the argument, we shall first focus on the asymptotic regime. In fact, we assume that at long times the transverse component of the velocity field has almost relaxed ($\partial_x v_x \gg \partial_y v_y$), and we retain the y-dependence of v_x. The solution of this problem reads, in Fourier space

$$\tilde{v}_x(k_x, k_y, \omega) = \frac{i\omega v_0}{-\omega^2 + i\omega(\Gamma k_x^2 + \nu k_y^2) + c^2 k_x^2}, \tag{3.3}$$

with $\Gamma = \nu + \xi$, the sound wave damping coefficient. Due to the anisotropy induced by the y dependence of the x component of the velocity, this equation shows that purely diffusive modes can be excited in the tube if $4c^2k_x^2 < (\Gamma k_x^2 + \nu k_y^2)^2$, implying that, for a fixed value of k_y, there will always be a k_x^* such that when $k_x < k_x^*$ only diffusive modes show up. In general, due to the fact that there exists a minimum k_y (because of the finite width of the tube), there will always exist a fraction of the sound modes that are overdamped and will behave diffusively. In the hydrodynamic regime ($k_x \to 0$) the modes in the system are

$$\begin{aligned} \omega_1 &\sim i\nu k_y^2 + i\left(\Gamma - \frac{c^2}{\nu k_y^2}\right) k_x^2 + \mathcal{O}(k_x^4), \\ \omega_2 &\sim i\frac{c^2}{\nu k_y^2} k_x^2 + \mathcal{O}(k_x^4). \end{aligned} \tag{3.4}$$

At small k_x, the first mode decays with a finite rate, determined by the minimum value of k_y. However, in the limit $k_x \to 0$, the ω_2 mode behaves as a diffusive hydrodynamic mode. The prefactor multiplying k_x^2 can be interpreted as an effective diffusion coefficient which characterizes the diffusion of density perturbations. It scales as

$$D^* \sim \frac{c^2 R^2}{\nu}, \tag{3.5}$$

where R is half the width of the channel. The possibility of exciting such overdamped sound modes has been discussed in ref. [46], where the hydrodynamics of a thin fluid layer in contact with a solid substrate is modelled as a 2-D fluid with an extra dissipation force accounting for the liquid-solid interaction. Recently, it has been argued that sound waves in fluid membranes may also be overdamped [47]. This suggests that the dynamics of particles embedded in such membranes will exhibit the same features as we discuss here.

The power-law characterizing the decay of this second mode can be obtained by transforming the velocity back to real space and time. An asymptotic analysis of this time decay leads to

$$v_x(t) \sim -\frac{v_0}{\sqrt{\nu} t^{3/2}} + \mathcal{O}(t^{-5/2}). \tag{3.6}$$

This is in agreement with the simulations of the two-dimensional system. An analogous analysis for the three-dimensional fluid between two plates shows that

$$v_x(t) \sim -\frac{v_0}{t^2} + \mathcal{O}(t^{-3}). \tag{3.7}$$

The derivation considers a fluid element, but the result should not depend on the specific way the momentum has been introduced - it only depends on the amount of momentum that is inserted. By changing the viscosity of the fluid, we could also verify that the tails scale with viscosity as predicted by equations 3.6 and 3.7.

3.4 Diffusion of sound

In order to investigate the diffusive decay of sound, predicted by equation 3.5, we performed a simulation in which we actually measured this effective diffusion constant. To do this, we increased the density of the fluid at a point in the center of a two dimensional slit, and computed the second moment of the evolving spatial density distribution. The diffusion coefficient was obtained by differentiation $D^* = \frac{1}{2}\frac{d}{dt}\langle r^2(t)\rangle$. The diffusion coefficient is plotted in figure 3.3, as a function of the kinematic viscosity. By varying the channel width and the viscosity, we find

$$D^* = \frac{c^2(R^2 - 1/4)}{3\nu} + \frac{1}{2}, \tag{3.8}$$

which is in agreement with equation 3.5 (except for the factors of $-1/4$ [17] and $1/2$ [48] which are, in fact, lattice artifacts).

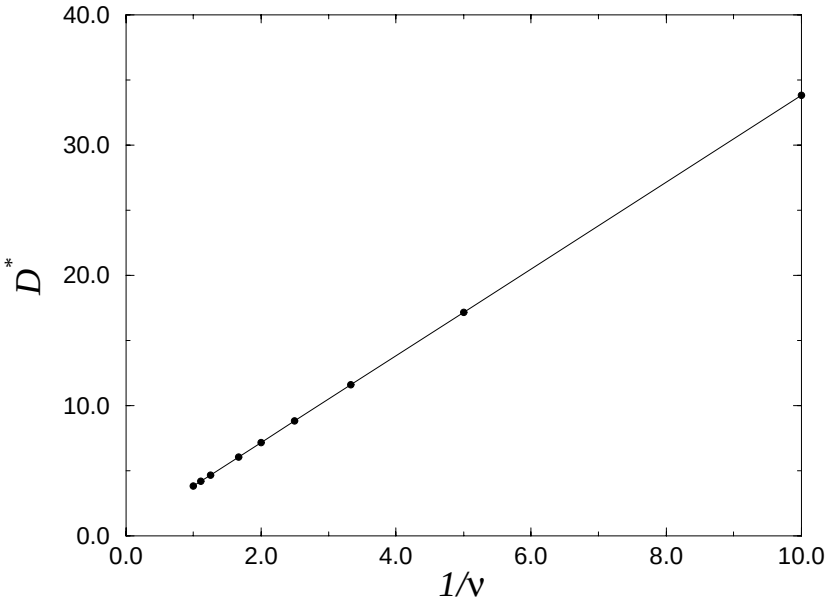

Figure 3.3 The effective diffusion coefficient of density perturbations D^* as a function of $1/\nu$, where ν is the dimensionless kinematic viscosity. Results were obtained in a two dimensional slit of half width $R = 4.5$. The points denote the simulation results, and the line is a guide to the eye.

This analysis allows us to give a more intuitive picture for the appearance of the negative algebraic decay. The initial motion of the particle in the tube sets up a density dipole in the fluid. If we consider that only overdamped modes are present in the system, this density dipole will decay diffusively

$$\rho(x,t) = \frac{x \exp\left(-x^2/4D^*t\right)}{\sqrt{4\pi(D^*t)^3}}, \tag{3.9}$$

where x is the distance from the particle along the tube and the density profile in the transverse direction is essentially flat. This leads to a mass flux around the origin which is proportional to the gradient in density $j(0,t) \sim -\partial_x \rho(0,t)$. The motion of the particle (or fluid element) that caused the initial dipole, will (at long times) be slaved to this mass flux and the velocity of the particle will be $v(t) \sim -1/t^{3/2}$. For the particle diffusing between two plates (in three dimensions), the diffusion of the density will be two-dimensional, and, arguing along similar lines, we find $v(t) \sim -1/t^2$. This shows that the long-time tail is driven by a diffusive pressure relaxation mechanism. We argue that this phenomenon is general and that

$$C_x(t) \sim -\frac{1}{t^{1+d^*/2}}, \tag{3.10}$$

where d^* is the number of dimensions that are not geometrically confined. In table 3.1 we list the value of d^* for some simple geometries. We also considered a colloidal particle

geometry	d^*
sphere in tube	1
disk between two walls	1
sphere between two plates	2

Table 3.1 Relation between geometry and number of directions which are not geometrically confined.

diffusing between regular rectangles as sketched in figure 3.4. We found that first the diffusion was in accordance with $d^* = 1$, but at longer times there was a changeover to behaviour with $d^* = 2$. This suggests that for diffusion in a three dimensional array of "bricks", we might expect to observe a changeover from $d^* = 2$ to $d^* = 3$.

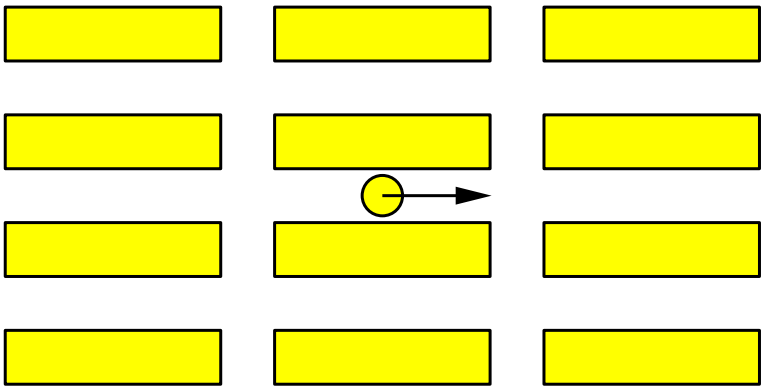

Figure 3.4 Colloidal particle in a regular simple geometry.

The requirement for finding the behaviour in equation 3.10 is that sound modes are overdamped in the geometry. The result in equation 3.10 differs from the velocity correlation function predicted by Bocquet and Barrat [45], who used a mode-coupling approach [2], in which the coupling of velocity with sound at long times was not taken into account. We also note that the form of velocity correlation function that we observe is the same as that found in a purely diffusive system - the Lorentz gas [5]. The physical origins of the two effects are, however, quite different.

3.5 Flow field in the tube

In this section we focus on the features of the flow, vorticity and density fields for a particle diffusing along the axis of the tube. We used the lattice spacing of the lattice-Boltzmann model as our unit of length, and the lattice-Boltzmann time step as our unit of time. The simulation are of a neutrally buoyant sphere of radius $r = 2.5$ lattice units in the center of tube of radius $R = 8.5$ lattice units. The kinematic shear viscosity was

set equal to $\nu = 1/6$. The simulation was performed with stick boundary condition at the wall and a colloidal particle with (initially) a velocity in the positive x direction. The system size was big enough to exclude finite system size effects. The fluid is initially at rest. In figure 3.5 we show the normalized velocity correlation function $C_x(t)/C_x(0)$. The total simulation time corresponds to $\tau \approx 10$. The flow, vorticity and density fields

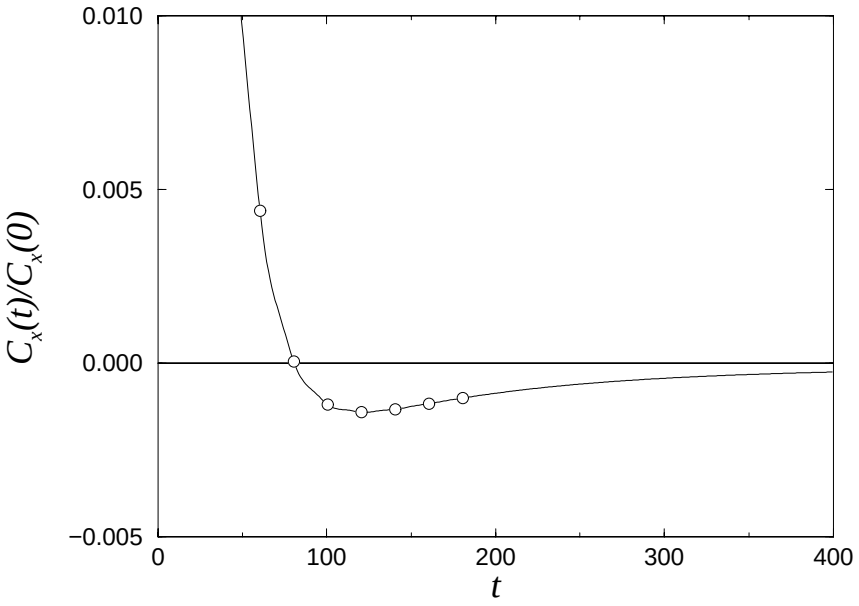

Figure 3.5 Normalized velocity correlation function. The times for which we show the flow, vorticity and density fields are indicated by the open circles. The open circles for $t = 20$ and $t = 40$ are off scale.

depend on the three spatial coordinates. The fields are examined in the $z = 0$ plane. The velocity field and density are directly calculated in the lattice-Boltzmann scheme. The vorticity, ω, at a lattice point (x, y), which is a local quantity is given by

$$\omega(x,y) = \frac{1}{2}\big(v_y(x+1,y) - v_x(x,y+1) - v_y(x-1,y) + v_x(x,y-1)\big). \quad (3.11)$$

This is a two dimensional discretisation of $\omega = \nabla \times \mathbf{v}$, the three dimensional definition of vorticity. The time evolution of the various fields is shown in figures 3.6 - 3.14.

In figure 3.6 we see that the velocity field initially contains the vortex pair that is responsible for the positive long-time tail in the velocity correlation function for an unbounded fluid. Vortices creeping at the wall of the tube are also seen. The density field displays a rather complex behaviour. The most salient feature is that the density in front of the particle is higher than at the back. In figure 3.7 we see that the vortex near the particle is already moving closer to the particle, and again vortices are seen spreading at the wall. In figure 3.8 it is seen that the vortices propagating near the

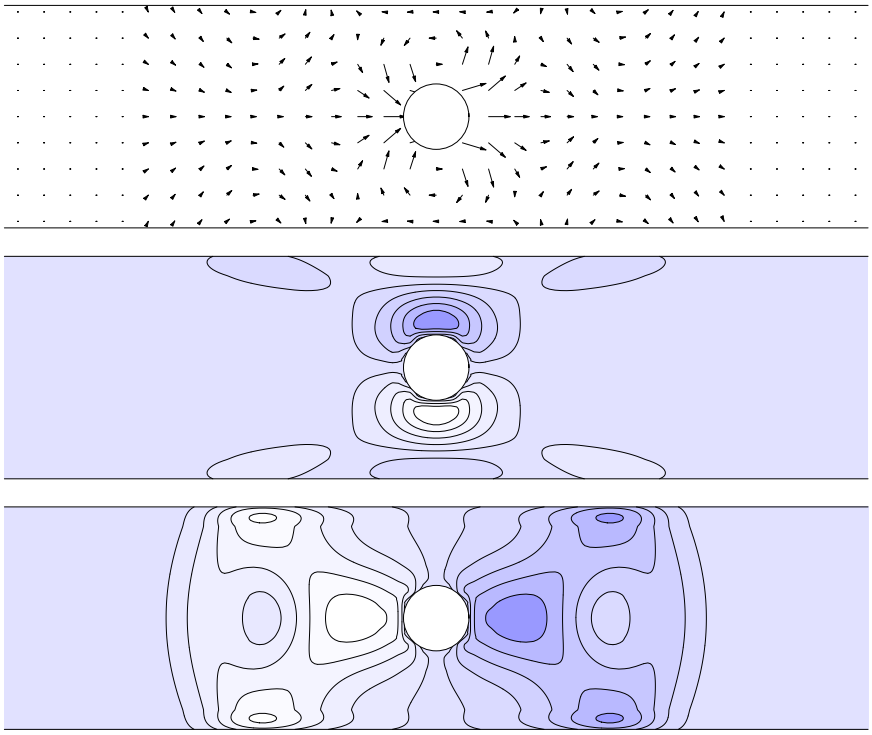

Figure 3.6 Flowfield, vorticity and density, from top to bottom, respectively ($t = 20$). The velocity field, which is at the top, is scaled with $s = \text{Max } v_x$ in the x direction, whereas for the y direction $4s$ is used to scale the arrows. For the sake of clarity one half of the velocity vectors in both directions are omitted from the picture. The vorticity field is obtained by applying equation 3.11 to the velocity field, and is shown in the middle. It is scaled such, that ten iso-vorticity lines are shown, at heights which vary linearly between the maximum and minimum vorticity. The largest vorticity is depicted by the darkest colour. The same procedure was performed for the density, the bottom picture.

wall have moved outside the observation window. The density plot indicates that in front of the particle there is a sizeable density increase. In figure 3.9 we see a clear change in behaviour for the flow field, compared with earlier pictures. Near the particle we see that over an appreachable area, the velocity in the x direction is *negative*. At this moment the velocity correlation function of the colloidal particle changes sign (see figure 3.5). In the next figure, figure 3.10 we see that the area of the flow field where the x component of the velocity is negative has grown. Due to the back flow around the particle, the vortices near the colloidal particle have almost disappeared. From here on (figures 3.11 - 3.14) we see that the negative flow field keeps growing in size, at the end spanning the total plotted region. The velocity field resembles the Poiseuille flow field for these times, which is the parabolic steady state flow profile for flow in a tube, with a pressure drop. As time progresses, the density field becomes more one-dimensional.

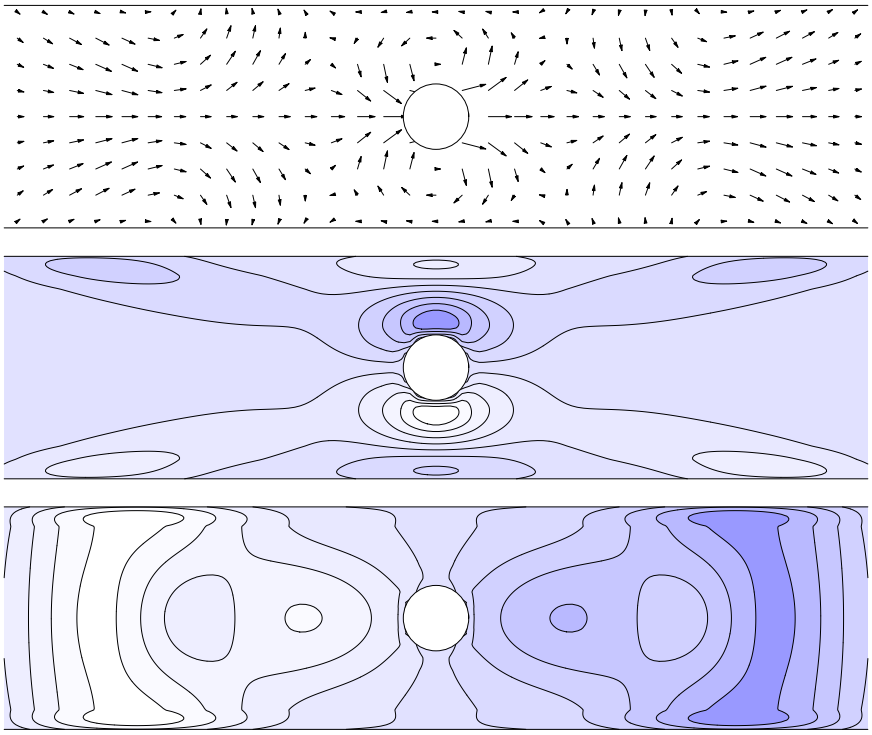

Figure 3.7 $t = 40$, for caption see figure 3.6.

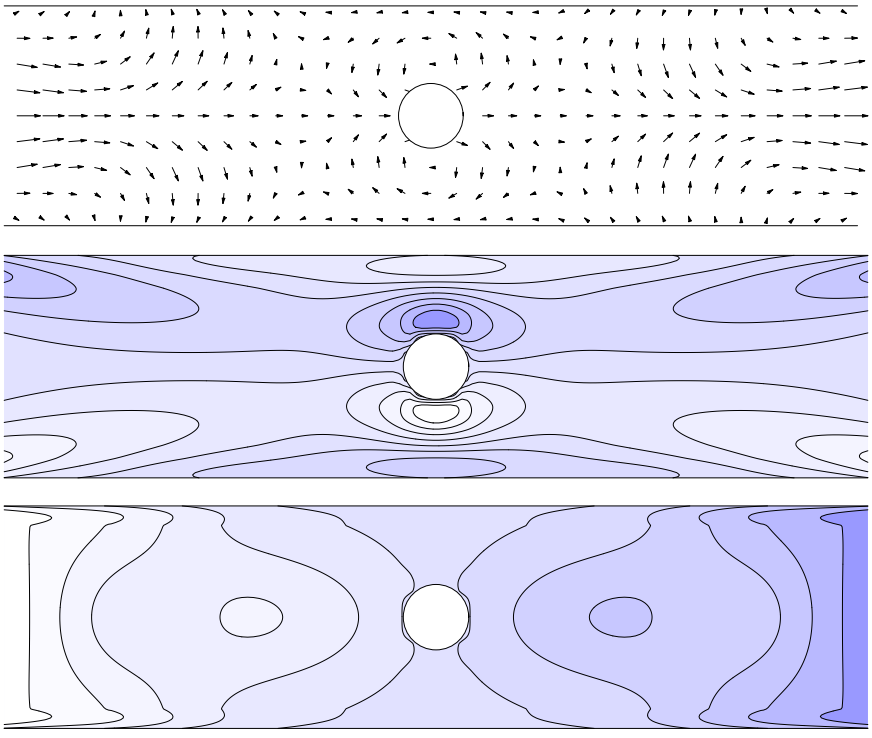

Figure 3.8 $t = 60$, for caption see figure 3.6.

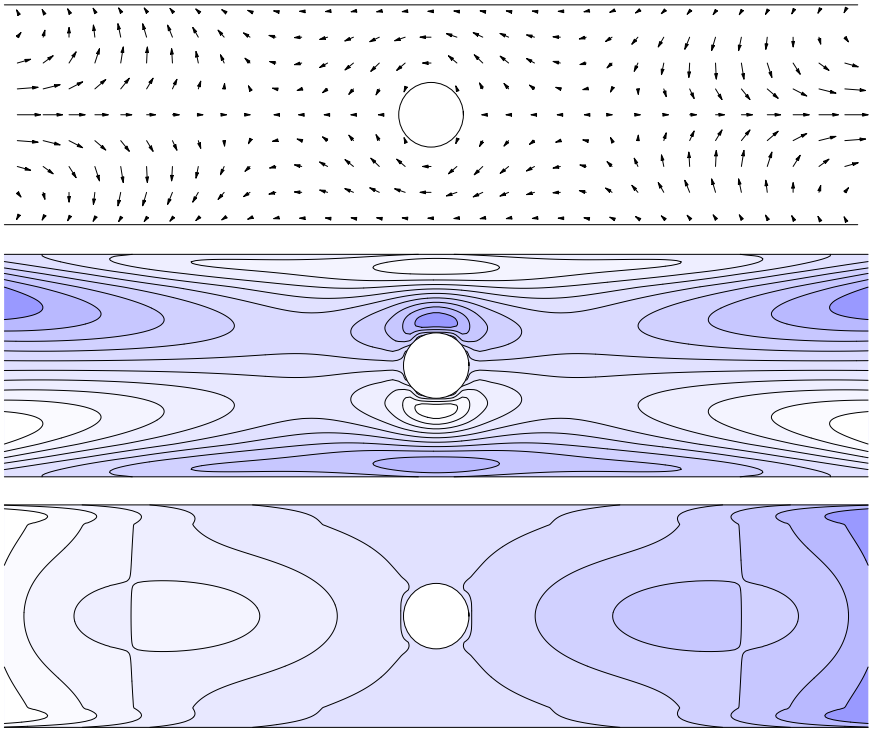

Figure 3.9 $t = 80$, for caption see figure 3.6.

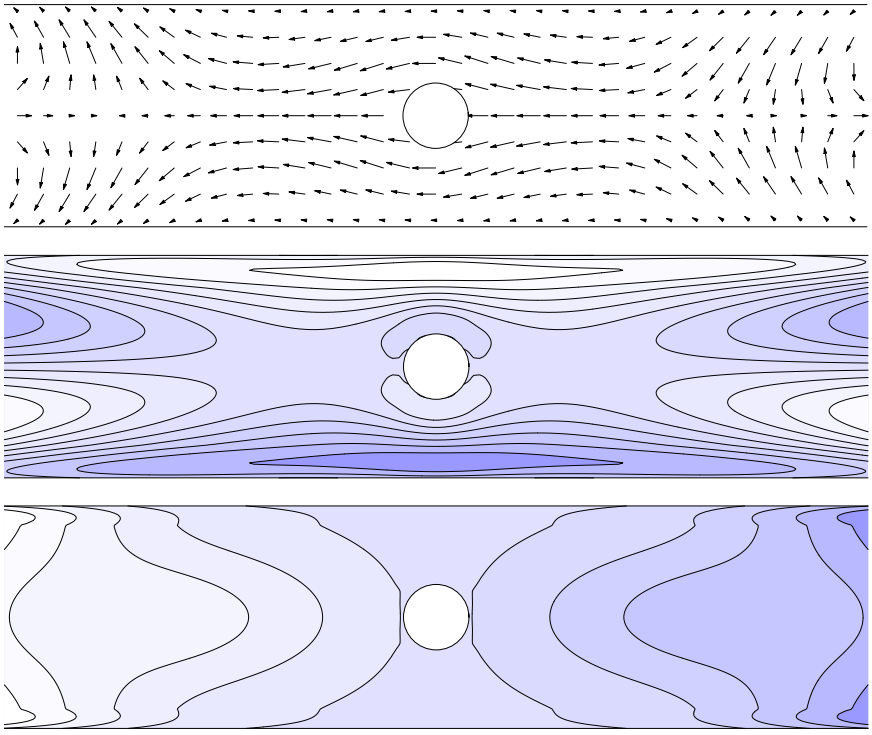

Figure 3.10 $t = 100$, for caption see figure 3.6.

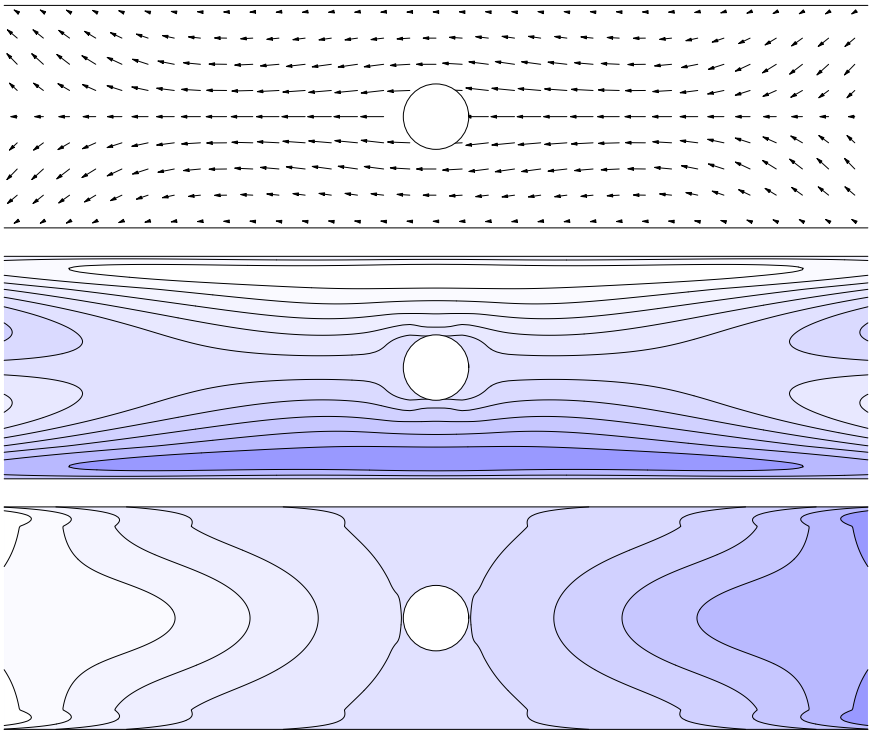

Figure 3.11 $t = 120$, for caption see figure 3.6.

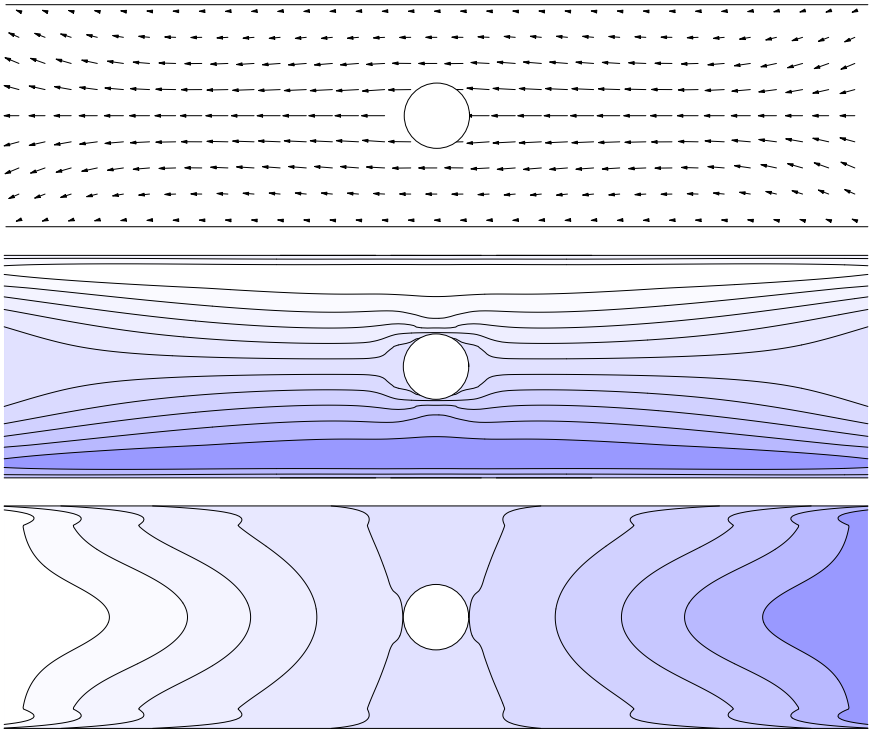

Figure 3.12 $t = 140$, for caption see figure 3.6.

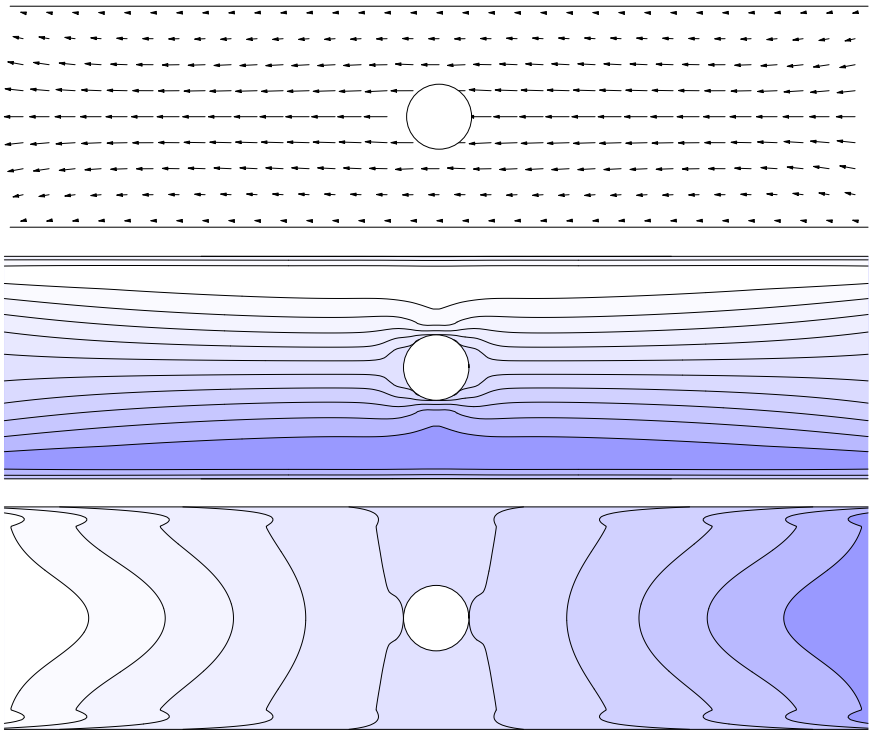

Figure 3.13 $t = 160$, for caption see figure 3.6.

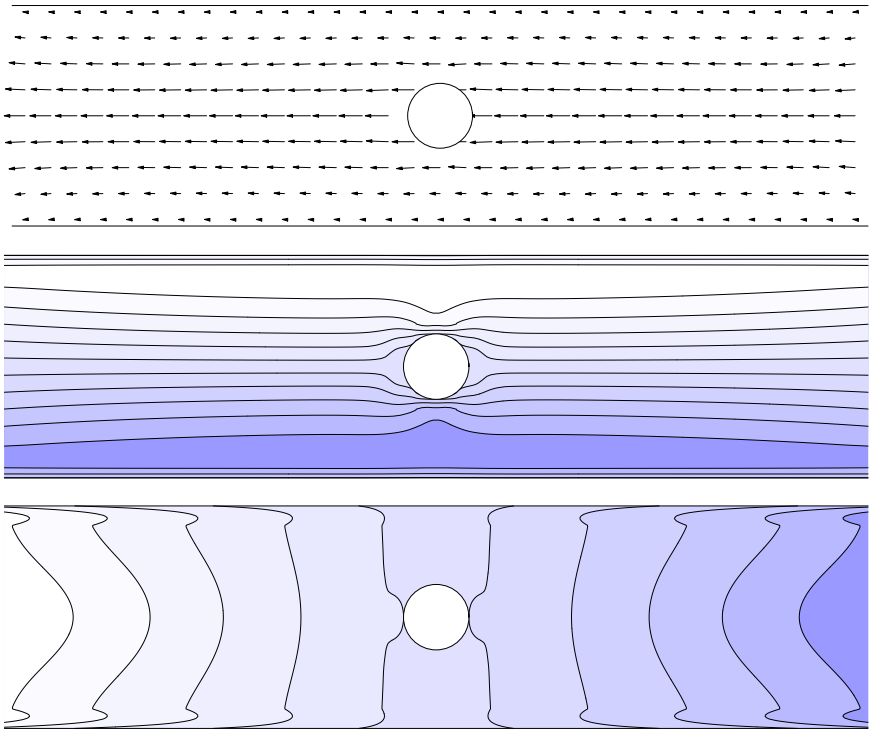

Figure 3.14 $t = 180$, for caption see figure 3.6.

3.6 Diffusion coefficient

By integrating the velocity correlation function we can calculate the diffusion coefficient for a particle in a tube to see whether this long-time tail contributes to the diffusion coefficient. The results, normalized by D_0, the diffusion coefficient in the absence of the tube, are shown in figure 3.15. Also plotted is the center-line approximation [44], calculated assuming a purely *incompressible* fluid (neglecting sound effects). The simulations yields the same diffusion coefficient as predicted by the theory for incompressible fluids. In fact, this is not surprising, because the long-time tail originates from the compressible modes. These modes do not affect the integral of the velocity correlation function - the contribution from equation 3.3 vanishes in the limit $\omega \to 0$. The diffusion coefficient is determined by the decay of transverse velocity perturbations [45, 49] which, in a confined system, is exponential. So, whilst compressibility effects dominate the long-time dynamics, they still do not contribute to the diffusion coefficient. Experimentally, one

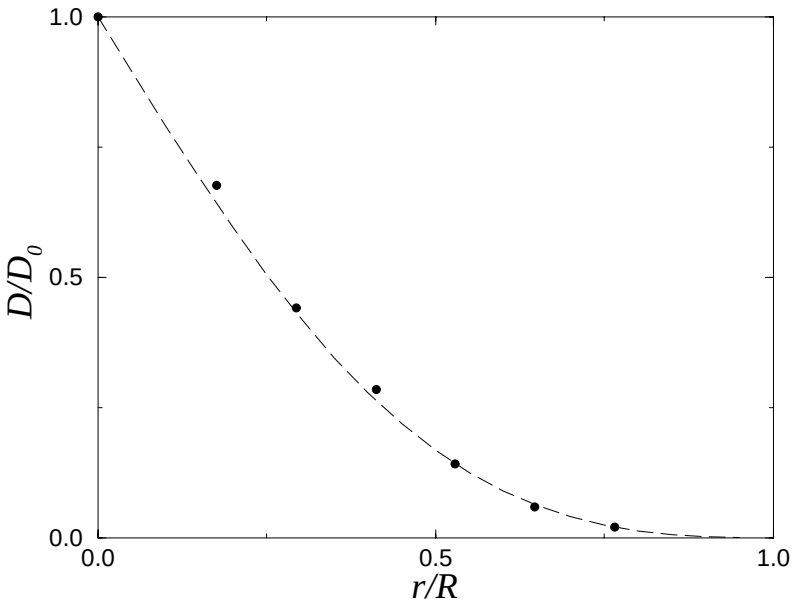

Figure 3.15 Normalized diffusion coefficient of a particle with radius r in the center of a cylindrical tube with radius R. The points denote simulation results, and the line corresponds to the center-line approximation (ref. [44]).

can expect to observe the long-time tail most easily if all the modes are overdamped, that is, when $k_y^2 > \frac{2c}{\nu}k_x$. If we consider a colloidal particle of radius r in a cylindrical tube of radius R and length L, this condition is satisfied if

$$\left(\frac{r}{R}\right)^2 > \frac{4}{\pi}\frac{cr}{\nu}\frac{r}{L}. \tag{3.12}$$

If we consider $\frac{r}{L} \sim 10^{-4}, \frac{r}{R} \sim \frac{1}{3}$, for water ($c \approx 1.5 \times 10^5$ cm/s, $\nu \approx 10^{-2}$ cm^2/s) we obtain the restriction that $r < 5 \times 10^{-5}$ cm, which is reasonable for colloidal particles. For a more viscous fluid, such as olive oil, the estimate is $r < 5 \times 10^{-3}$ cm. Here we considered a single particle in a tube, but, if particle-particle interactions within the pore are small compared with particle-wall interactions, the analysis also holds for a suspension of colloidal particles. A rough estimate of the appropriate volume fraction, ϕ, for which such condition is satisfied is given in ref. [34]: $\phi < \frac{2}{3}\frac{r}{R}$, with ϕ the solute volume fraction in the pore.

3.7 Conclusions

In conclusion, the simulations show that the velocity correlation function of a colloidal particle in a fluid confined by rigid walls displays a negative long-time tail. The mode-coupling analysis suggests that the mechanism driving the long-time tail is the diffusive decay of density perturbations. At long times, sound modes do not couple to the motion of a particle in an unbounded fluid - in a confined fluid this coupling is the dominant effect. We expect the same effect to be present for a molecular or atomic fluid confined between rigid walls, because the "colloidal" nature of the particle is not taken into account in the mode-coupling analysis.

4 Rotational diffusion coefficient of colloidal particles

4.1 Introduction

When studying the rotational diffusion coefficient of hydrodynamically interacting spheres, the dynamical correlation function that we should consider is the angular velocity correlation function. The expression for the rotational diffusion coefficient of a single sphere in an unbounded fluid was first given by Debye [36]

$$D_0^R = k_{\mathrm{B}}T/(8\pi\eta R^3), \tag{4.1}$$

where k_{B} is the Boltzmann constant, T is the absolute temperature, η the shear viscosity, and R the radius of the sphere. Degiorgio et al. [50] measured the rotational diffusion in concentrated colloidal dispersions of hard spheres by performing depolarized dynamic light scattering. In 1991 Clercx and Schram [51] gave an expression for the grand mobility matrix for a suspension of hydrodynamically interacting spherical particles. By taking into account two-particle interactions they found

$$D^R = D_0^R(1 - 0.63\phi - 1.02\phi^2), \tag{4.2}$$

where ϕ is the volume fraction. Later, by inclusion of three particle interactions, they derived [52]

$$D^R = D_0^R(1 - 0.63\phi - 0.74\phi^2). \tag{4.3}$$

Earlier Jones [53] had extended the generalized Smoluchowski equation to describe the diffusional relaxation of position and orientation in a suspension of interacting spherical colloidal particles. The one and two body cluster contributions were studied explicitly at short times. Working up to first order in volume fraction ϕ Jones found

$$D^R = D_0^R(1 - 0.63\phi). \tag{4.4}$$

The 1995 paper of Degiorgio et al. [50] reported an experimental and theoretical study of the rotational diffusion in concentrated colloidal dispersions of hard spheres. In their theoretical analisys, Degiorgio et al. considered the density dependence of the rotational diffusion coefficient they derived up to the ϕ^2 term. Again starting from the generalized

Smoluchowski equation

$$D^R = D_0^R(1 - 0.630\phi - 0.67\phi^2). \tag{4.5}$$

A fit to their experimental data gave [50]

$$D^R = D_0^R(1 - 0.55\phi - 1.1\phi^2). \tag{4.6}$$

Recently Kanetakis et al. [54] measured by nuclear magnetic resonance pulse experiments the rotational diffusion coefficient up to $\phi = 0.504$. A fit to their results is [54]

$$D^R = D_0^R(1 - 0.63\phi - 0.93\phi^2). \tag{4.7}$$

Clearly, the different theories only agree to leading order in ϕ. The aim of the present chapter is to study the ϕ dependence of D^R numerically. This chapter is structured as follows. First we describe the model that we have used to simulate the colloidal suspension. We then present the results of the simulations. Finally we conclude by comparing our results with the available theories and the experimental results.

4.2 Simulation method

We measured the angular velocity correlation function using the lattice-Boltzmann method as outlined in chapter 2. Non-overlapping randomly distributed solid spheres in a stationary lattice-Boltzmann fluid were all given an impulsive angular velocity $\omega_j(0)$ from a Maxwell-Boltzmann distribution. We computed the angular velocity correlation function by correlating the initial perturbation of the angular velocity with the angular velocity at some later time t

$$C_\omega(t) = \frac{1}{3}\left\langle \frac{1}{N}\sum_{j=1}^{N} \omega_j(0)\cdot\omega_j(t)\right\rangle, \tag{4.8}$$

with $\omega_j(t)$ the angular velocity of sphere j, and N is the total number of spheres. From this angular velocity correlation function (AVACF) one can compute the time-dependent rotational diffusion coefficient

$$\frac{D^R(t)}{k_\mathrm{B}T} = \frac{\int_0^t C_\omega(\tau)\mathrm{d}\tau}{IC_\omega(0)}, \tag{4.9}$$

where I is the moment of inertia of the sphere. In the limit $t \to \infty$, the rotational diffusion coefficient is obtained from

$$D^R = \lim_{t\to\infty} D^R(t). \tag{4.10}$$

In the previous equation we considered the limit $t \to \infty$ because in this limit the rotational diffusion coefficient has reached its asymptotic value. However, there are theoretical predictions [55, 56] that the AVACF has a long time tail $C_\omega(t) \sim t^{-5/2}$. A full description for the hydrodynamic theory of the angular velocity autocorrelation function of a single sphere was given by Berne [57]. The angular velocity correlation

function implies that $D^R(t) = A - Bt^{-3/2}$ at long times. Knowledge of this functional form will enable us to perform the extrapolation in equation 4.10. The explicit long-time behavior of the AVACF for a single sphere is given by [55, 56]

$$C_\omega(t) = C_\omega(0)\frac{\pi I}{\rho}\left(4\pi\nu t\right)^{-5/2}, \tag{4.11}$$

where I is the moment of inertia. The long-time tail in a suspension has the same exponent as for the case of the single sphere in a fluid. This is so because, at long times, a suspension behaves as a neat fluid, but with a different viscosity. At low volume fractions the viscosity η of the suspension is given by the Einstein result $\eta = \eta_0(1+\frac{5}{2}\phi)$, where η_0 is the solvent viscosity.

4.3 Results

Having set up the stationary lattice-Boltzmann fluid, we followed the time evolution of angular velocity correlation function of the suspended particles. In all simulations the viscosity ν of the fluid was equal to $\frac{1}{6}$ and the density ρ was 24 (all quantities are given in lattice units, where the mass of the lattice-gas particles, the lattice spacing and the time step are all unity). The density of the solid spheres was always equal to the density of the lattice Boltzmann fluid.

In order to obtain the normalized rotational diffusion coefficient (D^R/D_0^R) one also needs to determine D_0^R. D_0^R is measured by integrating the AVACF of a single sphere in a stationary lattice-Boltzmann fluid. The single particle rotational diffusion coefficient D_0^R gives a measure of the hydrodynamic radius of the colloidal particle. To this end we compare with the measured value of D_0^R with the Debye value $D_0^R = I/(8\pi\eta R^3)$, where I is the moment of inertia of the colloidal particle. For a sphere of radius $R = 4.5$ (lattice units) the hydrodynamic radius was found to be only 1.5% larger than the nominal radius. In what follows the difference between the nominal and hydrodynamic radius will be neglected. The normalized angular velocity correlation function together with the theoretical prediction for the asymptotic behaviour (equation 4.11) are shown in figure 4.1. As we can see from the figure the simulation results are compatible with both the functional form and the amplitude predicted by theory.

For the suspensions we generated non-overlapping hard sphere configurations at the desired volume fraction by using standard Monte Carlo simulations [19]. In the measurement of the angular velocity auto-correlation function, we also averaged over independent hard sphere configurations. The simulations were performed for volume fractions $\phi = 0.05$, 0.10,. . . ,0.45, 0.49, 0.55. The highest two densities are those of the coexisting phases of the hard sphere model at melting [58]. The last ($\phi = 0.55$) case is the FCC-solid. For the simulations at low densities ($\phi < 0.3$) many small spheres were simulated. When the volume fraction of spheres increases (at constant N) the interparticle distances

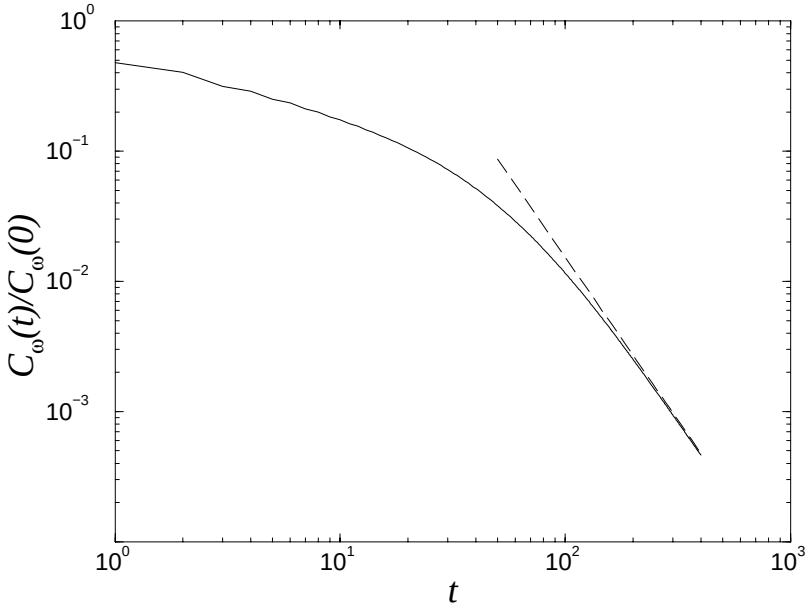

Figure 4.1 Normalized angular velocity correlation function for a single suspended sphere of radius $R = 4.5$ (lattice units). Time is expressed in units of the discrete time step used in the lattice model. The drawn line denotes the simulation result, the dashed line denotes the theoretical long-time behavior, equation 4.11.

(compared to the radius R of the particle) decreases. In order to correctly model the hydrodynamics there must be at least one layer of fluid nodes must be in between two neighbouring spheres. So, at higher volume fraction larger spheres were required. At $\phi = 0.55$ spheres with a radius as large as $R = 13.5$ (lattice units) were used. This puts an upper limit on the number of spheres used in the simulations at high volume fraction. For all solid volume fractions listed above, the normalized angular velocity auto correlation function ($C_\omega(t)/C_\omega(0)$) was determined. From $C_\omega(t)$, $D^R(t)$ was computed, using equation 4.9. The limiting value $D^R(\infty)$ was measured by plotting D^R as a function of $1/t^{3/2}$. The intercept at $1/t = 0$ yields the desired rotational diffusion coefficient. Extrapolation was done by fitting a quadratic function of $t^{-3/2}$ to $D^R(t)$. Note that this quadratic fit has no physical meaning, as $D^R(t)$ is *not* of the form $A + Bt^{-3/2} + Ct^{-3}$ In table 4.1 we show the simulation settings and results for all simulated suspensions. In figure 4.2 we plot D^R/D_0^R as a function of ϕ. In the same figure, we also show the experimental data of Degiorgio et al. [50] and the fit to the data by Kanetakis et al. [54] and virial expressions given by equations 4.3 [52] and 4.5 [50]. For the solid at $\phi = 0.55$, we also investigated the effect of the interparticle separations on the rotational diffusion coefficient. To do so, we prepared the colloidal suspension as follows: $N = 108$ spheres were placed on a regular (not thermally equilibrated) FCC lattice. We found that in this

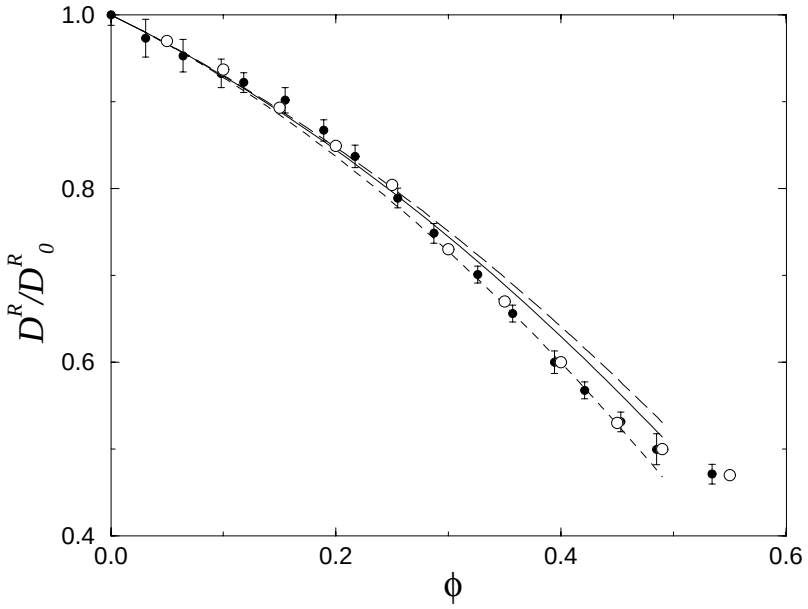

Figure 4.2 Rotational diffusion coefficient as a function of volume fraction. The open circles are the simulation results, whereas the filled circles with error bars are the experimental obtained values [50] the drawn curve is equation 4.5, the dashed curve is equation 4.3 and the dotted curve is the equation 4.7.

ϕ	R	N	D_0^R	D^R	D^R/D_0^R
0.05	2.5	1320	2.5	2.43	0.97
0.10	2.5	2640	2.5	2.34	0.94
0.15	4.5	679	8.1	7.23	0.90
0.20	4.5	905	8.1	6.88	0.85
0.25	4.5	1132	8.1	6.48	0.80
0.30	6.5	216	16.9	12.4	0.73
0.35	5.5	108	12.1	8.12	0.67
0.40	5.5	108	12.1	7.26	0.60
0.45	9.5	108	36.1	19.13	0.53
0.49	12.5	108	62.5	31.25	0.50
0.55	13.5	108	72.9	34.26	0.47

Table 4.1 Simulation settings and results, ϕ is the solid volume fraction, R is the radius of the spheres, N is the number of spheres, D_0^R is the single sphere rotational diffusion coefficient, D^R is the rotational diffusion coefficient at the specified setting and D^R/D_0^R is the normalized rotational diffusion coefficient.

system D^R/D_0^R was equal to 0.59. This is very different from the value of D^R/D_0^R for the equilibrated lattice, where D^R/D_0^R was equal to 0.47. So even, at constant volume fraction, the interparticle distances have an effect on the rotational diffusion coefficient. When close contacts are eliminated, the rotational diffusion coefficient is increased. This

situation might occur if the colloidal spheres have the long-ranged repulsive interactions found in charged systems. At lower volume fractions we also investigated the rotational diffusion coefficient for colloidal particles placed on a regular FCC lattice. The results of this simulation are shown in figure 4.3. Very recently Watzlawek and Nägele [59] studied

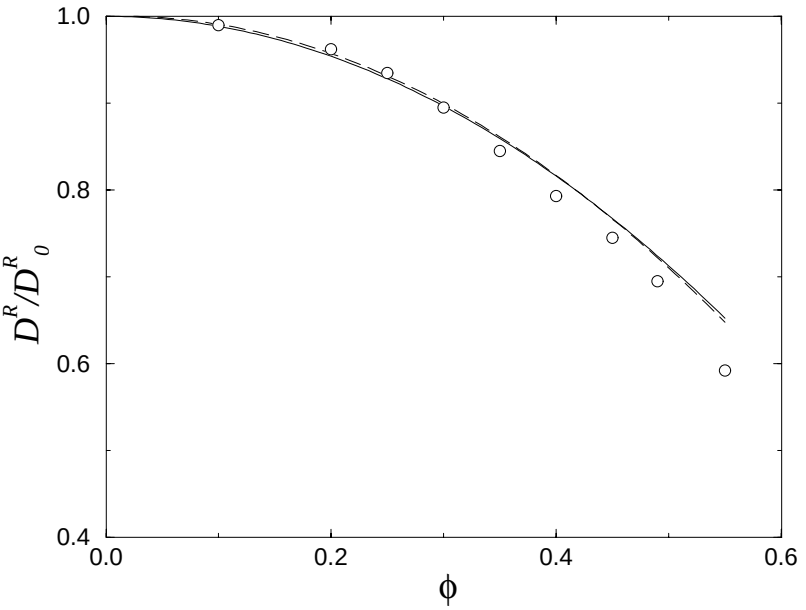

Figure 4.3 Rotational diffusion coefficient as a function of volume fraction for spheres placed on a regular FCC lattice. The open circles are the simulation results. The drawn line is equation 4.12 and the dashed line is equation 4.13.

the rotational diffusion coefficient for charged-stabilized particles. In contrast to hard sphere suspensions, charged stabilized systems have pronounced structure even at low densities. Watzlawek and Nägele fitted their data for D^R of charged colloidal particles in a deionized suspension to an expression of the form

$$D^R = D_0^R(1 - 1.15\phi^2), \tag{4.12}$$

for $\phi < 0.25$. When we fit our numerical data for D^R to a polynomial in ϕ ($\phi \leq 0.30$), we find

$$D^R = D_0^R(1 + 0.03\phi - 1.22\phi^2). \tag{4.13}$$

The most striking feature of equation 4.13 is that the prefactor of the linear term is small (and positive, which is unphysical), and our data are thus best described by a polynomial that contains no term linear in ϕ.

4.4 Conclusions

We computed the short-time rotational diffusion coefficient of a colloidal suspension of spheres. For the AVACF of a single particle, the amplitude and power of the long time tail are in agreement with theory. We find that the rotational diffusion coefficient are in agreement with available theories and experiment for low ($\phi < 0.3$) volume fractions. Above ($\phi = 0.30$) there is *only* agreement with experiment. This suggests that the theories could be improved by inclusion of higher order ϕ-terms in the virial expansion. With respect to the experiment, the agreement is excellent over the entire volume fraction range which has been studied. In our simulation we assumed that the spheres were smooth, and the the only interaction between the spheres was the hydrodynamic interaction. This was justified by the agreement of the simulation results with te experimental data. We have also computed the rotational diffusion coefficient for spheres placed on a regular FCC lattice. In that case, the linear term in the volume-fraction depence for D^R was found to be absent.

5 Non-Fickian diffusion in colloidal glasses

5.1 Introduction

Most theoretical treatments for problems involving mass transport are based on the classical diffusion equation

$$\frac{\partial}{\partial t}p(\mathbf{r},t) = D\nabla^2 p(\mathbf{r},t). \tag{5.1}$$

It describes the temporal evolution of the probability density at a position $\mathbf{r}$, $p(\mathbf{r},t)$, for the material undergoing transport, in terms of a single coefficient, the diffusion constant D. Two steps are required to arrive at this result. Firstly there is an *exact* relation between the microscopic current density $\mathbf{j}(\mathbf{r},t)$ and the probability density

$$\frac{\partial}{\partial t}p(\mathbf{r},t) = -\nabla\cdot\mathbf{j}(\mathbf{r},t). \tag{5.2}$$

This is the continuity equation and follows directly from the microscopic equations of motion. Secondly, there is the constitutive relation between $\mathbf{j}(\mathbf{r},t)$ and $p(\mathbf{r},t)$ which, according to Fick's law, is

$$\mathbf{j}(\mathbf{r},t) = -D\nabla p(\mathbf{r},t). \tag{5.3}$$

Whereas the continuity equation, equation 5.2, is exact, the constitutive equation, equation 5.3, is phenomenological. In cases where the diffusion equation applies, the diffusion coefficient itself can be related to the mean squared displacement of a single "tagged" particle $\Delta(t)$ as follows

$$D = \lim_{t\to\infty}\frac{\Delta(t)}{2dt}, \tag{5.4}$$

where d is the dimensionality. This is the Einstein definition of the diffusion coefficient. The mean squared displacement of a tagged particle can also be related to a correlation function of the microscopic particle velocity, $\mathbf{v}(t)$, namely the velocity autocorrelation function, $C_v(t)$

$$\frac{\Delta(t)}{2dt} = \int_0^t C_v(t')dt' - \frac{1}{t}\int_0^t t'C_v(t')dt'. \tag{5.5}$$

The velocity autocorrelation function is defined as

$$C_v(t) = \frac{1}{d} < \mathbf{v}(0) \cdot \mathbf{v}(t) >, \tag{5.6}$$

and, comparing equations 5.4 and 5.5, can be directly related to the diffusion coefficient

$$D = \lim_{t\to\infty} \frac{\Delta(t)}{2dt} = \int_0^\infty C_v(t')dt'. \tag{5.7}$$

This gives a definition of the diffusion coefficient of a tagged particle in terms of its microscopic dynamics.

One can consider the constitutive relation between flux and gradient (equation 5.3) as being the first term in an expansion involving higher derivatives of the gradient. These higher order terms represent corrections to Fick's law. However, the same mode-coupling theories which explain the existence of long-time tails also predict that at some point in the expansion the coefficients which precede the higher order terms (the Burnett coefficients) diverge.

It is convenient to consider higher order corrections to Fick's law in terms of the single particle probability density, $P(\mathbf{r}, t)$. The function $P(\mathbf{r}, t)$ is defined as the probability that a particle, initially located at the origin, is at position $\mathbf{r}$ at some later time t. Rather than studying $P(\mathbf{r}, t)$ itself, it is advantageous to consider its Fourier transform $F(\mathbf{k}, t)$, known as the self-dynamic structure factor (SDSF). There are two reasons for this. First it can be measured experimentally by several techniques. Second it is possible to express the SDSF in terms of the moments of $P(\mathbf{r}, t)$. This is most conveniently done by means of a cumulant expansion about a Gaussian. In terms of Cartesian components k and r, the first two terms in the expansion are

$$\begin{aligned} F(k,t) = \exp\Bigg(& -\frac{k^2}{2!} < r(t)^2 > \\ & + \frac{k^4}{4!}(< r(t)^4 > -3 < r(t)^2 >^2) + O(k^6) \Bigg). \end{aligned} \tag{5.8}$$

The solution to the diffusion equation (equation 5.1), for a particle starting from the origin at $t = 0$ is a Gaussian centered on the origin so, for a Fickian process, only the first term is non-zero and thus $F(k, t) = \exp(-k^2 Dt)$. Higher order terms in equation 5.8 reflect deviations in $P(\mathbf{r}, t)$ from a Gaussian or, equivalently, deviations from Fick's law. A general form which accounts for the deviations of the first and second term in the cumulant expansion from Fickian behaviour, is

$$F(k,t) = \exp\left(-k^2 \int_0^t D(t')dt' + k^4 \int_0^t B(t')dt' + O(k^6) \right), \tag{5.9}$$

from which it is convenient to define a "time and wavevector dependent" diffusion coefficient, $D(k,t)$,

$$D(k,t) = -\frac{d}{dt}\left(\frac{\ln F(k,t)}{k^2}\right) = D(t) - B(t)k^2 + O(k^4). \tag{5.10}$$

If a process is Fickian then $D(k,t)$ reduces to the diffusion coefficient. By definition the functions $D(t)$ and $B(t)$, the time dependent diffusion and super-Burnett coefficients respectively, are given by

$$D(t) = \frac{1}{2!}\frac{d}{dt} < r(t)^2 > \tag{5.11}$$

and

$$B(t) = \frac{1}{4!}\frac{d}{dt}(< r(t)^4 > -3 < r(t)^2 >^2). \tag{5.12}$$

Mode-coupling theory predicts that for a three dimensional Lorentz gas both converge. Only when we consider the next (k^4) term in equation 5.10 should we find a divergence [60]. One of our aims here is to examine the super-Burnett coefficient in this type of system. According to equation 5.9 deviations from Fick's law should be negligible if $k^2 << B(t)/D(t)$. So if B(t) and D(t) both approach constant values, deviations from Fick's law should to be limited to wavevectors larger than some fixed value, or, equivalently, to a short period of time. Here we argue that is not necessarily true.

If we assume that the diffusion and super-Burnett coefficients do converge as a function of time, then we expect to find an exponentially decaying self-dynamic structure factor. However, the fact that the higher Burnett coefficients diverge means that the behaviour at finite k, but long times, is more complex. In fact, a numerical study of the self-dynamic structure factor for a Lorentz gas (in which the fixed objects excluded volume), showed that it too decayed algebraically [61]. In three-dimensions the decay had the form $F(k,t) \sim 1/t^{3/2}$. Although this seemed surprising, the mode-coupling theory contained in ref. [60] actually predicted such an effect, although this was not appreciated at the time. Obviously, such a decay is not consistent with equation 5.8 meaning that the cumulant expansion for $F(\mathbf{k},t)$, in this type of system does not exist. This in turn implies that there are additional, non-analytic, terms in the expansion of the flux in terms of concentration gradients.

For the simulations reported in ref. [61], systems containing a low volume fraction of fixed obstacles (10 %) were studied and the amplitude of the long-time tail was found to be independent of the wavevector k. This is in agreement with a theoretical prediction based on solving the random walk problem in the presence of a single fixed object [62]. Based on these simulations one would have concluded that the algebraic decay of the SDSF was unlikely to be observed experimentally. The reasons for this are twofold. First the magnitude of the long-time tail was very small - it could only be observed with the aid

of a very accurate computational technique. Second, because the amplitude of the tail was independent of k, the effect became proportionately smaller for smaller wavevectors or, equivalently, at longer times. To see why, one must consider which wavevectors are relevant as time increases. By "relevant" we mean wavevectors which could in practice be observed decaying. If we examine equation 5.9 it is clear that, for a given wavevector, $F(k,t)$ decays at a time of the order $1/(k^2D)$. At shorter times the SDSF will hardly have decayed, at longer times it will be very small. Consequently it only makes sense to consider the problem in terms of a reduced time $\tau = k^2Dt$, which takes the shift to smaller wavevectors at longer times into account. In terms of the reduced time the asymptotic decay reported in ref. [61] has the form

$$F(k,\tau) \sim \frac{k^3}{\tau^{3/2}}, \tag{5.13}$$

and so the long-time tail rapidly becomes (proportionately) smaller as k decreases. The system studied in ref. [61] is however atypical. Systems found in nature, or studied experimentally, are typically much more dense. In this chapter we describe calculations of $F(\mathbf{k},t)$ for a particle diffusing in a more realistic system - namely, a glass composed of hard spheres. Diffusion in this type of material can indeed be studied experimentally, so our central question is: will the effects of the long-time tail in the SDSF be observable?

5.2 Description of the model

We consider a point particle performing a random walk on a three dimensional lattice. Certain sites on the lattice are excluded by the presence of impenetrable colloidal spheres. The particular lattice we used was the face-centered hypercubic lattice projected into three dimensions. A cubic lattice would formally suffice, but the face-centered hypercube has better symmetry properties and non-Gaussian effects intrinsic to the lattice are much smaller. For a given configuration of colloidal spheres we determine whether each site on the lattice is inside or outside a sphere. From this we construct a list of lattice links which connect sites outside spheres to sites inside spheres. These we refer to as boundary links. Any random walker which is traveling along such a link has its velocity reversed at half a time step. This ensures that the correct boundary conditions are imposed on the diffusing particle at the surface of the (impenetrable) spheres i.e., the flux and the equilibrium density gradient are zero. The configurations of spheres we used consisted of 1000 non-overlapping spheres at a volume fraction of $\phi = 0.59$, see figure 5.1. This is typical for a colloidal glass. The configurations were generated by the slow compression of an initially random distribution, using standard Monte-Carlo techniques.

For a given configuration of the colloidal glass, the best possible statistics we could obtain would come from averaging over all possible random walks in the system. To do this explicitly would be prohibitively time consuming but fortunately, by taking a given

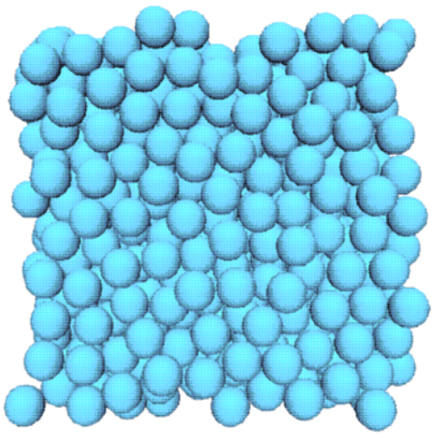

Figure 5.1
Picture of a $\phi = 0.59$ volume fraction configuration.

wavevector, the moment propagation method allows us to do this in one simulation [63]. A detailed description of the application of the method to the calculation of the SDSF is described in ref. [61] but, in summary, we proceed as follows. The lattice is initialized with a quantity we denote by $P_{tr}(\mathbf{r}, t)$,

$$P_{tr}(\mathbf{r}, 0) = \frac{1}{n} \sum_{\mathbf{i}_{nb}} \exp(-i\mathbf{k} \cdot \mathbf{r}) + \frac{1}{n} \sum_{\mathbf{i}_{b}} \exp(-i\mathbf{k} \cdot \mathbf{r}). \tag{5.14}$$

This quantity is then propagated in time according to

$$P_{tr}(\mathbf{r}, t+1) = \frac{1}{n} \sum_{\mathbf{i}_{nb}} P_{tr}(\mathbf{r} + \mathbf{i}, t) + \frac{1}{n} \sum_{\mathbf{i}_{b}} P_{tr}(\mathbf{r}, t), \tag{5.15}$$

where the summation is over all the n lattice vectors $\mathbf{i}$. The subscript b refers vectors that are boundary links and the subscript nb to those which are not. At any given time the SDSF, averaged over all possible random walks, is given by

$$F(\mathbf{k}, t) = \frac{1}{N} \sum_{\mathbf{r}} P_{tr}(\mathbf{r}, t) \exp(i\mathbf{k} \cdot \mathbf{r}). \tag{5.16}$$

The summation over $\mathbf{r}$ consists of the N sites on the lattice which lie outside the spheres.

5.3 Results

We consider the results of simulations performed on a lattice consisting of up to $L^3 = 144^3$ lattice sites. Applying periodic boundary conditions we used the scheme described above to calculate $F(\mathbf{k}, t)$. We only performed the simulations for times less than the minimum time it takes a particle to cross the simulation box. Thus, there are no finite-size effects to consider. The wavevector was chosen to lie along one of the Cartesian axes, and will be treated as a scalar, k. The product of the wavevector k and the particle radius R was used to define a dimensionless wavevector, $k^* \equiv kR/2\pi$. In these units wavevectors which probe length scales of the order of a colloidal particle radius correspond to $k^* \sim 1$. The simulations were performed for values of k^* less than,

or of the order of, unity. The units for the simulation were chosen such that the time step and lattice spacing were both unity, and the diffusion coefficient in the absence of any spheres, D_0 was equal to 1/4. To ascertain the level of numerical error introduced by representing the spheres on a lattice all the simulations were repeated using spheres of different radii. The difference between the results obtained using a sphere of radius 6.5 and 7.5 lattice units were of the same magnitude as the errors associated with averaging over a number of configurations. We therefore concluded that a sphere radius of 7.5 lattice units was adequate. All the results we show were obtained for this system.

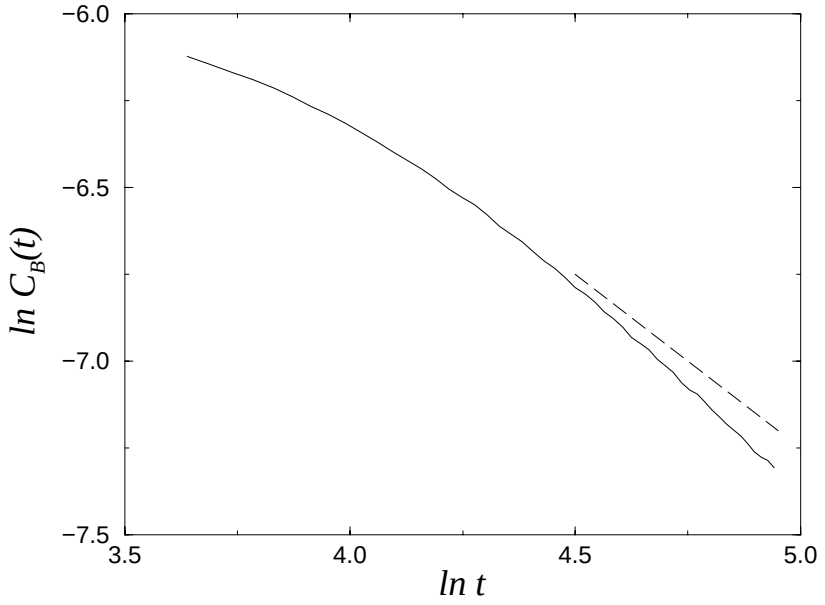

Figure 5.2 Correlation function $C_B(t)$ as drawn line. The dashed line is a curve with slope -1, provided for comparison.

5.3.1 Super-Burnett Coefficient

We start our analysis by looking at small ($\tau << 1$) values of the reduced time τ. Here we are looking at the very early stages of the decay of the SDSF where we expect equation 5.10 to be valid and any deviations from Fick's law to be small. We computed $D(t)$ and $B(t)$ by fitting our results for $F(k,t)$ to an equation with the form of equation 5.10. We stress that in order to calculate $D(t)$ it was essential to restrict ourselves to $\tau << 1$ i.e., to the initial decay of the SDSF. The diffusion coefficient, $D(t)$, reached an asymptotic value of $D/D_0 = 0.59 \pm 0.01$. This is in line with values measured experimentally for packed beds of spherical particle at roughly the same density [64]. From $B(t)$ we can obtain $C_B(t) = \frac{d}{dt}B(t)$, the correlation function associated with the super-Burnett coefficient. In figure 5.2 we have plotted $C_B(t)$, which clearly decays asymptotically faster

than $1/t$. The time dependent super-Burnett coefficient must therefore be converging as predicted in ref. [60]. The simulation results were not, however, sufficiently accurate to allow us to establish the long-time behaviour of $C_B(t)$.

5.3.2 Behaviour of $F(k,t)$

We now focus on the results for the self-dynamic structure factor at larger ($\tau > 1$) values of the reduced time. In figure 5.3 the self dynamic structure factor is plotted in a linear-log form. Clearly the SDSF is *not* decaying exponentially at longer times, otherwise the data in figure 5.3 would fall onto straight lines. Note that the apparent slowing down

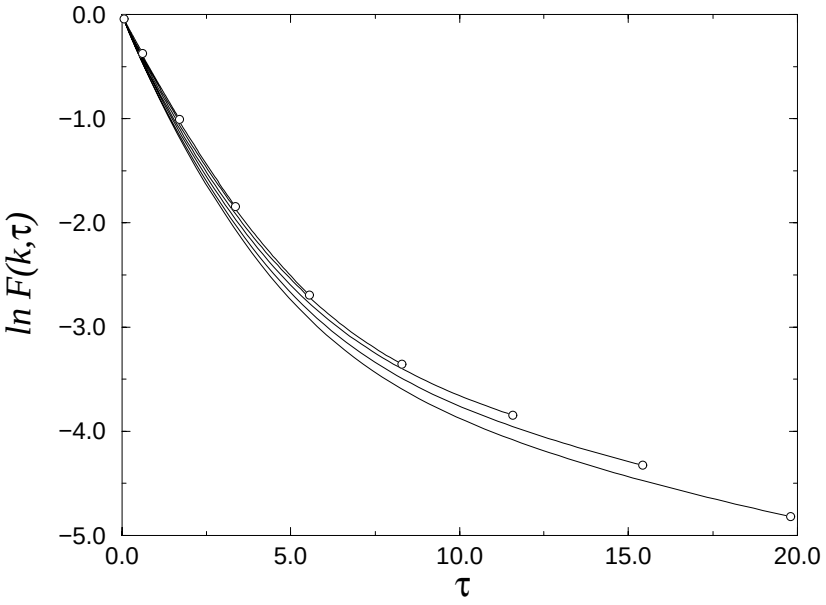

Figure 5.3 Linear-log plot of $F(k,\tau)$ for different values of k^*, $k^* = 0.052$, 0.156, 0.260, 0.365, 0.496, 0.573, 0.677, 0.781, 0.885. The open circles denote the end of the simulation for increasing values of k^* (from left to right). The errors are of the order of the circle size.

of the decay of the SDSF has nothing to do with the diffusion coefficient of the particle decreasing with time. As we mentioned above, $D(t)$ has to be calculated for $\tau << 1$. Rather that reflecting a change in the value of $D(t)$, the deviations from exponential behaviour shown in figure 5.3 reflect deviations of $P(\mathbf{r},t)$ from a Gaussian. It is somewhat surprising that such large deviations show up because we have restricted ourselves to times for which $F(k,\tau)$ is at least 1% of its initial value. If one were to look at the SDSF experimentally the decay could only be measured up until the time where its magnitude became of the same order as the statistical noise. If we assume a level of noise equal to about one hundredth of the initial value of the SDSF then figure 5.3 shows roughly the

range of values of τ that would be experimentally accessible. The simulations reported in ref. [61] required much longer times before any significant deviation from exponential behaviour was observed. Clearly, for this range of k^* deviations from Fick's law should indeed be observable. The remaining questions are, could the true asymptotic decay be observed? And would the effect still be observable at even smaller values of k^*? The reason for addressing the latter point is that the only length scale in the system is the size of the particles. If we can establish the behaviour of the SDSF for $k^* << 1$, i.e., over spatial length scales much longer than a particle radius, it would therefore be reasonable to assume that this represents the true small k behaviour. This is the most interesting case because it corresponds to particles undergoing large displacements in the colloidal glass. In figure 5.4 we have plotted the SDSF in log-log form. For comparison we also showed the asymptotic decay of $F(k,\tau) \sim 1/\tau^{3/2}$ that we expect based on the simulations reported in ref. [61] and on the theory reported in ref. [60]. For sufficiently long times,

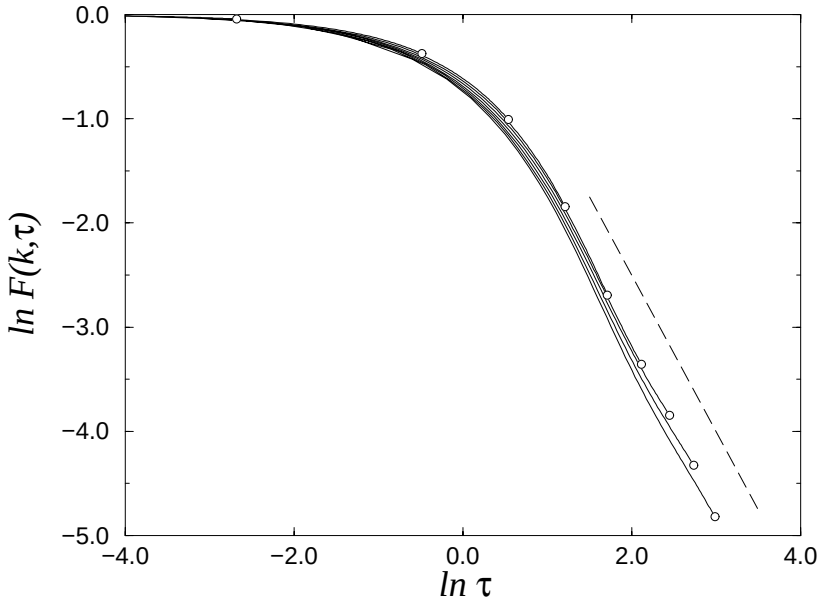

Figure 5.4 Log-log plot of $F(k,\tau)$ for different values of k^*, $k^* = 0.052$, 0.156, 0.260, 0.365, 0.496, 0.573, 0.677, 0.781, 0.885. The open circles denote the end of the simulation for increasing values of k^* (from left to right). The errors are of the order of the circle size. The dashed line is a curve with slope -1.5, provided for comparison.

the data are reasonably well represented by a power law decay. In fact, a linear fit to the long-time decay at $k^* = 0.885$ yields a power law exponent of -1.38 ± 0.02. A more accurate way of analysing the simulation data is to plot $\tau^{3/2}F(k,\tau)$ and see if this function reaches a constant value. This we show in figure 5.5. The figure strongly suggests that the function is reaching a plateau value, indicating that asymptotically

$1/\tau^{3/2}$ decay is approached. However, the asymptote is not quite reached within the simulation time even at the largest wavevector we have plotted ($k^* = 0.885$). This is

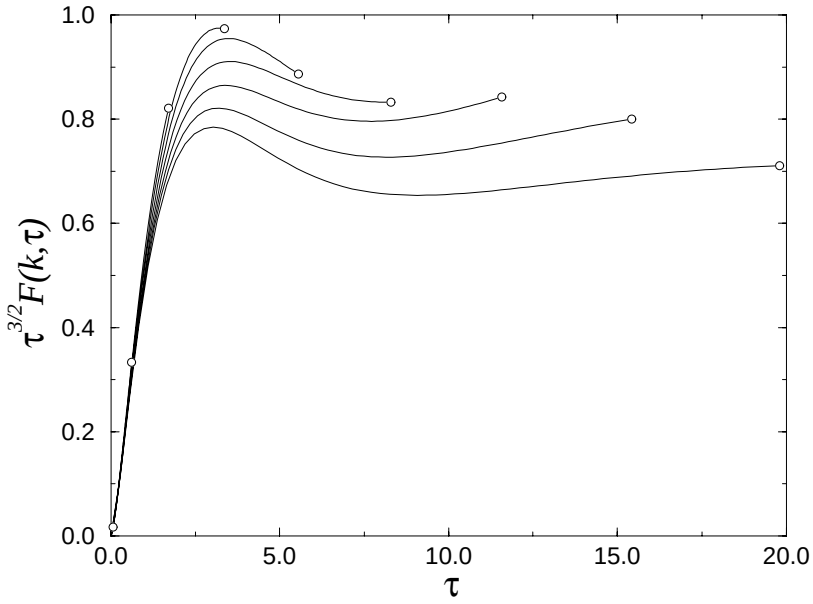

Figure 5.5 Plot of $\tau^{3/2}F(k,\tau)$ for different values of k^*, $k^* = 0.052$, 0.156, 0.260, 0.365, 0.496, 0.573, 0.677, 0.781, 0.885. The open circles denote the end of the simulation for increasing values of k^* (from left to right). The errors are of the order of the circle size.

why the linear fit to the log-log plot yielded a value for the algebraic exponent slightly different to the expected value of -1.5. We now turn to our second question; does the effect decrease with decreasing wavevector? Figure 5.5 suggests not. The value of the coefficient characterizing the magnitude of the long-time tail (the plateau value in figure 5.5) does not appear to be decreasing. On the contrary, it appears if anything to increase slightly (although the data does not extend to long enough times for us to establish the precise form of the scaling). This is in contrast to the behaviour at very low densities where the coefficient is proportional to k^3 and scales rapidly away with decreasing k [61]. There is no reason to expect that the results obtained for these dense packings should be the same as the low density results. The analysis which predicts the scaling of the tail coefficient with k is based on a single particle analysis. There will also be contributions from many particle interactions which this analysis neglects and which one would expect to become more important at higher volume fractions. Indeed, this is true of the velocity autocorrelation function which displays a pre-asymptotic decay which strongly depends on the density and a asymptotic decay with an amplitude which also depends strongly on the density [6]. Perhaps the most striking observation from

fig. 5.5 is just how little the dimensionless SDSF changes as a function of wavevector. This would suggest that, even for wavevectors smaller than those we have studied, the long-time tail in $F(k,\tau)$ should still make an experimentally observable contribution to the SDSF for a tracer particle in a colloidal glass.

5.4 Conclusions

We studied the diffusion of a small particle in a colloidal glass and found numerical evidence that the super-Burnett coefficient converges, in line with theoretical expectations. Since the super-Burnett coefficient should characterize the lowest order correction to Fick's law this might suggest that any deviations from an exponential decay of the SDSF should be small and not relevant to the analysis of experimental results. However, we found that this was not the case because the long-time tail in SDSF is a large effect in densely packed systems and its influence should be clearly observable in an experiment. In contrast to earlier work, we also find that the magnitude of the tail does not decrease (proportionately) as the wavevector decreases. This suggests that the effect should be observable, not just for the relatively large values of the wavevector we have studied, but also for the much smaller values accessible to experiment but not to simulation.

6 Non-Gaussian diffusion of particles

6.1 Introduction

In the study of the dynamics of colloids one often wishes to measure the diffusion coefficient, D. The value of D is usually extracted from the self-dynamic structure factor $F(\mathbf{k},t)$

$$F(\mathbf{k},t) = \frac{1}{N}\sum_{i=1}^{N}\left\langle \exp\bigl(i\mathbf{k}\cdot(\mathbf{r}_i(t)-\mathbf{r}_i(0))\bigr)\right\rangle . \tag{6.1}$$

If one assumes that the diffusive process is described by the diffusion equation,

$$\partial_t \rho(\mathbf{r},t) = D\nabla^2\rho(\mathbf{r},t), \tag{6.2}$$

then it follows that

$$F(\mathbf{k},t) = \exp(-k^2 Dt), \tag{6.3}$$

from which one can calculate D. If we now focus on the diffusion of a single particle nicely located at the origin, the solution to the diffusion equation (6.2) is a Gaussian of the form

$$\rho(\mathbf{r},t) = \frac{1}{(4\pi Dt)^{d/2}}\exp\left(-\frac{r^2}{4Dt}\right), \tag{6.4}$$

where d is the dimensionality of the system. From this solution of the diffusion equation one can calculate the moments of the distribution, see table 6.1. If we want to have

d	r	$< r^2(t) >$	$< r^4(t) >$	f_d
1	x	$2Dt$	$12D^2t^2$	1/3
2	$\sqrt{x^2+y^2}$	$4Dt$	$32D^2t^2$	1/2
3	$\sqrt{x^2+y^2+z^2}$	$6Dt$	$60D^2t^2$	3/5

Table 6.1 Moments of the Gaussian distribution.

a measure of the deviation from Gaussian behaviour, we can use combinations of the second and fourth moment of the distribution

$$\alpha_2(t) = f_d\frac{< r^4(t) >}{< r^2(t) >^2} - 1. \tag{6.5}$$

Rahman [65] was the first to study non-Gaussian behaviour of the SDSF by computer simulation. He computed $\alpha_2(t)$ (and higher order cumulants) for Lennard-Jones "argon" and found evidence for small deviation from Gaussian behaviour.

Thus far we have assumed that all particles have the same diffusion coefficient. However, in general the (short-time) diffusion coefficient depends on the configuration of the particle. In addition, in inhomogeneous systems the diffusion coefficient may depend on position. In this chapter we focus on these two aspects, which both can lead to non-Gaussian diffusion. To this end, we look at two cases: short-time diffusion of colloidal particles in suspension, and long-time diffusion of a colloidal particle confined between two plates.

6.2 Colloidal suspension at short-times

There have been several attempts to determine non-Gaussian effects in diffusion experimentally. These studies measured the possible deviations from Gaussian behaviour at rather long-times. Van Megen and Underwood [66] measured α_2 at very long times (of the order of 10^{-1} s) and found values $\alpha_2 \sim 0.2$ at maximum. On the other hand, Van Veluwen and Lekkerkerker [67] found value for α_2 that tended to become very large at shorter times. In fact, the reported values of α_2 were more than an order of magnitude larger than those found by Rahman [65] for Lennard-Jones "argon". Rahman found that $\alpha_2(t)$ started off at 0, peaked, and at longer times decayed to zero again. In this chapter we study non-Gaussian behaviour of colloidal particles at short-times. To be more precise, our simulations focus on a time scale where particle diffusion is still small, although hydrodynamic effects are important. The times that we consider are very long compared to the initial "ballistic" regime where α_2 *must* be zero because the Maxwell-Boltzmann distribution is Gaussian.

If we have a suspension of N colloidal particles, we can calculate the average short-time diffusion coefficient

$$< D >= \frac{1}{N} \sum_{i=1}^{N} D_i \tag{6.6}$$

After the hydrodynamics fields have developed, every particle has its own short-time diffusion coefficient D_i. If we assume that the diffusion of individual particles is Gaussian, then we can write for the self-dynamic structure factor

$$F(k,t) = \exp(-k^2 < D > t) \left(1 + k^4(< D^2 > - < D >^2)t^2 + \dots\right). \tag{6.7}$$

This leads to the following measure for the deviations from Gaussian behaviour

$$\alpha_2 = \frac{< D^2 >}{< D >^2} - 1, \tag{6.8}$$

which was also used in refs. [32] and [68]. The non-Gaussian behaviour of $F(k,t)$ is thus caused by the spread in the distribution of the diffusion coefficient D. We also note that there are non-Gaussian effects associated with the presence of the long-time tail in the velocity correlation function [69]. These should be present even for a single particle (where D has a unique value). However, at long times this contribution to $\alpha_2(t)$ decays to zero, so here we choose to neglect it.

The quantity that we need to calculate therefore is the spread in the diffusion coefficients. Ideally one would calculate the short-time diffusion coefficient of every individual particle in the suspension. To do this by calculating the mobility of each particle, using the lattice-Boltzmann technique (or any other technique for that matter), would require three simulations for every particle in the suspension. This is prohibitively time consuming. Therefore we use in the same approach that we used in the calculation of the mean diffusion coefficient. That is, if we perform a dissipative lattice Boltzmann simulation in which, we first assign independent velocities to all particles in the suspension from a Gaussian distribution. After this we calculate, for every particle, the velocity correlation function $C_v^{ij}(t)$, where the superscript i denotes the particle, j is the number of the run, all for the same starting configuration. In total, for this single configuration, M runs are performed. It should be stressed that $C_v^{ij}(t)$ is *not* yet the velocity correlation function of the particle - the latter quantity is only obtained after averaging over initial conditions. The velocity correlation function is related to the diffusion coefficient by

$$\overline{D^i(t)}_M = \frac{1}{M}\sum_{j=1}^{M}\int_0^t C_v^{ij}(\tau)d\tau, \tag{6.9}$$

where the bar denotes the estimate for the diffusion coefficient of particle i after M runs. Of course ideally, we would like to compute

$$\begin{aligned} < D(t) > &= \lim_{M\to\infty}\frac{1}{N}\sum_{i=1}^{N}\overline{D^i(t)}_M, \\ < D^2(t) > &= \lim_{M\to\infty}\frac{1}{N}\sum_{i=1}^{N}\left(\overline{D^i(t)}_M\right)^2. \end{aligned} \tag{6.10}$$

However, as we are necessarily limited to finite M we need to investigate the dependence of $\overline{D^i(t)}_M$ on M. To this end, we compute

$$\left(\overline{D^i(t)}_M\right)^2 = \left(\frac{1}{M}\sum_{j=1}^{M}\int_0^t C_v^{ij}(\tau)d\tau\right)^2 \tag{6.11}$$

If we now write $\overline{D^i(t)}$ for $\lim_{M\to\infty} \overline{D^i(t)}_M$, then we can define $\Delta^{ij}(t)$

$$\left(\overline{D^i(t)}_M\right)^2 = \left(\frac{1}{M}\sum_{j=1}^{M}\left(\overline{D^i(t)} + \Delta^{ij}(t)\right)\right)^2 . \tag{6.12}$$

As $\overline{\Delta}^{ij}(t) = 0$ (by definition) we can write

$$\left(\overline{D^i(t)}_M\right)^2 = \overline{D^i(t)}^2 + \frac{1}{M^2}\sum_{j=1}^{M}\left(\Delta^{ij}(t)\right)^2 . \tag{6.13}$$

If we now define $\sum_{j=1}^{M}\left(\Delta^{ij}(t)\right)^2 = M(\Delta^i(t))^2$ we find

$$< D^2(t) >_M = \frac{1}{N}\sum_{i=1}^{N}\overline{D^i(t)}^2 + \frac{1}{M}\frac{1}{N}\sum_{i=1}^{N}(\Delta^i(t))^2. \tag{6.14}$$

The important point to note is that our numerical estimate for $< D^2(t) >$ has a *systematic* $1/M$ dependence (unlike $\overline{D^i(t)}$ itself). Hence, when computing $< D^2 > - < D >^2$ it is essential to eliminate the M-dependence by extrapolation to $1/M = 0$. If we find the scaling with $1/M$ predicted by equation 6.14 then we can use it to give $< D^2(t) >$ for an extrapolated infinite number of simulations. Up to this point, we have assumed that $< D(t) >$ and $< D^2(t) >$ depend on time. We now proceed to take the limit $t \to \infty$. That is, we consider the "long-time" limit of the short-time behaviour. The time dependence of $< D(t) >$ is given by $< D(t) >= \overline{D} + A/\sqrt{t}$, because the velocity correlation function decays as $C_v(t) \sim 1/t^{3/2}$. By virtue of equation 6.11, we expect $< D^2(t) >= \overline{D^2} + A'/\sqrt{t} + B'/t$. B' was explicitly included because it need not be small. In practice, we use the following procedure

- Do M runs with different initial velocities, for the same configuration.
- Calculate (as a function of M): $< D(t) >_M$ and $< D^2(t) >_M$.
- Extrapolate $< D^2(t) >_M$ as a function of $1/M$, to give $< D^2(t) >$.
- Extrapolate $< D^2(t) >$ as a function $1/\sqrt{t}$, to give $< D^2(\infty) >$.
- Extrapolate $< D(t) >$ as a function $1/\sqrt{t}$, to give $< D(\infty) >$.
- Compute α_2 from equation 6.8.

6.2.1 Simulation results

In this section we report the results of the numerical simulation of α_2 for three different packing fractions. The parameters characterizing the simulations we give in table 6.2. As an illustration of the data analysis we focus on the data obtained for $\phi = 0.30$. All simulations were performed in a box of size $L^3 = 200^3$ lattice units. In figure 6.1 we show the dependence of $< D^2 >_M$ on $1/M$. As can be seen in the figure, the $1/M$ dependence predicted by equation 6.14 is recovered. If we now perform the extrapolation to $M \to \infty$,

ϕ	N	M	R	α_2
0.10	686	50	4.5	0.04
0.20	1377	60	4.5	0.04
0.30	2066	50	4.5	0.06

Table 6.2 Simulation settings, ϕ is the volume fraction, N is the number of particles, M is the total number of runs for the configuration, R is the radius of the sphere, measured in lattice units, α_2 is the measure of non-Gaussian behaviour.

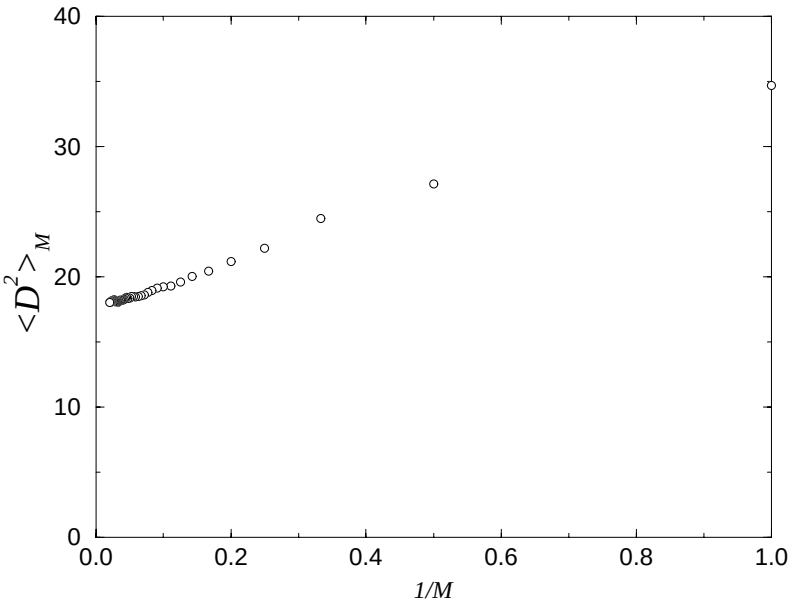

Figure 6.1 $< D^2(t = 200) >_M$ as a function of $1/M$.

we obtain $< D^2(t) >$. This quantity is shown in figure 6.2. After extrapolation to $t \to \infty$, we recover $< D(t) >$. Then, using equation 6.8, we compute α_2. The resulting values we give in table 6.2.

6.2.2 Conclusion

Our simulation results suggest that the deviations from Gaussian behaviour in the diffusion of monodisperse colloidal particles are observable, but small. Our data pertain to the time regime where all velocity correlations have decayed, yet particles have not yet diffused over an appreciable distance. We note that, in this regime, the diffusion coefficient of every particle is different (because of the difference in initial position). It is this spread in the diffusion coefficients that leads to apparent non-Gaussian behaviour. We note also that our results for α_2 are of the same order of magnitude as the values found in the experiments of Van Megen and Underwood [66]. This is however somewhat

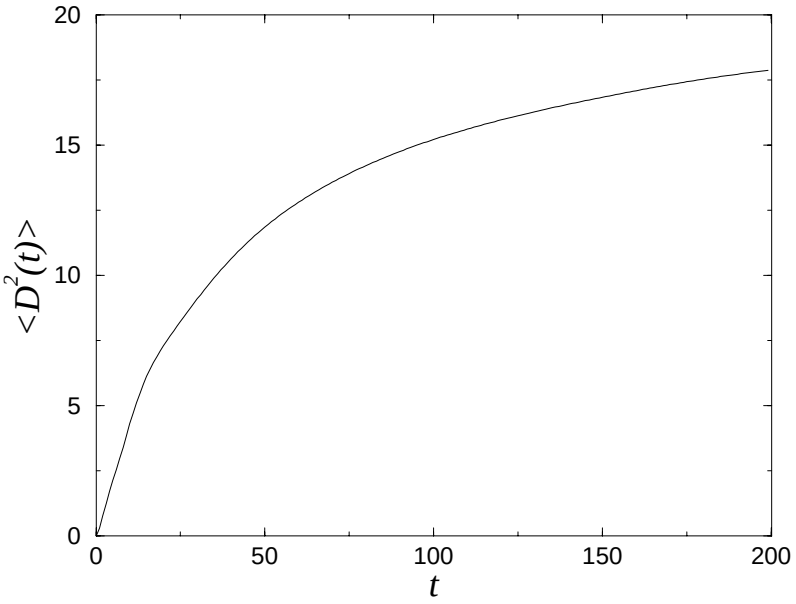

Figure 6.2 $< D^2(t) >$ obtained from $< D^2(t) >_M$ after extrapolation to $1/M = 0$. Time is expressed in the time step used in the lattice-Boltzmann model.

surprising because the shortest time considered in ref. [66] is of the order of 10^{-2} s. On this time scale, colloidal particles can diffuse over appreciable distances. We also note that we do not find the very large values for α_2 reported by Van Veluwen and Lekkerkerker [67]. In particular, we find no evidence for a divergence of α_2 when $t \to 0$.

6.3 Non-Gaussian diffusion between plates.

The non-Gaussian effects in the short-time diffusion coefficient considered in the previous section were due to a positional dependence of the short-time diffusion coefficient. In the present section we focus on a system where we expect to see a much stronger positional dependence, namely a system in which a particle is confined between between two plates. Such a system has, in fact, been studied experimentally by Marcus et al. [70]. However, whereas ref. [70] studied a colloidal suspension a low but finite volume fraction (in order to compare with the theory of ref. [71]), we shall focus on the infinite dilution limit. We shall use the same geometry studied in the experiments of ref. [70]. Marcus et al. studied a suspension of particles with a diameter of 1 μm between two plates at a distance of about 3 μm. We use the ratio of the particle radius to the plate separation to characterize the geometry of the system. The experiments correspond to $\lambda = R/L = 1/3$, where R is the radius of the particle L is half the plate separation. In our simulation we first determined the positional dependence of the diffusion coefficient.

We did this using the lattice-Boltzmann method. The diffusion coefficient of a colloidal particle at a distance r from the middle of the gap between the plates can be computed by integrating the velocity correlation function of the colloidal particle. In figure 6.3 we show the results of this calculation for both components of the diffusion coefficient tensor. The data shown in figure 6.3 pertain to the short-time diffusion coefficient. Let us next

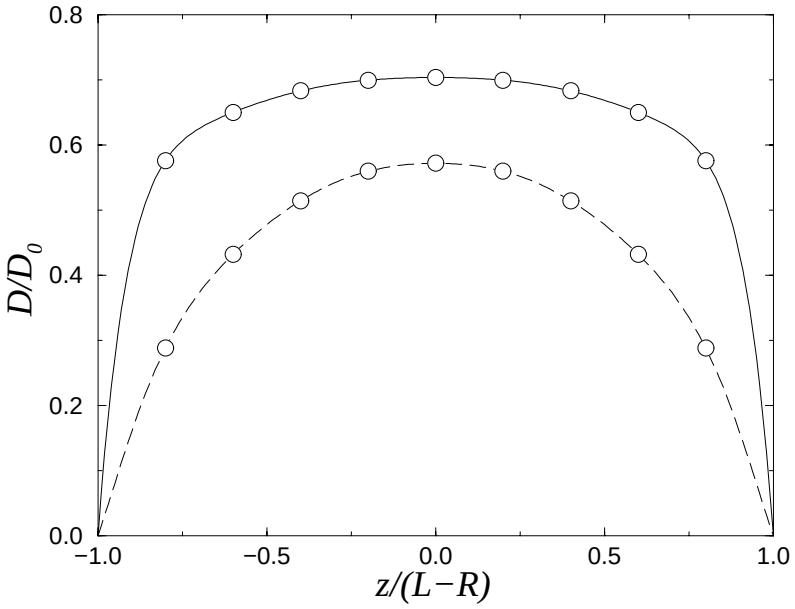

Figure 6.3 Positional dependence of the short-time diffusion coefficient for a colloidal particle between two plates ($\lambda = 1/3$). The drawn curve is a fit to the simulated points for the in plane diffusion coefficient, The dashed curve is a fit to the simulated points for the perpendicular diffusion coefficient.

focus on the calculation of the long-time self diffusion coefficient. Using our numerical results for the position dependent diffusion coefficient we employed Brownian Dynamics simulations [19, 29] to compute the in-plane diffusion. The Brownian-dynamics method is a numerical method for solving the Smoluchowski equation (a generalisation of the classical diffusion equation) in a system where the diffusion coefficient varies with position. In the absence of external forces the Brownian-dynamics algorithm to update the position of a particle in a time interval δt takes the following form

$$\mathbf{r}(t + \delta t) = \mathbf{r}(t) + \nabla \cdot \mathbf{D}(t)\delta t + \delta \mathbf{r}^G, \tag{6.15}$$

where $\mathbf{D}$ is the diffusion tensor of the particle. The components of $\delta \mathbf{r}^G$ are random variables selected from a Gaussian distribution with zero means and covariance

$$< \delta \mathbf{r}^G \delta \mathbf{r}^G >= 2\mathbf{D}\delta t. \tag{6.16}$$

The second term on the right hand side in equation 6.15 is needed to maintain the correct spatial distribution of the diffusing particle. As the particles are displaced over finite distances during the simulation, it may happen, that the change in position would cause the particle to cross the wall. This is clearly unphysical. If this happens, we let the particle perform bounce back from the wall such that the total displacement of the particle (including the reflection from the wall) is the same.

We now focus on the in-plane diffusion for one coordinate, say x. As before, we compute the reduced fourth cumulant as a measure for deviation from Gaussian behaviour

$$\alpha_2(t) = \frac{< (\Delta x)^4(t) >}{3 < (\Delta x)^2(t) >^2} - 1 \tag{6.17}$$

In the absence of external forces, the particles are distributed uniformly between the

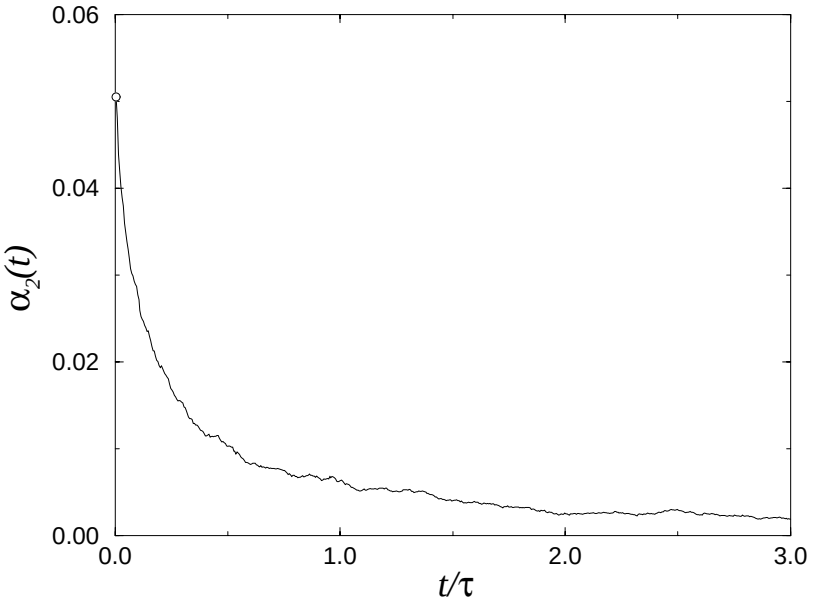

Figure 6.4 The non-Gaussian behaviour α_2 as a function of time. Drawn curve: Brownian dynamics simulations. Time is scaled by $1/\tau =< D_\perp >$, where $< D_\perp >$ is calculated from figure 6.3. The open circle denotes the value predicted by equation 6.19.

plates. It is straightforward to compute $< (\Delta x)^2(\delta t) >$ and $< (\Delta x)^4(\delta t) >$

$$\begin{aligned} < (\Delta x)^2(\delta t) > &= \frac{1}{N}\sum_{i=1}^{N}(\Delta x)^2 = \frac{1}{N}\sum_{i=1}^{N} 2D_{\parallel i}\delta t = 2 < D_\parallel > \delta t, \\ < (\Delta x)^4(\delta t) > &= \frac{1}{N}\sum_{i=1}^{N}(\Delta x)^4 = \frac{1}{N}\sum_{i=1}^{N} 12D_{\parallel i}^2(\delta t)^2 = 12 < D_\parallel^2 > (\delta t)^2. \end{aligned} \tag{6.18}$$

Combining the two previous two equations leads to

$$\alpha_2(\delta t) = \frac{< D_\parallel^2 >}{< D_\parallel >^2} - 1. \tag{6.19}$$

At times short compared to the time it takes the particle to diffuse an appreacheable distance we can compute the initial non-Gaussian behaviour (eq. 6.19), using

$$< D_\parallel^n >= \frac{1}{2L} \int_{-L}^{L} D_\parallel^n(z) dz, \tag{6.20}$$

and the values of $D_\parallel$ which are given in figure 6.3. For longer times, we need to perform the Brownian dynamics simulations referred to above.

In the Brownian-dynamics simulation we followed 7.2×10^6 independent trajectories starting from initial positions randomly located between the two plates. We had fitted the data of figure 6.3 to a polynomial of the form

$$D(z) = \sum_{n=1}^{5} a_n (1 - z^{2n}). \tag{6.21}$$

These diffusion coefficient profiles were then used in the Brownian-dynamics algorithm (eq. 6.15). We used a time step $\delta t = 0.0125$. A plot of the time dependence of $\alpha_2(t)$ is shown in figure 6.4. Note that the results of the Brownian dynamics simulations extrapolate nicely to the $t = 0$ value computed using equation 6.19. We stress that $< D_\parallel >$ is itself is time independent. Hence all non-Gaussian effects are due to the Δx^4 term. Analysis of the data showed that, at long times, $(\Delta x)^4 \approx At + Bt^2$, where A and B are constants. The term linear in t leads to the slow $(1/t)$ decay of $\alpha_2(t)$. We note that Marcus et al. found no evidence for non-Gaussian effects in the diffusion of confined colloidal particles. This may be due to the fact that, on the time scale of their experiment, $\alpha_2(t)$ was too small compared to the level of statistical error, to be observable.

7 Diffusion of colloidal particles in porous media

7.1 Introduction

Let us now consider the diffusion of colloidal particles in a more complex geometry, namely a medium with randomly distributed obstacles. A possible candidate for such a system is a dense random packing of spheres. Here we study the effect of the confining matrix on the motion of a single colloidal particle. In order to investigate the diffusion process, we distinguish the diffusion process in two time scales. First there is the short-time regime, during which the hydrodynamic interactions between the colloidal particle and the medium have fully developed, yet the particle has not yet diffused appreciably. In this time regime the particle motion is characterized by the short-time diffusion coefficient. Then there is time scale during which the particle diffuses over a distance that is not small compared to its radius. On this time scale the particle might collide with the fixed particles that constitute the matrix. At present, the theoretical description of the short-time diffusion in dense porous media, is limited to rather simplified or idealized models. Some progress can be made if one assumes that the medium under consideration is a network composed of tubes [72, 73]. A further simplification can be made by assuming tracer diffusion in a two dimensional network [74]. In contrast, the description of long-time diffusion (ignoring variations in the short-time diffusion coefficient due to hydrodynamic interactions), has been subject of several studies [75–77]. Viramontes-Gamboa et al. [78, 79] reported a numerical study of a binary mixture of colloidal particles, using Brownian dynamics (ignoring hydrodynamic interactions). They used this approach to model a porous matrix, by fixing the coordinates of the particles of one species.

Experiments to study colloidal particle diffusion in a glassy matrix of larger particles are underway at the Van 't Hoff laboratory in Utrecht [80]. In the present chapter we aim to model this colloidal tracer diffusion process. The model system that we studied at is a computer generated packing of $N = 10000$ spheres at a volume fraction of

$\phi = 0.636$ [81, 82]. This chapter begins with a discussion of the short-time dynamics. Subsequently, we discuss the long-time (non-hydrodynamic) diffusion. Finally, we discuss a combination of the two calculations.

7.2 Short-time diffusion

Our first aim is to determine the reduction of the Stokes-Einstein diffusion coefficient of a single colloidal particle due to the hydrodynamic interaction with the fixed matrix. To this end we use the Lattice-Boltzmann method for neutrallay buoyent particles. as described in chapter 2. The kinematic shear viscosity was set equal to $\nu = 1/6$. Due to the size difference between the small diffusing particle, and the big (non-diffusing) particles the lattice-Boltzmann method becomes computationally very demanding. To see this, let us consider a practical example. Let us denote the size ratio of the small and the large particles by $\lambda = r/R$, where r is the radius of the small sphere, and R the radius of the big, stationary sphere. In order to have diffusion of the small spheres, the latter must be able to move trough the narrowest constrictions created by the large spheres. As we see in figure 7.1 this puts an upper limit $\lambda^* = \frac{2}{3}\sqrt{3} - 1$ on the size ratio. The size of the small colloidal particle puts an upper limit on the lattice spacing of our lattice-Boltzmann model. Let us take the (rather extreme) case that the diameter of the small colloidal particle is only three lattice spacings. And let us consider a reasonable value of $\lambda < \lambda^*$, e.g., $\lambda = 0.1$. In that case the diameter of the large colloidal particle would be thirty lattice spacings. For the simulation of a system consisting of 10000 large particles,

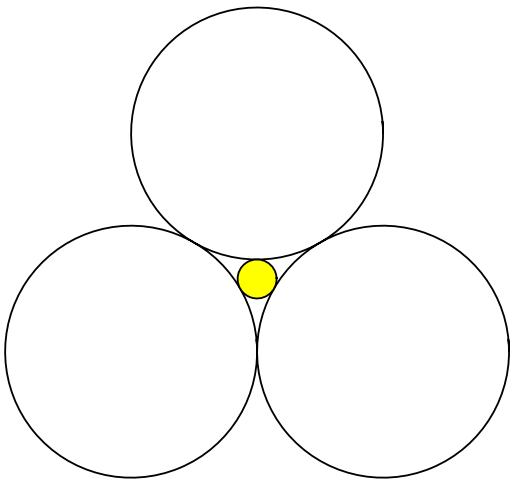

Figure 7.1
The largest "small" diffusing particle simulated, indicated in grey, in the matrix composed of white spheres.

we would need a lattice-Boltzmann model of size $L^3 = 606^3$ lattice nodes. As simulation of such a model would require more computer memory then we have currently at our disposal. In order to make progress we do not therefore simulate the entire system but only a part in the vicinity of the small colloidal particle. We thus first insert the small particle in an off-lattice model of a system of ten thousand large spheres. We then map

the particles that surround the small particle onto a lattice. During the simulation large particles are fixed (i.e., an external force and torque are applied such that $\mathbf{v} = \omega = 0$). For the small, neutrally buoyant, particle we calculate the velocity correlation function $C_v(t)$. This velocity correlation function can subsequently be integrated to give the diffusion coefficient

$$D^S = \lim_{t\to\infty} \int_0^t C_v(\tau) d\tau. \tag{7.1}$$

As the large and small particles are assumed to have a hard, repulsive interaction, the density of the small particles between the big spheres is uniform. Before we proceed, let us first note that, in the limit $\lambda \to 0$, the effect of the hydrodynamic interactions between the small particle and the wall becomes negligible. As a result, the short-time diffusion constant of a small particle becomes equal to D_0, the diffusion constant of the same particle in a bulk fluid. This does not mean that the matrix has no effect on the tracer diffusion, but simply that all such effects are "long-time" phenomena due to the physical blocking of the tracer diffusion by the matrix. In contrast, for non-zero λ there *is* an effect of the matrix on the short-time diffusion coefficient. This is shown in figure 7.2 where we show the time dependence of the diffusion coefficient, of a small sphere with $\lambda = 0.103$, and compare it with the time dependence $D(t)$ for the same sphere sphere in absence of the matrix. Similar simulations were carried out for two other values of λ. The parameters characterizing these simulations have been collected in table 7.1. To see the effect of the geometry of the confining medium we also considered tracer diffusion in a close packed FCC crystal of large spheres. In table 7.2 we have collected

λ	r	R	N_{run}	D^S/D_0
0.000				1.000
0.034	0.5	14.5	300	0.834
0.059	0.5	8.5	300	0.731
0.103	1.5	14.5	300	0.527

Table 7.1 Simulation settings and results for tracer diffusion in a martix of randomly close packed hard spheres ($\phi = 0.636$). r is the radius of the small particle, R is the radius of the large particle (both in lattice units) $\lambda = r/R$. N_{run} is the number of runs. D^S/D_0 is the short-time diffusion coefficient.

the simulation parameters and the main results. As before, we see that the diffusion coefficient decreases when λ is increased, but now it decreases faster. In figure 7.3 we compare the diffusion coefficients for the two systems studied. The results of the linear fits to the data are

$$D^S_{\text{RCP}}(\lambda)/D_0 \approx 1 - 4.68\lambda, \tag{7.2}$$

$$D^S_{\text{FCC}}(\lambda)/D_0 \approx 1 - 5.85\lambda. \tag{7.3}$$

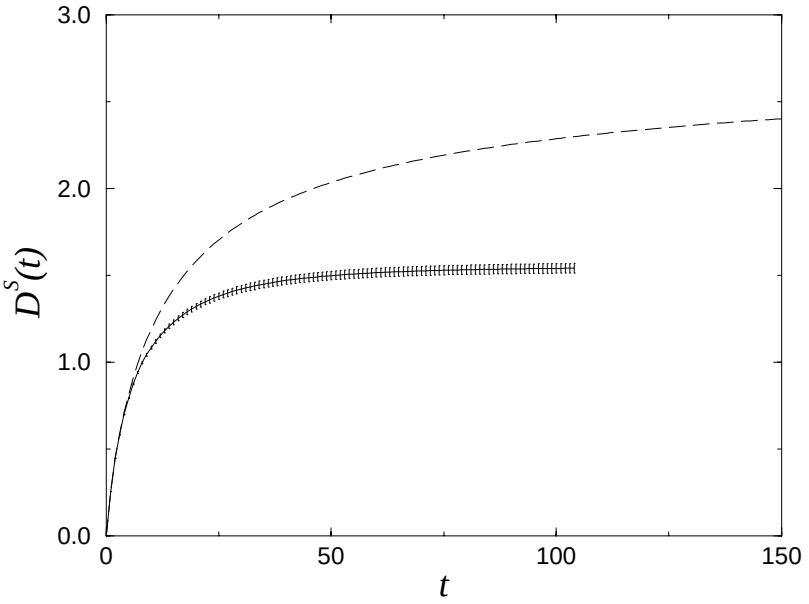

Figure 7.2 Plot of the time dependence of the diffusion coefficient of a colloidal particle. Both curves are for particles with radius $r = 1.5$ in lattice units, The dashed curve is for a colloidal particle in an unbounded fluid (increases to $D_0 = 3$). The drawn curve is for the same particle ($\lambda = 0.103$) in a matrix of randomly close-packed hard spheres. Time is expressed in the unit of time used in the lattice model.

λ	r	R	N_{run}	D^S/D_0
0.000				1.000
0.034	0.5	14.5	100	0.800
0.059	0.5	8.5	100	0.655
0.103	1.5	14.5	100	0.433

Table 7.2 Simulation settings and results for tracer diffusion in a matrix of regularly close-packed hard spheres ($\phi = 0.740$), FCC crystal r is the radius of the small particle, R is the radius of the large particle (both in lattice units) $\lambda = r/R$. N_{run} is the number of runs. D^S/D_0 is the short-time diffusion coefficient.

Note that the *short-time* diffusion coefficient is non-zero for $\lambda = \lambda^*$, even though the *long-time* diffusion coefficient must vanish for a value of λ close to this value (see figure 7.6, below). In a close packed FCC lattice, D^L vanishes for $\lambda = \lambda^*$. We should be aware that equations 7.2 and 7.3 may be subject to a small but systematic error. The reason is the following. As can be seen in figure 7.2 the diffusion coefficient appears to be a monotonically increasing function of time. Yet as we have seen in chapter 3 there may be an effect on the velocity correlation function due to the compressibility of the fluid. As discussed in chapter 3, long-wavelength sound modes become diffusive in a porous medium, and in principle we should expect the same to happen in the present case. If

so, then after some time the velocity correlation function would become negative

$$C_v(t) \sim -\frac{1}{t^{5/2}}. \tag{7.4}$$

As was discussed, the presence of this negative long-time tail does not change the diffusion coefficient from the value it would have in an incompressible fluid. However if we *ignore* the contribution of the negative tail of the velocity correlation function to the diffusion coefficient, we would be overestimating be overestimating $D^S(\lambda)$.

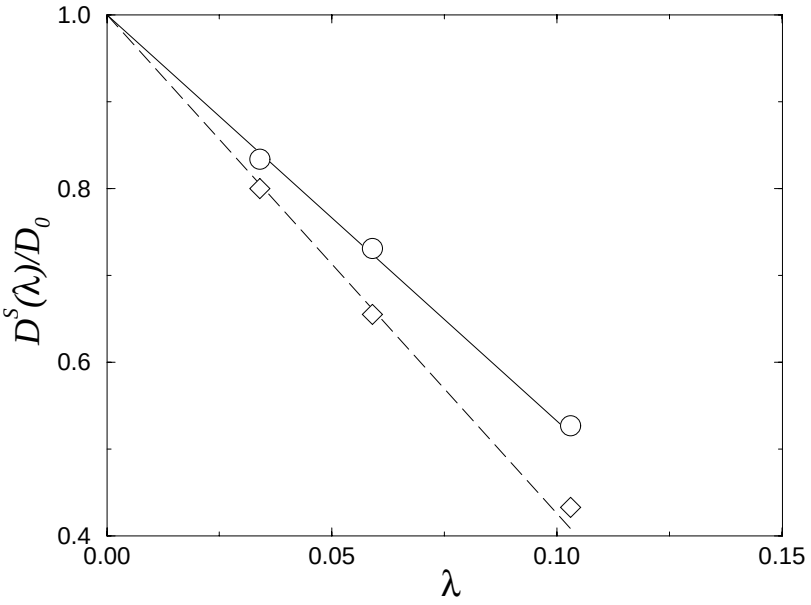

Figure 7.3 λ dependence for the short-time diffusion coefficient. The open circles denote the result for the randomly close-packed matrix (RCP), the drawn line is a linear fit to the data. The open diamonds denote the result for the close packed FCC crystal, the dashed line is a linear fit to the data.

7.3 Long-time diffusion

The second part of this chapter focusses on the long-time diffusion of a tracer particle in a porous medium. Long-time diffusion takes place when a particle diffuses over a distance that is significant compared to its radius. The model that we use to study the long-time diffusion is a diffusive Lorentz-gas model. In this model, a point tracer performs a random walk until it encounters a fixed scatterer. When this happens, the tracer bounces back from the surface of the impenetrable sphere. The implementation of the bounce-back rule should be such that detailed balance is satisfied. We take the following approach. We assume that δ, the size of the jump carried out by the tracer particle is constant (see figure 7.4). The procedure for updating the position of the tracer

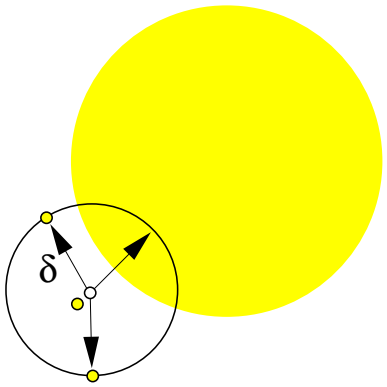

Figure 7.4
The hopping Lorentz gas. The open circle denotes the initial position of the tracer. The particle will be moved after the update to one of the filled open circles.

is as follows. First select a random direction. Along that direction find the intersection point (if any) with the sphere that is nearest along that line. We move the particle over a distance δ along the line, bouncing it off the surface of the sphere if required. To obtain reasonable statistics, we need to average over a large number of trajectories of tracers diffusing in the medium. The finite size of the tracer, relative to the size of the

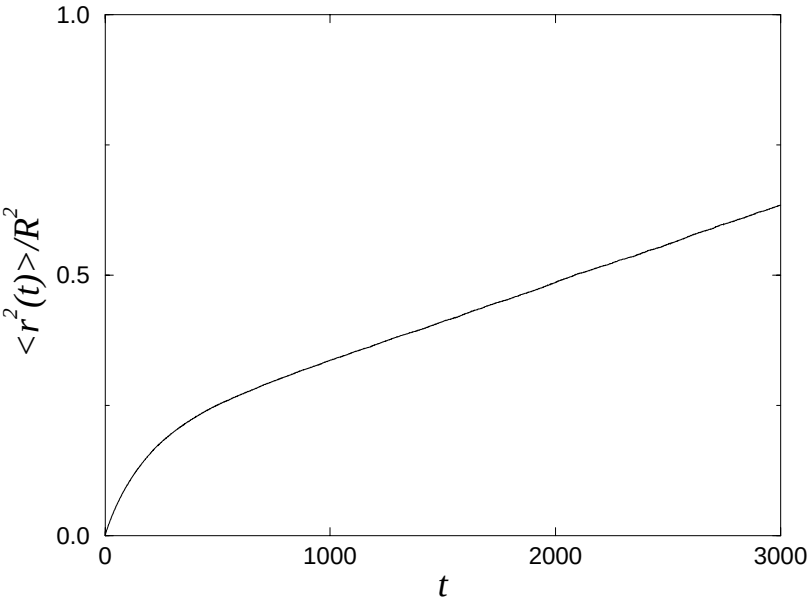

Figure 7.5 The mean squared displacement $< r^2(t) > /R^2$ for tracer ($\lambda = 0.13$) diffusion in a matrix of regularly close-packed hard spheres ($\phi = 0.740$), R is the radius of the large spheres.

big spheres, is taken into account by expanding the radius of the large spheres to be not R but $r + R$. From then on we treat the tracer as a diffusing point particle. The quantity that we determine in the simulation is the mean squared displacement of the

tracer

$$< r^2(t) >= \frac{1}{N}\sum_{i=1}^{N}\big(\mathbf{r}_i(t) - \mathbf{r}_i(0)\big)^2, \tag{7.5}$$

where t is the number of jumps. Once we know $< r^2(t) >$ as a function of t, we can compute the (time dependent) diffusion coefficient

$$D^L(t) = \frac{1}{6}\frac{d}{dt} < r^2(t) > . \tag{7.6}$$

In general, the results that we obtain may still depend on the ratio $\delta/(r+R)$. We

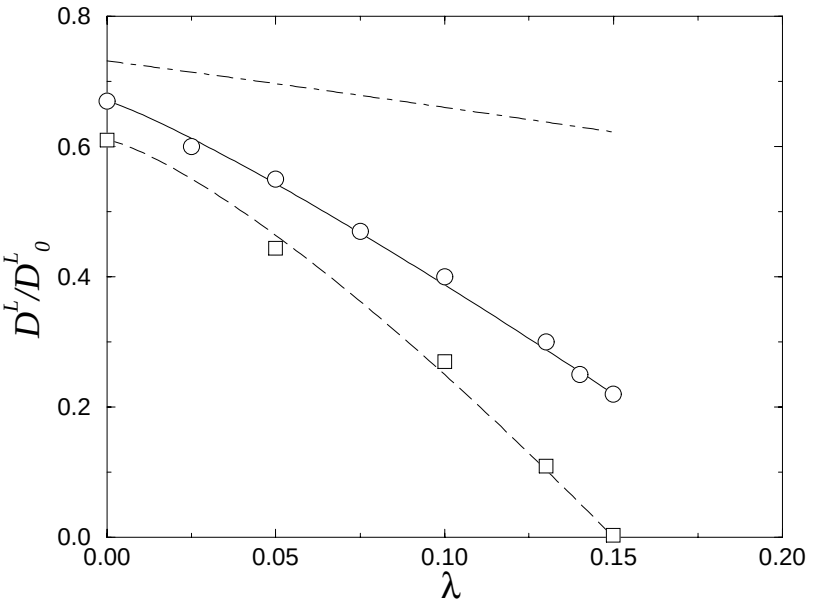

Figure 7.6 λ dependence for the long-time diffusion coefficient D^L/D_0^L for tracer diffusion in a matrix. The open circles denote the result for the diffusion in a matrix composed of randomly close packed hard spheres ($\phi = 0.636$), where the drawn curve is a guide to the eye. The open squares denote the result for diffusion in a matrix of regularly close-packed hard-spheres, where the dashed line is a guide to the eye. The dot-dashed curve is the prediction by Kim and Torquato [77].

are interested in the limit that the step size δ is much smaller than the particle radius. Hence we consider the quantity $D^L(t)/D_0^L$ in the limit $\delta/(r+R) \to 0$, where D_0^L is the diffusion coefficient of the tracer in the absence of the fixed obstacles

$$D_0^L = \frac{1}{6}\delta^2. \tag{7.7}$$

To obtain the long-time diffusion coefficient, we consider the limit

$$\frac{D^L}{D_0^L} = \lim_{t\to\infty}\frac{D^L(t)}{D_0^L}. \tag{7.8}$$

In our simulations, we collected statistics on 10^5 trajectories. Every trajectory contained up to 2.5×10^4 steps. During the simulation the tracer moved typically over a distance of $\sqrt{r^2} \sim 3R$, where R is the radius of the large spheres. As an example, we show in figure 7.5 the mean-squared displacement of a tracer particle in a close packed FCC crystal of large spheres, as function of the simulation time for $\lambda = 0.13$. We see that

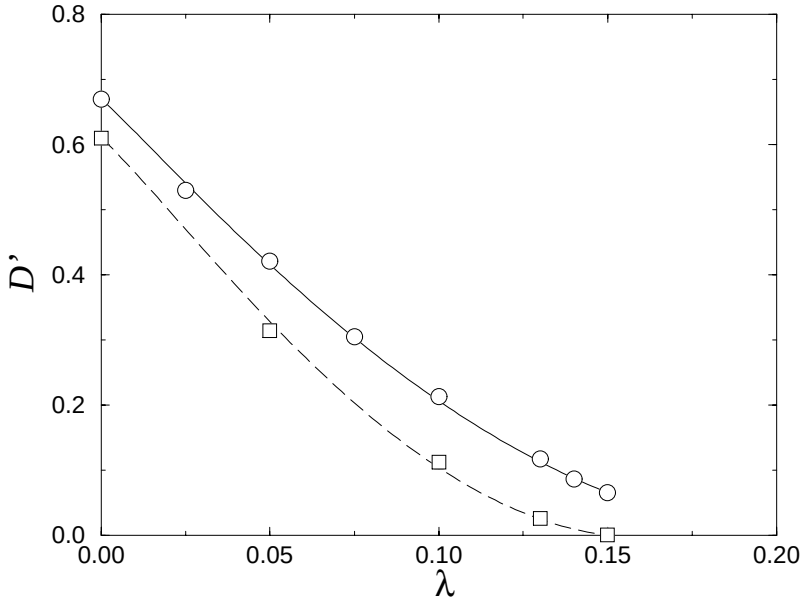

Figure 7.7 λ dependence for the scaled long-time self diffusion-coefficient D'. The open circles denote the result for tracer diffusion in the matrix of randomly close-packed spheres, where the drawn line is a guide to the eye. The open squares denote the result for tracer diffusion in the regularly close-packed FCC crystal, where the dashed line is a guide to the eye.

on this time scale there is a clear time dependence for the diffusion coefficient, diffusive behaviour is only found after some 1000 steps. This crossover to diffusive behaviour was most clearly observed for the close packed FCC crystal, when λ was close to λ^*. Similar simulations were performed for random close-packed hard spheres. We note that the crossover to diffusive behaviour was less sharp for the random close packed matrix. Simulations on both the random close-packed and the regular close-packed matrix were performed to determine D^L/D_0^L. The results of these simulations are shown in figure 7.6. In the figure we see that, for the tracer diffusion in the close packed FCC matrix, the long-time diffusion coefficient vanishes at $\lambda = \lambda^*$. However for the case of the tracer diffusion in the random close-packed matrix the long-time diffusion is still finite at this value of λ. Also we see in figure 7.6 that the prediction by Kim and Torquato [77] is an

overestimate of the long-time diffusion coefficient compared with the long-time diffusion coefficient measured by simulation.

7.4 Combination of the results

Now we combine the results for the short-time diffusion with those for the long-time diffusion of a tracer diffusion a a porous matrix. We follow the approach of Medina-Noyola [83]. This author approach was to separate the hydrodynamic interaction from the effects caused by the direct interaction as follows

$$D' = \frac{D^S}{D_0}\frac{D^L}{D_0^L}, \tag{7.9}$$

where D^S is the short-time diffusion coefficient, D_0 is the Stokes-Einstein diffusion coefficient and D^L/D_0^L is the long-time diffusion coefficient. For the short-time diffusion coefficient we use the expressions 7.2 and 7.3. Combination of those data with the results fromm figure 7.6 leads to the *true* scaled long-time diffusion coefficient D'. This is shown in figure 7.7 where we show the λ dependence of D'. The results shown in figure 7.7 should be compared with experimental data for tracer diffusion in regularly or randomly packed arrays of colloidal spheres.

8 Diffusion of a colloidal particle near a wall

8.1 Introduction

In the previous chapters, we studied the diffusion of colloidal particles in different confined geometries. In the present chapter we focus on the dynamics of a colloidal particle near *one* wall. The geometry is depicted in figure 8.1. We assume that, at

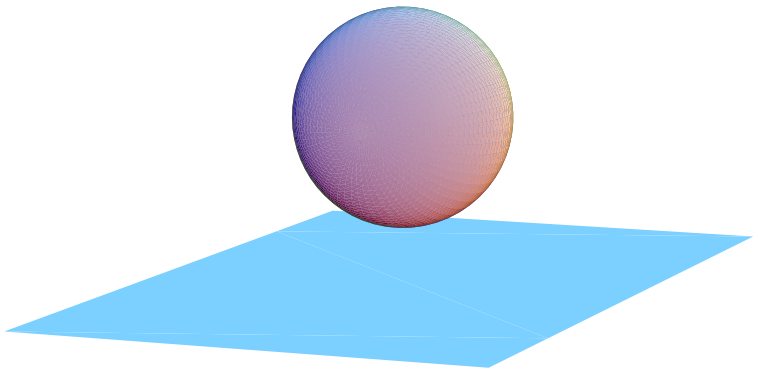

Figure 8.1 Colloidal particle near a single wall.

this wall, stick boundary conditions ($\mathbf{u}(z=0)=\mathbf{0}$) are imposed. We recall that, in a bulk fluid, the translational and angular velocity correlation functions have the following asymptotic form

$$C_v(t) \sim \frac{1}{t^{d/2}} \tag{8.1}$$

and

$$C_\omega(t) \sim \frac{1}{t^{d/2+1}}, \tag{8.2}$$

where $C_v(t)$ denotes the translational velocity correlation function, $C_\omega(t)$, the angular velocity correlation function and d is the dimensionality of the system ($d>1$). The algebraic decay of the (angular) velocity correlation function can be understood qualatively if we assume that the evolution of the flow field surrounding the colloidal particle is

described by the Navier-Stokes equation for an incompressible fluid in the low-Reynolds number limit. If we restrict ourselves to the transverse velocity field, we can ignore the pressure term in the Navier-Stokes equation and we obtain

$$\partial_t \mathbf{u}(\mathbf{r},t) = \nu \nabla^2 \mathbf{u}(\mathbf{r},t). \tag{8.3}$$

This is a simple diffusion equation for the (transverse) flow field. It only needs to be supplemented with the appropriate boundary conditions (in space and time). If we consider an unbounded fluid, and $\mathbf{u}(\mathbf{r},0) = \delta(\mathbf{r})$, then equation 8.1 follows directly from the solution of equation 8.3. In the presence of a wall, the long-time behaviour of the velocity correlation functions will be modified. Gotoh and Kaneda [84] reported a theoretical analisys of behaviour of the translational velocity correlation functions of a colloidal particle at a distance l from the $z = 0$ plane. They found that for times $t >> l^2/\nu$

$$C_v^{\parallel}(t) = \frac{d^{\parallel}}{t^{5/2}} \tag{8.4}$$

and

$$C_v^{\perp}(t) = \frac{d^{\perp}}{t^{7/2}}, \tag{8.5}$$

where $C_v^{\parallel}$ is the in-plane velocity correlation function, $C_v^{\perp}$ is the out of plane velocity correlation function. These correlation functions are the only ones studied by Gotoh and Kaneda [84]. The amplitudes in equation 8.4 and 8.5 are given by

$$d^{\parallel} = \frac{MC_v^{\parallel}(0)}{\nu\rho} \frac{l^2}{(4\pi\nu)^{3/2}} \tag{8.6}$$

and

$$d^{\perp} = \frac{MC_v^{\perp}(0)}{4\nu^2\rho} \frac{l^4}{(4\pi\nu)^{3/2}}, \tag{8.7}$$

where M is the mass of the colloidal particle and ρ is the density of the solvent. In the present chapter we report numerical results of simulations of various velocity correlation functions in the presence of hard walls. We look at both translational and angular velocity correlation functions, in two and three dimensions.

8.2 Disk in two dimensions

To study diffusion near a wall in two dimensions we performed lattice-Boltzmann simulations of a neutrally buoyant disk of radius $r = 1.5$ lattice units, using techniques described in chapter 2. The kinematic shear viscosity of the solvent was set to $\nu = 0.6$, chosen such that the time scale on which the effect of the wall on $C_v(t)$ is observable, is sufficiently short. The system size was $L^2 = 400^2$. The position of the particle was such that there was one layer of lattice nodes between the disk and the hard wall. The particle

was placed so near the wall to make the effect of the wall on $C_v(t)$ more easily observable. In figure 8.2, 8.3 and 8.4 we show, respectively the in-plane and perpendicular velocity correlation functions, and the angular velocity correlation function. In every case we have multiplied the correlation function with t^n, where n was chosen such that, if the the correlation function was multiplied by t^n, it tended to a constant value. In all cases,

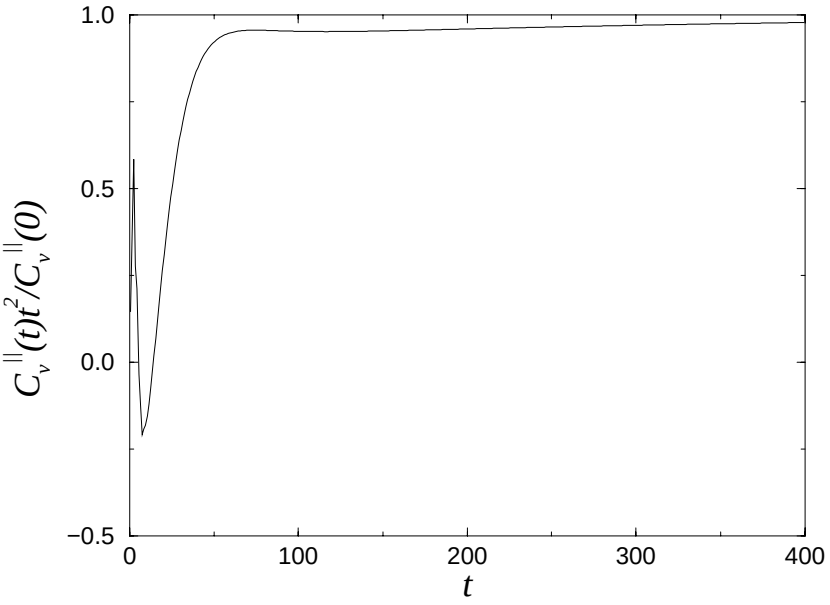

Figure 8.2
$C_v^{\parallel}(t)t^2/C_v^{\parallel}(0)$ for a disk in two dimensions near a wall. Time is expressed in lattice units.

we observe that the correlation function is initially positive (which would persist if the particle was in an unbounded system), then negative and finally positive again.

8.3 Sphere in three dimensions

In order to determine the translational velocity correlation function of a sphere near a wall in a three dimensional system, we simulated a lattice-Boltzmann fluid containing a neutrally buoyant sphere of radius $r = 0.5$ lattice units. The kinematic shear viscosity was chosen to be $\nu = 0.6$. The system size was $L^3 = 150^3$. The position of the particle was such that there were two layers of lattice nodes between the sphere and the stick boundary wall ($l = 2.5$ lattice units). Again the particle was placed so near the wall because then the effect of the boundary was most easily observable. The appropriately multiplied normalized translational velocity correlation functions are shown in figures 8.5 and 8.6. For the translational velocity correlation functions of a sphere in three dimensions, we find behaviour that is similar to that of a disk in two dimensions (after multiplication with the appropriate power of t). We note that the exponent of the asymptotic decay of both $C_v^{\parallel}(t)$ and $C_v^{\perp}(t)$ agrees reasonably well with the predictions by

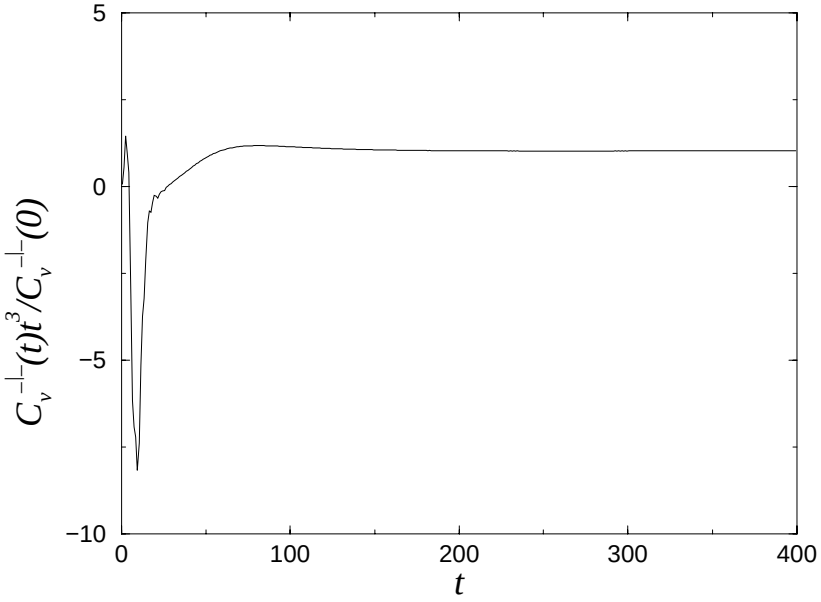

Figure 8.3
$C_v^{\perp}(t)t^3/C_v^{\perp}(0)$ for a disk in two dimensions near a wall. Time is expressed in lattice units.

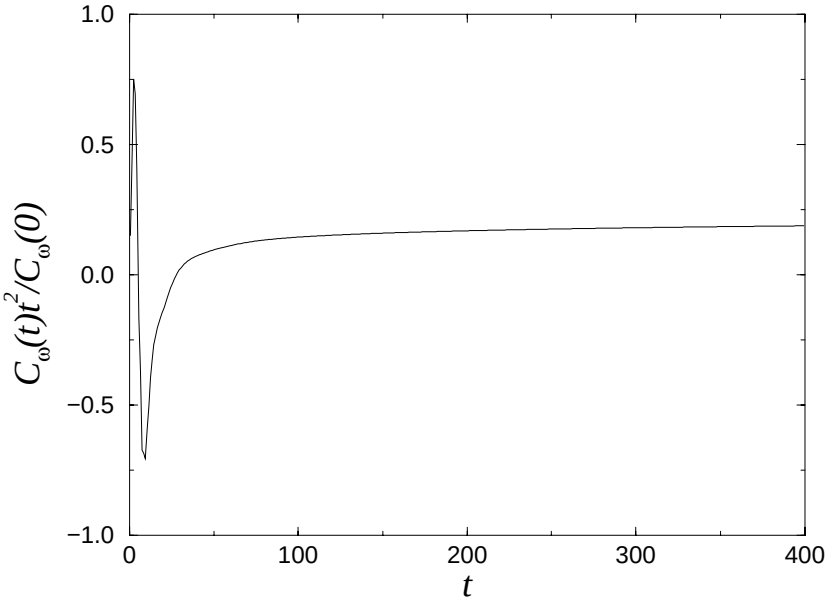

Figure 8.4
$C_\omega(t)t^2/C_\omega(0)$ for a disk in two dimensions near a wall. Time is expressed in lattice units.

Gotoh and Kaneda [84]. The amplitude of the velocity correlation function can be obtained from extrapolation. The predicted amplitudes $d^{\parallel}$ and $d^{\perp}$ are respectively 5% and 13% larger than the amplitudes obtained from simulation. For the theoretical estimate we used $l = 2.5$ lattice units. However, if we would have chosen $l = 2.4$ lattice units, then the agreement between simulation and theory would have been perfect. Within

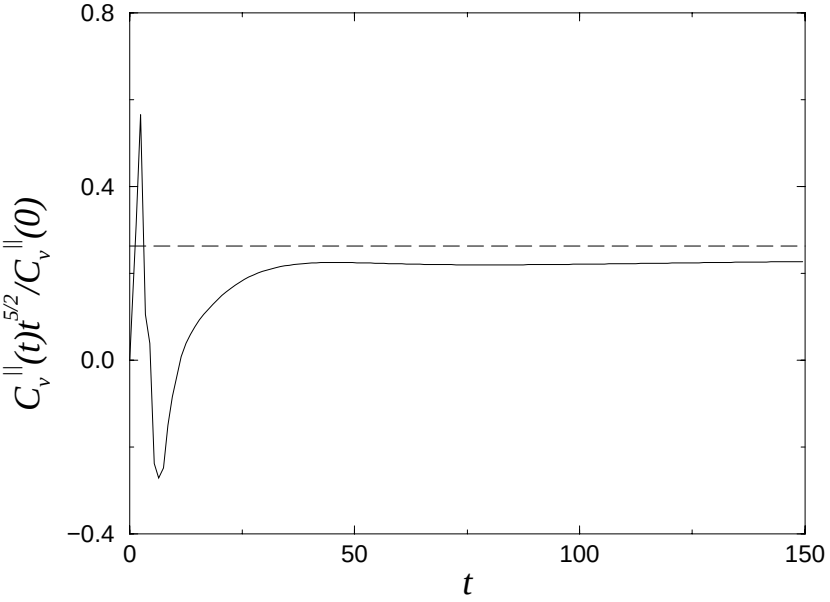

Figure 8.5
$C_v^{\parallel}(t)t^{5/2}/C_v^{\parallel}(0)$ for a sphere in three dimensions near a wall. Time is expressed in lattice units. The dashed line denotes $d^{\parallel}$, from equation 8.6.

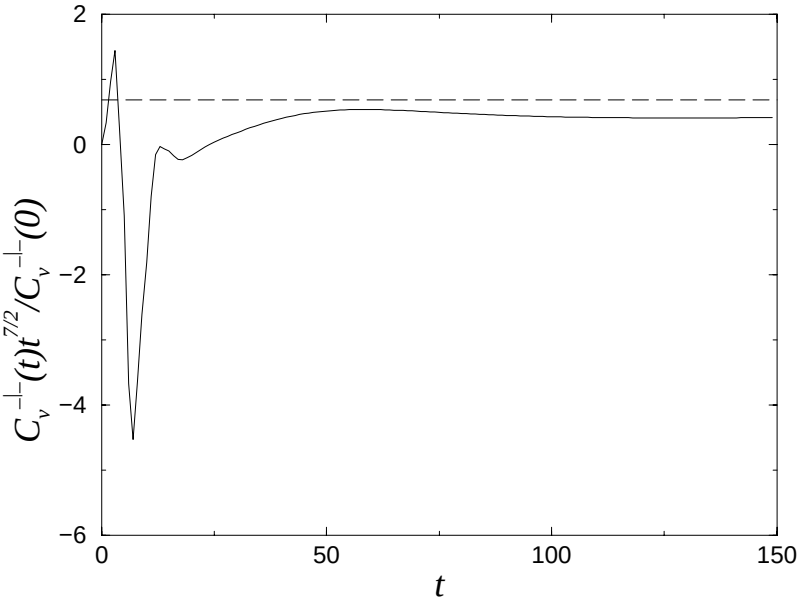

Figure 8.6
$C_v^{\perp}(t)t^{7/2}/C_v^{\perp}(0)$ for a sphere in three dimensions near a wall. Time is expressed in lattice units. The dashed line denotes $d^{\perp}$, from equation 8.7.

the uncertainty of the position of the wall, due to the lattice nature of the simulation, the agreement with the predicted amplitudes is therefore satisfactory. For the angular velocity correlation function in three dimensions, a neutrally buoyant sphere of radius $r = 1.5$ lattice units was used. The kinematic shear viscosity was set to $\nu = 0.6$. The system size was $L^3 = 150^3$. The position of the particle was such that there was one

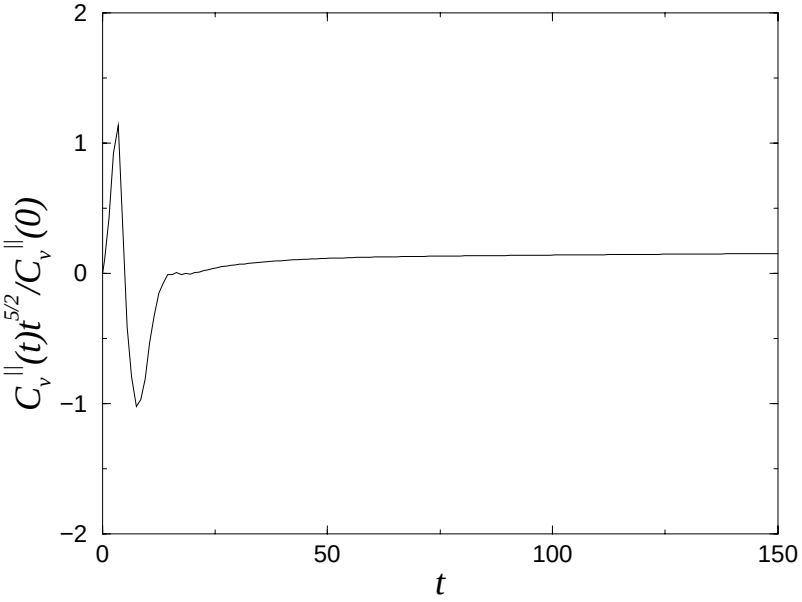

Figure 8.7
$C_\omega^{\parallel}(t)t^{5/2}/C_\omega^{\parallel}(0)$ for a sphere in three dimensions near the wall. The rotation axis is parallel to the wall. Time is expressed in lattice units.

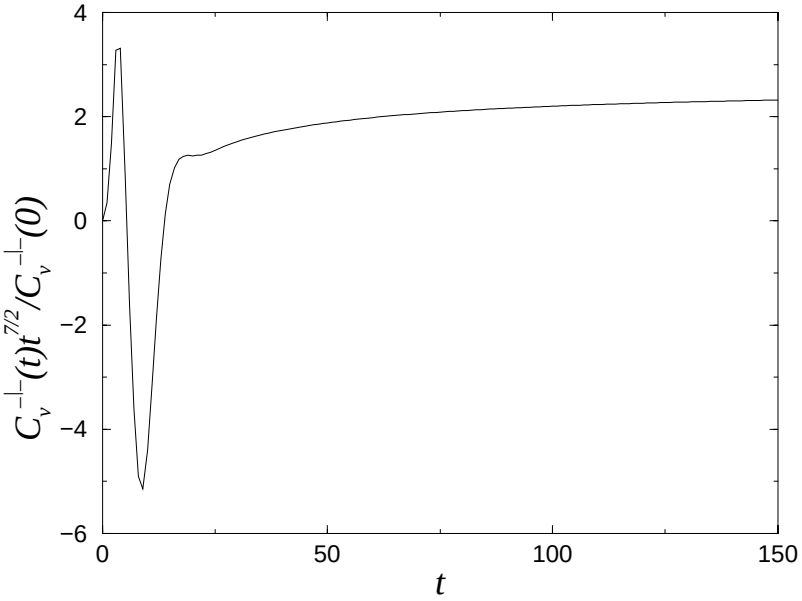

Figure 8.8
$C_\omega^{\perp}(t)t^{7/2}/C_\omega^{\perp}(0)$ for a sphere in three dimensions near a wall. The rotation axis is perpendicular to the wall. Time is expressed in lattice units.

layer of lattice nodes between the sphere and the wall. In figures 8.7 and 8.8 we show respectively the in-plane and perpendicular angular velocity correlation function. In every case we have multiplied the correlation function with $t^{n+1/2}$, where n was chosen such that, if the the correlation function was multiplied by $t^{n+1/2}$ it tended to a constant

value. As before, we find that the angular velocity correlation functions approach an asymptotic power law decay after an initial, oscillatory transient.

8.4 Intuitive argument

Using the approach of images we can along simple lines make predictions for the observed exponents for the long-time behaviour. For translation parallel to the wall the colloidal particle and the direction of the image is shown in figure 8.9. The initial velocities are given by

$$\begin{aligned} u_x(x=0, z= \quad l, t=0) &= \quad u_0, \\ u_x(x=0, z=-l, t=0) &= -u_0. \end{aligned} \tag{8.8}$$

Solution of the diffusion equation for transverse momentum(eq. 8.3), with initial con-

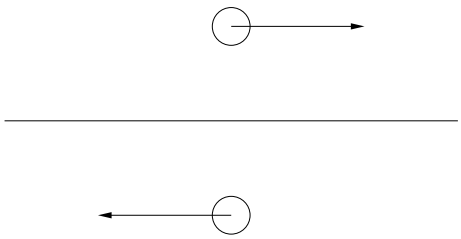

Figure 8.9
Picture of the colloidal particle, which is above the wall, and the position of the image below it, the arrows denotes the velocity.

dition 8.8 in two dimensions gives

$$u_x(t) = \frac{M u_0}{\rho} \frac{1}{4\pi\nu t} \left(\exp\left(-\frac{x^2 + (z-l)^2}{4\nu t} \right) - \exp\left(-\frac{x^2 + (z+l)^2}{4\nu t} \right) \right). \tag{8.9}$$

For long times the previous equation, when evaluated in $(x = 0, z = l)$ leads to

$$C_v^{\parallel}(t) \sim \frac{1}{t^2}. \tag{8.10}$$

Along similar lines one derives in three dimensions

$$C_v^{\parallel}(t) \sim \frac{1}{t^{5/2}}, \tag{8.11}$$

which is in agreement with equation 8.4, and the results in figure 8.2 and figure 8.5. For rotation the initial velocities are given by

$$\begin{aligned} u_x(x=0, z= \quad r, t=0) &= \quad u_0, \\ u_x(x=0, z=-r, t=0) &= -u_0. \end{aligned} \tag{8.12}$$

The velocity field can again be calculated, like in equation 8.9. From the vorticity $(\partial_z u_x)$ in the origin, the angular velocity correlation function is derived to be

$$C_\omega(t) \sim \frac{1}{t^{d/2+1}}. \tag{8.13}$$

Using this approach, we proceed to evaluate the in-plane angular velocity correlation function in the presence of a wall. In two and three dimensions the positions and direction of the initial velocities are given by (see figure 8.10)

$$\begin{aligned} u_x(x=0, z= \quad l+r, t=0) &= \quad u_0, \\ u_x(x=0, z= \quad l-r, t=0) &= -u_0, \\ u_x(x=0, z=-l+r, t=0) &= \quad u_0, \\ u_x(x=0, z=-l-r, t=0) &= -u_0, \end{aligned} \tag{8.14}$$

which leads to

$$C_\omega^{\parallel}(t) \sim \frac{1}{t^{d/2+1}}, \tag{8.15}$$

where the vorticity was evaluated at $(x = 0, z = l)$, which is in agreement with the result of the simulation in figure 8.4 and figure 8.8. The perpendicular angular velocity

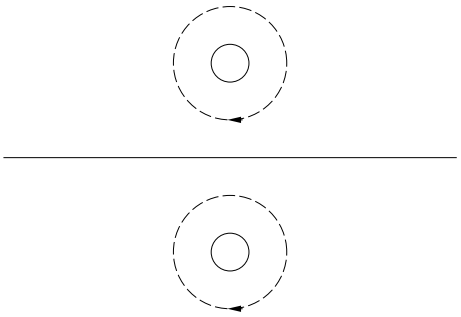

Figure 8.10
Picture of the colloidal particle, which is above the wall, and the position of the image below it, the arrows denotes the direction of the angular velocity.

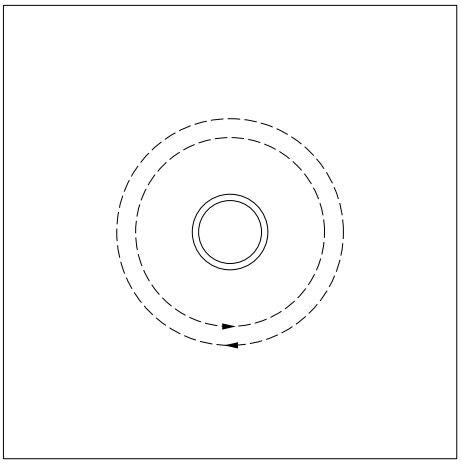

Figure 8.11
Top view picture of the colloidal particle, which is above the wall. The smaller colloidal particle is the image, which is below the wall. The arrows denote the angular velocity, which is for the colloidal particle above the wall clockwise, and for the image rotating counterclockwise.

correlation function can be derived along similar lines. For a wall in three dimensions,

see figure 8.11. The initial velocities are given by

$$\begin{aligned} u_x(x=0, y=r, z=l, t=0) &= u_0, \\ u_x(x=0, y=-r, z=l, t=0) &= -u_0, \\ u_x(x=0, y=r, z=-l, t=0) &= -u_0, \\ u_x(x=0, y=-r, z=-l, t=0) &= u_0, \end{aligned} \tag{8.16}$$

from which we derive

$$C_\omega^\perp(t) \sim \frac{1}{t^{7/2}}, \tag{8.17}$$

which is in agreement with the simulation result in figure 8.8. In all the previously mentioned examples the images were chosen such that the x-component of the in-plane velocity at the wall vanished.

8.5 Conclusions

The simulations reported in this chapter provide the first numerical evidence that the hydrodynamic long-time tail is changed by the presence of the wall. Not only is the exponent characterizing the algebraic decay of the velocity correlation function changed, but the functional form depends on the orientation of the velocity relative to the wall. Shown was that, using the methods of reflections, an intuitive derivation of the exponent of the long-time tail can be performed. In their 1982 article, Gotoh and Kaneda [84] expressed the hope that the long-time tails that they predicted would be verified by either experiment or numerical simulation. The present simulations provide a first step in this direction.

A Stress autocorrelation function

We wish to study the stress autocorrelation function in the lattice-Boltzmann model. The mode coupling prediction for the stress autocorrelation function is given by [2]

$$C_{xy}(t) = \frac{1}{\rho d(d+2)} \left(\frac{d^2-2}{(8\pi\nu t)^{d/2}} + \frac{1}{(4\pi\Gamma t)^{d/2}} \right), \tag{A.1}$$

where $C_{xy}(t)$ is the correlation function for the xy component of the stress tensor, d is the dimensionality, ρ is the number density, ν is the bare kinematic viscosity, and $\Gamma = 2(d-1)\nu/d + \xi$, the sound-damping coefficient, with ξ the kinematic bulk viscosity.

In chapter 2 we used for the equilibrium momentum flux density tensor

$$\Pi^{\mathrm{eq}} = p\mathbf{I}. \tag{A.2}$$

In the linear lattice-Boltzmann model, equation A.2, Π_{xy} can only decay exponentially. To observe the long-time behaviour of the stress autocorrelation function, a coupling to the momentum is essential. The nonlinear expression for the local momentum flux density tensor is given by

$$\Pi^{\mathrm{eq}} = p\mathbf{I} + \rho\mathbf{u}\mathbf{u}. \tag{A.3}$$

The second term in the previous equation, which is usually only taken into account to study high Reynolds number flow, does take into account a coupling to the momentum. In order to observe the long-time tail in the stress autocorrelation function, the full non-linear stress had to be considered.

The stress in the system, which is a collective property is given by

$$\Sigma = \sum_{\mathbf{r}} (\Pi - p\mathbf{I}). \tag{A.4}$$

For the sake of convenience, we consider only one component of the traceless symmetric part of the stress tensor viz. the xy component. Other components give rise to the same correlation functions. We compute the stress autocorrelation function by correlating the initial perturbation of the stress with the stress at some later time t

$$C_{xy}(t) = \frac{\langle \Delta\Sigma_{xy}(0)\Delta\Sigma_{xy}(t)\rangle}{\langle (\Delta\Sigma_{xy}(0))^2\rangle}, \tag{A.5}$$

where $\Delta\Sigma_{xy} = \Sigma_{xy}(t) - \Sigma_{xy}(\infty)$. It is important to subtract the steady state ($t = \infty$) value of the stress tensor because, in a finite system, the initial stress perturbation will relax to a uniform velocity field with an associated stress given by equation A.3

$$\Sigma_{xy}(\infty) = \frac{\Sigma_{xy}(0)}{V}, \tag{A.6}$$

where V is the volume of the fluid. In a lattice gas cellular automata, where the stress is purely kinetic in origin, the stress at site $\mathbf{r}$ at time t is uncorrelated to the stress at that same time at any other lattice point. In our calculations we have therefore chosen to consider the simplest possible initial condition viz. a small perturbation of the stress *at one lattice site only*.

In ref. [85] we report the results of the simulations to measure $C_{xy}(t)$ in both two and three dimensions. If the viscosity was determined using the linearized version of the equilibrium part of the momentum flux density, equation A.3, it was found that the "bare" viscosity was recovered. Also shown was that upon including the non-linear term in equation A.3, that the stress autocorrelation function could be measured. Both the exponent and the amplitude were found to be in agreement with equation A.1. Due to the long-time tail in the stress autocorrelation function an increased viscosity, compared to the "bare" viscosity was found. In this thesis we use the linear lattice-Boltzmann model, where the viscosity is the "bare", prescribed viscosity.

A Stress autocorrelation function

We wish to study the stress autocorrelation function in the lattice-Boltzmann model. The mode coupling prediction for the stress autocorrelation function is given by [2]

$$C_{xy}(t) = \frac{1}{\rho d(d+2)} \left(\frac{d^2-2}{(8\pi\nu t)^{d/2}} + \frac{1}{(4\pi\Gamma t)^{d/2}} \right), \tag{A.1}$$

where $C_{xy}(t)$ is the correlation function for the xy component of the stress tensor, d is the dimensionality, ρ is the number density, ν is the bare kinematic viscosity, and $\Gamma = 2(d-1)\nu/d + \xi$, the sound-damping coefficient, with ξ the kinematic bulk viscosity.

In chapter 2 we used for the equilibrium momentum flux density tensor

$$\Pi^{\mathrm{eq}} = p\mathbf{I}. \tag{A.2}$$

In the linear lattice-Boltzmann model, equation A.2, Π_{xy} can only decay exponentially. To observe the long-time behaviour of the stress autocorrelation function, a coupling to the momentum is essential. The nonlinear expression for the local momentum flux density tensor is given by

$$\Pi^{\mathrm{eq}} = p\mathbf{I} + \rho\mathbf{u}\mathbf{u}. \tag{A.3}$$

The second term in the previous equation, which is usually only taken into account to study high Reynolds number flow, does take into account a coupling to the momentum. In order to observe the long-time tail in the stress autocorrelation function, the full non-linear stress had to be considered.

The stress in the system, which is a collective property is given by

$$\Sigma = \sum_{\mathbf{r}} (\Pi - p\mathbf{I}). \tag{A.4}$$

For the sake of convenience, we consider only one component of the traceless symmetric part of the stress tensor viz. the xy component. Other components give rise to the same correlation functions. We compute the stress autocorrelation function by correlating the initial perturbation of the stress with the stress at some later time t

$$C_{xy}(t) = \frac{\langle \Delta\Sigma_{xy}(0)\Delta\Sigma_{xy}(t)\rangle}{\langle (\Delta\Sigma_{xy}(0))^2\rangle}, \tag{A.5}$$

where $\Delta\Sigma_{xy} = \Sigma_{xy}(t) - \Sigma_{xy}(\infty)$. It is important to subtract the steady state ($t = \infty$) value of the stress tensor because, in a finite system, the initial stress perturbation will relax to a uniform velocity field with an associated stress given by equation A.3

$$\Sigma_{xy}(\infty) = \frac{\Sigma_{xy}(0)}{V}, \tag{A.6}$$

where V is the volume of the fluid. In a lattice gas cellular automata, where the stress is purely kinetic in origin, the stress at site $\mathbf{r}$ at time t is uncorrelated to the stress at that same time at any other lattice point. In our calculations we have therefore chosen to consider the simplest possible initial condition viz. a small perturbation of the stress *at one lattice site only*.

In ref. [85] we report the results of the simulations to measure $C_{xy}(t)$ in both two and three dimensions. If the viscosity was determined using the linearized version of the equilibrium part of the momentum flux density, equation A.3, it was found that the "bare" viscosity was recovered. Also shown was that upon including the non-linear term in equation A.3, that the stress autocorrelation function could be measured. Both the exponent and the amplitude were found to be in agreement with equation A.1. Due to the long-time tail in the stress autocorrelation function an increased viscosity, compared to the "bare" viscosity was found. In this thesis we use the linear lattice-Boltzmann model, where the viscosity is the "bare", prescribed viscosity.

B Generalized Einstein equation

B.1 Single particle

We wish to study the short-time diffusion coefficient of a suspension of particles. On this time scale the colloidal configuration is essentially fixed, and the friction is position dependent. We start of by writing the generalized Langevin equation for a particle, with no external and random forces acting on it

$$M\frac{dv}{dt} = -\int_0^t \xi(t-s)v(s)ds, \tag{B.1}$$

with mass M, velocity v, and friction kernel $\xi(t-s)$. If the previous equation is Laplace transformed we find

$$M(z\tilde{v}(z) - v(0)) = -\tilde{\xi}(z)\tilde{v}(z). \tag{B.2}$$

If we substitute $z = 0$, we find

$$Mv(0) = \tilde{\xi}(0)\tilde{v}(0), \tag{B.3}$$

or equivalently

$$\tilde{v}(0) = \frac{1}{\tilde{\xi}(0)}Mv(0). \tag{B.4}$$

If both sides are now multiplied by $v(0)$ we find

$$v(0)\tilde{v}(0) = \frac{1}{\tilde{\xi}(0)}Mv^2(0), \tag{B.5}$$

From which we can proceed via two routes. First we take on both sides the velocity average

$$< v(0)\tilde{v}(0) >= \frac{1}{\tilde{\xi}(0)} < Mv^2(0) > . \tag{B.6}$$

The left hand side in the previous equation is the diffusion coefficient D (from the Green-Kubo relation for the diffusion coefficient) and on the right hand side we can use

equipartition to arrive at

$$D = \frac{k_{\mathrm{B}}T}{\tilde{\xi}(0)}, \tag{B.7}$$

which is the famous Einstein relation. Secondly we can look at equation B.5 in a different way. After giving the particle an initial velocity $v(0)$ we can can measure $v(0)\tilde{v}(0)$, like in linear response

$$v(0)\tilde{v}(0) = \frac{Mv^2(0)}{\tilde{\xi}(0)}. \tag{B.8}$$

So, if we integrate the velocity correlation function, we obtain $1/\tilde{\xi}(0)$, and by equation B.7 the diffusion coefficient.

Thus far, we considered a system in which no external force acted on the colloid. Let us now explicitly add a (time-dependent) external force $f(t)$ in equation B.1

$$M\frac{dv}{dt} = -\int_0^t \xi(t-s)v(s)ds + f(t), \tag{B.9}$$

which after Laplace transformation gives

$$M(z\tilde{v}(z) - v(0)) = -\tilde{\xi}(z)\tilde{v}(z) + \tilde{f}(z). \tag{B.10}$$

If we substitute $z = 0$ then we find

$$Mv(0) = \tilde{\xi}(0)\tilde{v}(0) - \tilde{f}(0). \tag{B.11}$$

If we set the initial velocity of the particle to $v(0) = 0$ we find

$$\tilde{v}(0) = \frac{1}{\tilde{\xi}(0)}\tilde{f}(0), \tag{B.12}$$

From which it can be seen that $1/\tilde{\xi}(0)$ is the mobility, often written as μ

$$\tilde{v}(0) = \mu\tilde{f}(0). \tag{B.13}$$

B.2 Suspension

For a suspension the situation is more involved. From this point on, we consider a single configuration of colloids. For a suspension the generalized Langevin equation, again with no external and random force, is

$$M\frac{dv_i}{dt} = -\sum_j \int_0^t \xi_{ij}(t-s)v_j(s)ds, \tag{B.14}$$

which after Laplace transformation gives

$$M(z\tilde{v}_i(z) - v_i(0)) = -\sum_j \tilde{\xi}(z)_{ij}\tilde{v}_j(z). \tag{B.15}$$

If we substitute $z = 0$, we find

$$Mv_i(0) = \sum_j \tilde{\xi}(0)_{ij}\tilde{v}_j(0), \tag{B.16}$$

which is a matrix equation. Inversion gives:

$$\tilde{v}_i(0) = M\sum_j (\tilde{\xi}(0)^{-1})_{ij}v_j(0). \tag{B.17}$$

If we multiply both sides with $v_i(0)$ we find

$$v_i(0)\tilde{v}_i(0) = M\sum_j (\tilde{\xi}(0)^{-1})_{ij}v_i(0)v_j(0), \tag{B.18}$$

Now again we can proceed via two routes. First we take the velocity average we obtain

$$< v_i(0)\tilde{v}_i(0) >= (\tilde{\xi}(0)^{-1})_{ii} < Mv_i^2(0) > . \tag{B.19}$$

After which we recover (using Green-Kubo and equipartition)

$$D_{ii} = k_{\mathrm{B}}T(\tilde{\xi}(0)^{-1})_{ii}, \tag{B.20}$$

the Einstein relation. From equation B.16 one can also derive

$$D_{ij} \equiv< v_i(0)\tilde{v}_j(0) >= k_{\mathrm{B}}T(\tilde{\xi}(0)^{-1})_{ij}, \tag{B.21}$$

where D_{ij} is the generalized diffusion tensor. As before we could have looked at equation B.18 in a different way. If the velocities of different particles are uncorrelated ($[v_i(0)v_j(0)] = \delta_{ij}[v_i^2(0)]$) we find, upon averaging

$$[v_i(0)\tilde{v}_i(0)] = M(\tilde{\xi}(0)^{-1})_{ii}[v_i^2(0)]. \tag{B.22}$$

From which it can be seen that, if the initial velocities are appropriately chosen and averaging is performed, the diffusion coefficient can be measured in simulation. Thus one can measure

$$[D] = \left[\frac{1}{N}\sum_i v_i(0)\tilde{v}_i(0)\right] = \int_0^\infty \left[\frac{1}{N}\sum_i v_i(0)v_i(t)\right] dt \tag{B.23}$$

Alternatively, one could have opted to make all the velocities except $v_i(0)$ in equation B.18 equal to zero, then one finds

$$v_i(0)\tilde{v}_i(0) = M(\tilde{\xi}(0)^{-1})_{ii}v_i^2(0), \tag{B.24}$$

a direct way to measure $(\tilde{\xi}(0)^{-1})_{ii}$ in simulation.

If we now add external forces acting on the colloids, equation B.14 becomes

$$M\frac{dv_i}{dt} = -\sum_j \int_0^t \xi_{ij}(t-s)v_j(s)ds + f_i(t), \tag{B.25}$$

which after Laplace transformation gives

$$M(z\tilde{v}_i(z) - v_i(0)) = -\sum_j \tilde{\xi}(z)_{ij}\tilde{v}_j(z) + \tilde{f}_i(z). \tag{B.26}$$

If we substitute $z = 0$ then we find

$$Mv_i(0) = \sum_j \tilde{\xi}(0)_{ij}\tilde{v}_j(0) - \tilde{f}_i(0). \tag{B.27}$$

If we set the initial velocity of the particle to $v(0) = 0$ and rewrite the previous equation we find

$$\tilde{v}_i(0) = \sum_j (\tilde{\xi}(0)^{-1})_{ij}\tilde{f}_j(0), \tag{B.28}$$

So $\tilde{\xi}(0)^{-1}$ is the mobility matrix, often written as μ

$$\tilde{v}_i(0) = \sum_j \mu_{ij}\tilde{f}_j(0). \tag{B.29}$$

If now only particle i is forced one finds

$$\tilde{v}_i(0) = (\tilde{\xi}(0)^{-1})_{ii}\tilde{f}_i(0), \tag{B.30}$$

as in equation B.12.

Combination of equation B.21 and equation B.29 gives

$$D_{ij} =< v_i(0)\tilde{v}_j(0) >= k_{\mathrm{B}}T(\tilde{\xi}(0)^{-1})_{ij} = k_{\mathrm{B}}T\mu_{ij}, \tag{B.31}$$

which is the generalized Einstein equation.

B.3 More variables

Thus far, we have treated the velocity v as a scalar and in addition rotation of the colloid was ignored. The extension to vectorial notation is straightforward.

$$D = \frac{1}{d}\sum_\alpha < v_\alpha(0)\tilde{v}_\alpha(0) >= \frac{k_{\mathrm{B}}T}{d}\mathrm{Tr}\left(\tilde{\xi}(0)^{-1}\right) = \frac{k_{\mathrm{B}}T}{d}\mathrm{Tr}\left(\mu\right), \tag{B.32}$$

where d is the dimensionality. When we consider the coupling of rotation and translation, we get

$$\begin{aligned} M\frac{dv}{dt} &= -\int_0^t \xi^{TT}(t-s)v(s)ds - \int_0^t \xi^{TR}(t-s)\omega(s)ds, \\ I\frac{d\omega}{dt} &= -\int_0^t \xi^{RT}(t-s)v(s)ds - \int_0^t \xi^{RR}(t-s)\omega(s)ds, \end{aligned} \tag{B.33}$$

Where I is the moment of inertia ω is the angular velocity and T and R denote translation and rotation respectively. Laplace transformation and taking the limit $z \to 0$ gives

$$\begin{pmatrix} Mv(0) \\ I\omega(0) \end{pmatrix} = \begin{pmatrix} \tilde{\xi}^{TT}(0) & \tilde{\xi}^{TR}(0) \\ \tilde{\xi}^{RT}(0) & \tilde{\xi}^{RR}(0) \end{pmatrix} \begin{pmatrix} \tilde{v}(0) \\ \tilde{\omega}(0) \end{pmatrix}, \tag{B.34}$$

or

$$\begin{pmatrix} \tilde{v}(0) \\ \tilde{\omega}(0) \end{pmatrix} = \begin{pmatrix} \tilde{\xi}^{TT}(0) & \tilde{\xi}^{TR}(0) \\ \tilde{\xi}^{RT}(0) & \tilde{\xi}^{RR}(0) \end{pmatrix}^{-1} \begin{pmatrix} Mv(0) \\ I\omega(0) \end{pmatrix}, \tag{B.35}$$

again

$$\begin{pmatrix} \tilde{\xi}^{TT}(0) & \tilde{\xi}^{TR}(0) \\ \tilde{\xi}^{RT}(0) & \tilde{\xi}^{RR}(0) \end{pmatrix}^{-1} = \begin{pmatrix} \mu^{TT} & \mu^{TR} \\ \mu^{RT} & \mu^{RR} \end{pmatrix} \tag{B.36}$$

If we again calculate the diffusion coefficients we find from velocity averaging

$$\begin{pmatrix} D_i^T \\ D_i^R \end{pmatrix} = \frac{k_B T}{d} \begin{pmatrix} \mathrm{Tr}(\mu_i^{TT}) \\ \mathrm{Tr}(\mu_i^{RR}) \end{pmatrix}, \tag{B.37}$$

where we have now explicitly inserted the particle index i and have taken into account that both $\mathbf{v}$, and ω are vectors. We stress that the analysis presented in this appendix applies to a single realization of the configuration of the colloids. To obtain the true transport properties, averaging over colloid configurations needs to be performed.

Bibliography

[1] B.J. Alder and T.E. Wainwright, Phys. Rev. A **1**, 18 (1970).

[2] M.H. Ernst, E.H. Hauge and J.M.J. van Leeuwen, Phys. Rev. Lett. **25**, 1254 (1970).

[3] J.R. Dorfman and E.G.D. Cohen, Phys. Rev. Lett. **25**, 1257 (1970).

[4] Y. Pomeau and P. Résibois, Phys. Rep. **19**, 63 (1974).

[5] M.H. Ernst and A. Weyland, Phys. Lett. **34A**, 39 (1971).

[6] C.P. Lowe and A.J. Masters, Physica A **195**, 149 (1993).

[7] U. Frisch, B. Hasslacher and Y. Pomeau, Phys. Rev. Lett. **56**, 1505 (1986).

[8] U. Frisch, D. d'Humières, B. Hasslacher, P. Lallemand, Y. Pomeau and J.-P. Rivet, Complex Systems **1**, 649 (1987).

[9] M.A. van der Hoef and D. Frenkel, Phys. Rev. Lett. **66**, 1591 (1991).

[10] A.J.C. Ladd, M.E. Colvin and D. Frenkel, Phys. Rev. Lett. **60**, 975 (1988).

[11] M.A. van der Hoef and D. Frenkel, in *Microscopic Simulation of Complex Hydrodynamic Phenomena*, edited by M. Mareschal and B.L. Holian, Plenum, New York (1992).

[12] G.R. McNamara and G. Zanetti, Phys. Rev. Lett. **61**, 2332 (1988).

[13] F. Higuera, S. Succi and R. Benzi, Europhys. Lett. **9**, 345 (1989).

[14] G.R. McNamara and B.J. Alder, in *Microscopic Simulation of Complex Hydrodynamic Phenomena*, edited by M. Mareschal and B.L. Holian, Plenum, New York (1992).

[15] A.J.C. Ladd, Phys. Rev. Lett. **70**, 1339 (1993).

[16] L.D. Landau and E.M. Lifshitz, *Fluid Mechanics*, Pergamon, Oxford, 2nd edition (1993).

[17] A.J.C. Ladd, J. Fluid Mech. **271**, 285 (1994).

[18] A.J.C. Ladd, J. Fluid Mech. **271**, 311 (1994).

[19] M.P. Allen and D.J. Tildesley, *Computer Simulation of Liquids*, Oxford University Press, Oxford (1987).

[20] D. Frenkel and B. Smit, *Understanding Molecular Simulation: From Algorithms to Applications*, Academic Press, Boston (1996).

[21] P.J. Hoogerbrugge and J.M.V.A. Koelman, Europhys. Lett. **19**, 155 (1992).

[22] J.M.V.A. Koelman and P.J. Hoogerbrugge, Europhys. Lett. **21**, 363 (1992).

[23] P. Español and P. Warren, Europhys. Lett. **30**, 191 (1995).

[24] P. Español, Phys. Rev. E **52**, 1734 (1995).

[25] C.A. Marsh and J.M. Yeomans, Europhys. Lett. **37**, 511 (1997).

[26] C.A. Marsh, G. Backx and M.H. Ernst, Europhys. Lett. **38**, 411 (1997).

[27] C.A. Marsh, G. Backx and M.H. Ernst, Phys. Rev. E **56**, 1676 (1997).

[28] J.F. Brady and G. Bossis, Ann. Rev. Fluid Mech. **20**, 111 (1988).

[29] D.L. Ermak and J.A. McCammon, J. Chem. Phys. **69**, 1352 (1978).

[30] D.J. Pine, D.A. Weitz, J.X. Zhu and E. Herbolzheimer, J. Phys. France **49**, 2101 (1990).

[31] J.X. Zhu, D.J. Durian, J. Müller, D.A. Weitz and D.J. Pine, Phys. Rev. Lett. **68**, 2559 (1992).

[32] P.N. Pusey, in *Liquids, Freezing and Glass Transition*, edited by J.P. Hansen, D. Levesque and J. Zinn-Justin, North-Holland, Amsterdam (1991).

[33] A. van Blaaderen, J. Peetermans, G. Maret and J.K.G. Dhont, J. Chem. Phys. **96**, 4591 (1992).

[34] H. Happel and H. Brenner, *Low Reynolds Number Hydrodynamics*, Martinus Nijhof, Dordrecht, 4th edition (1983).

[35] A. Einstein, *Investigations on the Theory of the Brownian Movement*, Dover, New York (1956).

[36] P. Debye, *Polar Molecules*, Dover, New York (1929).

[37] G.K. Batchelor, J. Fluid Mech. **74**, 1 (1976).

[38] C.W.J. Beenakker and P. Mazur, Physica A **120**, 388 (1983).

[39] C.W.J. Beenakker and P. Mazur, Physica A **126**, 349 (1983).

[40] J.K.G. Dhont, *An Introduction to Dynamics of Colloids*, Elsevier, Amsterdam (1996).

[41] H.J.H. Clercx, *The Dependence of Transport Coefficients of Suspensions on Quasistatic and Retarded Hydrodynamic Interactions*, Ph.D. Thesis, Technical University Eindhoven, The Netherlands (1991).

[42] C.P. Lowe, D. Frenkel and A.J. Masters, J. Chem. Phys. **103**, 1582 (1995).

[43] J.M. Deutch and I. Oppenheim, Faraday Discuss. Chem. Soc. **83**, 1 (1987).

[44] P.M. Bungay and H. Brenner, Int. J. Multiph. Flow **1**, 25 (1973).

[45] L. Bocquet and J.-L. Barrat, J. Phys.: Condens. Matter. **8**, 9297 (1996).

[46] S. Ramaswamy and G.F. Mazenko, Phys. Rev. A **26**, 1753 (1982).

[47] W. Cai and T.C. Lubensky, Phys. Rev. Lett. **73**, 1186 (1994).

[48] T. Naitoh, M.H. Ernst, M.A. van der Hoef and D. Frenkel, Phys. Rev. A **44**, 2484 (1991).

[49] L. Bocquet and J.-L. Barrat, Europhys. Lett. **31**, 455 (1995).

[50] V. Degiorgio, R. Piazza and R.B. Jones, Phys. Rev. E **52**, 2707 (1995).

[51] H.J.H. Clercx and P.P.J.M. Schram, Physica A **174**, 293 (1991).

[52] H.J.H. Clercx and P.P.J.M. Schram, J. Chem. Phys. **96**, 3137 (1992).

[53] R.B. Jones, Physica A **150**, 339 (1988).

[54] J. Kanetakis, A. Tölle and H. Sillescu, Phys. Rev. E **55**, 3006 (1997).

[55] E.H. Hauge and A. Martin-Löf, J. Stat. Phys. **7**, 259 (1973).

[56] T.S. Chow, Phys. Fluids **16**, 31 (1973).

[57] B.J. Berne, J. Chem. Phys. **56**, 2164 (1972).

[58] W.G. Hoover and F.H. Ree, J. Chem. Phys. **49**, 3609 (1986).

[59] M. Watzlawek and G. Nägele, Physica A **235**, 56 (1997).

[60] M.H. Ernst, J. Machta, H. van Beijeren and J.R. Dorfman, J. Stat. Phys. **34**, 477 (1984).

[61] C.P. Lowe, D. Frenkel and M.A. van der Hoef, J. Stat. Phys. **87**, 1229 (1997).

[62] H. van Beijeren, personal communication.

[63] D. Frenkel and M.H. Ernst, Phys. Rev. Lett. **63**, 2165 (1989).

[64] J.J. Fried and M.A. Combarnous, Adv. in Hydr. Sci. **7**, 169 (1971).

[65] A. Rahman, Phys. Rev. **136**, A405 (1964).

[66] W. van Megen and S.M. Underwood, J. Chem. Phys. **88**, 7841 (1988).

[67] A. van Veluwen and H.N.W. Lekkerkerker, Phys. Rev. A **38**, 3758 (1988).

[68] R.J.A. Tough, P.N. Pusey, H.N.W. Lekkerkerker and C. van den Broeck, Mol. Phys. **59**, 595 (1986).

[69] I.M. de Schepper, H. van Beijeren and M.H. Ernst, Physica A **75**, 1 (1974).

[70] A.H. Marcus, B. Lin and S.A. Rice, Phys. Rev. E **53**, 1765 (1996).

[71] B. Cichocki and B.U. Felderhof, J. Phys.: Condens. Matter. **6**, 7287 (1994).

[72] M. Sahimi and V.L. Jue, Phys. Rev. Lett. **62**, 629 (1989).

[73] M. Sahimi, J. Chem. Phys. **96**, 4718 (1992).

[74] J. Alvarez-Ramírez, S. Nieves-Mendoza and J. González-Trejo, Phys. Rev. E **53**, 2298 (1996).

[75] I.C. Kim and S. Torquato, J. Appl Phys. **68**, 3892 (1990).

[76] I.C. Kim and S. Torquato, J. Appl Phys. **69**, 2280 (1991).

[77] I.C. Kim and S. Torquato, J. Chem. Phys. **96**, 1498 (1992).

[78] G. Viramontes-Gamboa, J.L. Arauz-Lara and M. Medina-Noyola, Phys. Rev. Lett. **75**, 759 (1995).

[79] G. Viramontes-Gamboa, J.L. Arauz-Lara and M. Medina-Noyola, Phys. Rev. E **52**, 4035 (1995).

[80] S.G.J.M. Kluijtmans and A.P. Philipse, personal communication.

[81] B.D. Lubashevsky, F.H. Stillinger and E.N. Pinson, J. Stat. Phys. **64**, 501 (1991).

[82] A. van Blaaderen and P. Wiltzius, Science **270**, 1177 (1995).

[83] M. Medina-Noyola, Phys. Rev. Lett. **60**, 2705 (1988).

[84] T. Gotoh and Y. Kaneda, J. Chem. Phys. **76**, 3193 (1982).

[85] M.H.J. Hagen, C.P. Lowe and D. Frenkel, Phys. Rev. E **51**, 4287 (1995).

Summary

In this thesis the diffusion of confined colloidal particles has been investigated using computer simulation.

Chapter 1 and chapter 2 contain a general discussion of particle diffusion. The history of Brownian motion and the dynamics of colloidal particles is discussed. This is followed by a discussion of computational, experimental and theoretical approaches to the dynamics of colloidal particles. Chapter 2 concludes with a discussion of the lattice-Boltzmann method to simulate the dynamics of colloidal particles on a short-time scale - this is the method that we employ in this thesis.

In chapter 3 we calculate the velocity correlation function for a particle in a liquid-filled tube. We find that the velocity correlation function in the direction of the tube decays with a negative long-time tail. The functional form of this negative long-time tail appears to depend on the number of unconfined dimensions. The behaviour of the velocity correlation function can be explained in terms of the diffusive decay of density perturbations. The short-time diffusion coefficient of the particle is unaffected by the temporal behaviour of the velocity correlation function.

In chapter 4 we calculate the rotational diffusion coefficient of a suspension of colloidal particles at short times. We find that our simulations of the angular velocity correlation function of the colloidal particle are in good agreement with theory. Our results for the rotational diffusion coefficient for the suspension also agree with recent experimental results. We find that for colloids placed on a regular FCC lattice the linear term in the volume-fraction dependence for the rotational diffusion coefficient is absent.

In chapter 5 computations of the self-dynamic structure factor for tracer particles diffusing in a dense colloidal packing are reported. Our simulations show that, although the super-Burnett coefficient converges, the self-dynamic structure factor does not decay exponentially. The self-dynamic structure factor decays with a power-law decay. We argue that the long-time behaviour of the self-dynamic structure factor might be observable in experiment.

Chapter 6 describes the results of simulations to measure deviations from Gaussian diffusive behaviour. In the first part of the chapter we present evidence for non-Gaussian behaviour caused by the positional dependence of the diffusion coefficient. In the second part of the chapter we show the results for calculations of the deviations of Gaussian behaviour for a single colloid, which is confined between two parallel plates. There the time dependence of the non-Gaussian behaviour was measured at long times.

In chapter 7 we present the calculations for the diffusion coefficient of a small colloidal particle in dense colloidal packings. Both, the short and the long time scale we considered. On the short time scale, the hydrodynamic interactions develop and the diffusion coefficient reaches its short-time value. After this time scale the particle diffuses a distance comparable to its radius and the diffusion coefficient reaches another plateau value, the long-time diffusion coefficient. By combination of the results for the diffusion on the short time scale and a calculation in which the hydrodynamic interactions are neglected we calculated the long-time self diffusion coefficient in an array of randomly and regularly close packed spheres.

In the final chapter, we show the results of a calculation of the velocity correlation function of a particle diffusing near a single wall. The simulations show that the decay of the angular and the translational velocity correlation function are modified due to the hydrodynamic interaction with the wall. For the situations where the colloidal particle diffuses perpendicular and parallel to the flat wall agreement with the relevant theoretical predictions is found.

Samenvatting voor iedereen

Op deze plek in het proefschrift is het gebruikelijk om een samenvatting te maken voor mensen die geen of een beperkte achtergrond hebben in de beta-wetenschappen.

Het onderwerp van dit proefschrift is diffusie van kleine deeltjes in de omgeving waarin zich obstakels (bijvoorbeeld wanden) bevinden. Die kleine deeltjes kan men beschouwen als kleine balletjes, met een straal van die ongeveer 100 tot 1000 maal zo groot is als die van een water molecuul (H_2O). Die kleine deeltjes, ook wel colloïdale deeltjes genoemd, zijn vaak opgelost in water, of in een ander oplosmiddel. Voorbeelden van colloïdale suspensies zijn: melk, verf, bloed en ook mayonaise. Als zo'n colloïdaal deeltje zo licht is dat het niet (of slechts langzaam) naar beneden zakt onder invloed van de zwaartekracht, dan is diffusie waar te waar te nemen.

Diffusie is goed te illustreren aan de hand van een eenvoudig voorbeeld. Na het laten vallen van een druppel inkt in een glas met water is te zien dat de kleur van van het water na verloop van tijd homogeen is. De inkt deeltjes, ook dit zijn weer colloïden, diffunderen door de oplossing. Hoe snel de diffusie verloopt wordt aangegeven door de diffusie coefficient D. Hoe hoger die is, des te sneller verloopt de diffusie. Einstein heeft laten zien dat als de straal van het colloïdale deeltje verkleind wordt, of als de stroperigheid van het oplosmiddel verlaagd wordt, dat dan de diffusie coefficient omhoog gaat. Dit komt omdat dan de wrijving die het deeltje in de vloeistof "voelt" vermindert. Nog voordat een inkt-deeltje botst met de wand van het glas, is het effect van de wand op de diffusie van het deeltje al waar te nemen, namelijk, de wrijving neemt toe door de aanwezigheid van de wand, en daardoor neemt de diffusie coefficient af. Nog later zullen de deeltjes ook gaan botsen met de wand, en de wand dus ook direct gaan voelen.

Zoals al aangegeven komen colloïdale deeltjes veelvuldig voor in de natuur en in voedingsmiddelen. Daarom is het interessant om de eigenschappen en het gedrag van die deeltjes te begrijpen. Er zijn verschillende mannieren om dit te doen. Men kan experimenten doen, en bijvoorbeeld onder een microscoop kijken naar de diffusie van de colloïdale deeltjes. Anders kan men theorie, een serie vergelijkingen opstellen om daarmee de diffusie te voorspellen. Ook kan men een model van de werkelijkheid maken (zoals in de theorie), maar dan gedetailleerder. Vanwege de complexiteit van dergelijke modellen kan het gedrag alleen nog maar worden voorspeld door het op de computer door te rekenen - dit is *computer simulatie*.

Voor een deel van het werk dat in dit proefschrift beschreven is maken wij gebruik van een model waarin de wisselwerking tussen een deeltje (het colloïdale deeltje), en het

oplosmiddel (de vloeistof) en eventuele wanden of andere deeltjes op eenvoudige wijze wordt beschreven. Door de resultaten van de simulaties te vergelijken met al bekende resultaten van theorieën en experimenten, kan men laten zien dat het model goed werkt. Hiermee ontkom je dan (hopelijk) aan het grote gevaar van computer berekeningen, zoals omschreven door Richard Feynman: "Garbage in, garbage out". Als je een goed functionerend model hebt, dan kan je dat gebruiken om voorspellingen te doen waarvoor theoretische en experimentele gegevens nog ontbreken. Computer simulaties kunnen dus voorspellingen doen over effecten die nog niet experimenteel zijn waargenomen.

In hoofdstuk 3 van dit proefschrift kijken we naar het systeem van een colloïdaal deeltje dat in een nauwe, met vloeistof gevulde, buis is geplaatst (zie figuur 3.1). In dat hoofdstuk is te lezen dat, als het deeltje een zetje in de richting van de buis krijgt, het na verloop van tijd *omkeert* in beweging. Als de buis er niet zou zijn zou je verwachten dat het deeltje in de oorspronkelijke richting zou blijven bewegen.

Colloïdale deeltjes verplaatsen niet alleen door de vloeistof, ze roteren ook. In hoofdstuk 4 is te lezen, wat het effect is van de volume fractie op de rotatie diffusie coefficient van colloïdale deeltjes. De volume fractie geeft aan hoe dicht op elkaar de deeltjes gepakt zijn. Als de volume fractie van de deeltjes hoger wordt, dan neemt de rotatie diffusie snelheid af. De resultaten van de computer simulatie zijn in uitstekende overeenstemming met de resultaten van experimenten.

In hoofdstuk 5 wordt gekeken naar een aspect van de diffusie van een zeer klein colloïdaal deeltje in een pakking van stilstaande harde bollen, zie figuur 5.1. In dat hoofdstuk laten wij zien, dat er een afwijking is van eenvoudige diffusie. Verder laten wij zien dat dat die afwijking zodanig groot is dat die experimenteel waarneembaar zou moeten zijn.

In hoofdstuk 6 beschouwen we ook andere afwijkingen van eenvoudige diffusie. In het begin van dat hoofdstuk is te lezen wat de oorzaak is van de afwijking. Verder in dat hoofdstuk is te lezen hoe groot, of beter hoe klein het effect is voor een systeem van colloïdale deeltjes en voor een eenvoudig systeem van één deeltje dat tussen twee platen diffundeert.

In hoofdstuk 7 komen wij terug op het systeem van een colloïdaal deeltje dat diffundeert in een systeem van stilstaande bollen. Hier bepalen we het effect van de toegenomen wrijving door de aanwezigheid van de grote bollen. Dit heeft een effect op de diffusie van het deeltje. De diffusie van het deeltje neemt sterk af als de grootte van het deeltje vergelijkbaar wordt met de breedte van de poriën.

In het laatste hoofdstuk van dit proefschrift is te lezen hoe de beweging van een colloïdaal deeltje wordt beïnvloed door de aanwezigheid van één wand, zie figuur 8.1. Het is verrassend dat de aanwezigheid van een wand in het systeem de beweging van het deeltje zelfs op een afstand al kwalitatief anders maakt.